

ABSTRACT

Title of Dissertation: DEVELOPMENT OF HYBRID
BIOMATERIALS FOR RECONSTRUCTION
OF CARDIOVASCULAR TISSUE

Laura Bracaglia, Doctor of Philosophy, 2017

Dissertation directed by: Fischell Family Distinguished Professor &
Department Chair John P. Fisher,
Department of Bioengineering

Congenital heart defects in the pediatric population require severe surgery to reconstruct vessels and structures in malformed heart tissue. Reconstructive surgery at an early age leaves many patients with synthetic, non-living and possibly failing grafts that require subsequent surgeries. A biodegradable scaffold can support regeneration of the vascular wall by the patient's own tissues, and eventually degrade away, leaving a functional and patient maintained tissue in its place. Extracellular matrix (ECM) based scaffolds are uniquely equipped to enhance host cell recruitment and modulate the immune response. Natural healing responses are initiated by native biochemical and physical cues provided by the ECM to endothelial cells and key immune system responders. However, ECM-based scaffolds may degrade rapidly or not possess the elastic strength required for vascular grafts. The work presented here is aimed at the development of a biohybrid scaffold, consisting of the ECM-based material pericardium and synthetic polymers. This combination results in a single

material that retains mechanical integrity from the polymer and provides bioactivity from the pericardium matrix. The first aim of this research develops a compliant patch material as a replacement for chemically crosslinked pericardium currently used in surgical applications. Reinforcing pericardium with the polymer PPF creates a mechanically resilient scaffold, with reduced inflammatory markers compared to chemically crosslinked or untreated controls. In addition to cues provided by the matrix molecules of pericardium, the polymer layer can serve as a platform to further facilitate or direct the remodeling by releasing bioactive cargo from the polymer layer to the pericardium matrix. The benefits of the hybrid material are not limited to a layered scaffold, as demonstrated in the second aim. Here, the applicability of the pericardium polymer hybrid is expanded to control shape and mechanical properties in a hydrogel scaffold. In this dissertation, we have successfully developed two distinct hybrid materials that maintain the bioactivity of an ECM-based material to support native cell remodeling, and incorporate control over degradation and magnitude of host response from the polymer. Used as vascular scaffolds, these materials have potential to reduce subsequent surgical intervention by creating a lasting and living vascular patch.

DEVELOPMENT OF HYBRID BIOMATERIALS FOR RECONSTRUCTION OF
CARDIOVASCULAR TISSUE

by

Laura Bracaglia

Dissertation submitted to the Faculty of the Graduate School of the
University of Maryland, College Park, in partial fulfillment
of the requirements for the degree of
Doctor of Philosophy
2017

Advisory Committee:

Professor John P. Fisher, Chair

Associate Professor Christopher Jewell

Assistant Professor Kimberly Stroka

Assistant Professor Steven M. Jay

Associate Professor John Cumings, Dean's Representative

© Copyright by
Laura Bracaglia
2017

Acknowledgements

I would like to thank my advisor, Dr. John Fisher, for his terrific mentorship and the opportunity to work in the Tissue Engineering and Biomaterials Lab. I would also like to extend my appreciation to my committee members for providing guidance and suggestions that have improved the outcome of my research throughout this process. I am grateful to my friends and lab mates in the Tissue Engineering and Biomaterials Lab and in the BIOE department, who have taught me, helped me learn and laughed with me over the course of this project. A special thank you to Michael Messina, Casey Vantucci, Shira Winston and Maria Pascale for their hard work and contributions to the hybrid material projects. Finally, a big thank you to Dan, who lent me enthusiasm and momentum along the way, and especially to my parents and sisters, who encourage me to “discover something” every day.

Table of Contents

Acknowledgements.....	ii
Table of Contents.....	iii
List of Tables.....	v
List of Figures.....	vi
Chapter 1: Introduction to Tissue Engineered Vascular Scaffolds.....	1
Chapter 2: ECM-Based Biohybrid Materials for Engineering Compliant, Matrix-Dense Tissues.....	8
2.1 Role of ECM in Engineering Tissue.....	8
2.2 Methods.....	12
2.3 Types of Biohybrid Materials.....	13
2.3.1 Materials Fabricated with Interwoven Fibers.....	19
2.3.2 Materials Fabricated Using the Layering Technique.....	29
2.3.3 Cell-Built ECM Layer Fabrication Method.....	35
2.3.4 Materials Fabricated By Blending Hydrogel Components.....	36
2.5. Conclusion.....	46
2.6 Acknowledgments.....	46
Chapter 3: PPF Reinforced Pericardium as a Hybrid Material for Cardiovascular Applications.....	47
3.1 Introduction.....	47
3.2 Methods.....	52
3.2.1 Polymer Synthesis and Composition.....	52
3.2.2 Mechanical Testing of Polymer Compositions.....	53
3.2.3 Sample Preparation.....	53
3.2.4 <i>In vitro</i> Evaluation- Degradation Test.....	54
3.2.5 <i>In vitro</i> Evaluation- Calcification Test.....	55
3.2.6 <i>In vivo</i> Evaluation.....	55
3.2.7 Statistical Analysis.....	57
3.3 Results.....	57
3.4 Discussion.....	67
3.5 Conclusion.....	70
3.6 Acknowledgements.....	71
Chapter 4: Inflammatory Response to PPF Reinforced Pericardium in a Rat Model.....	72
4.1 Introduction.....	72
4.2 Methods.....	75
4.2.1 Material Synthesis.....	75
4.2.2 <i>In vitro</i> Studies.....	76
4.2.3 <i>In vivo</i> Studies.....	78
4.3 Results and Discussion.....	79
Chapter 5: Controlled Delivery of Tissue Inductive Factors in a Cardiovascular Hybrid Biomaterial Scaffold.....	90
5.1 Introduction.....	90
5.2 Methods.....	96

5.2.1 Preparation of the Microspheres	96
5.2.2 Polymer Synthesis and Composite Film Assembly	96
5.2.3 Degradation Assessment.....	97
5.2.4 Release from Films and Free Microspheres.....	98
5.2.5 Construction and Assessment of Hybrid Material	99
5.2.6 Demonstration of Effect on Cells <i>In vitro</i>	101
5.2.7 Demonstration of Directional Release	105
5.3 Results and Discussion	105
5.4 Acknowledgements.....	119
Chapter 6: 3D Printed Pericardium Hydrogels Promote Wound Healing Response in Vascular Tissue Scaffolds.....	121
6.1 Introduction.....	121
6.2 Methods.....	127
6.2.1 Tissue Homogenization	127
6.2.2 HPM Characterization	127
6.2.3 PEG +HPM Hydrogel Formation	129
6.2.4 Evaluation of PEG+HPM hydrogels.....	130
6.2.5 Cell Metabolic Activity Assay.....	131
6.2.6 Isolation of Bone Marrow	132
6.2.7 Macrophage response to HPM components	133
6.2.8 Quantitative reverse transcriptase-polymerase chain reaction (QT-PCR).....	133
6.2.9 Co-culture experiment to evaluate response to ECM Hydrogel	134
6.2.10 Statistical Analysis.....	135
6.3 Results and Discussion	136
Chapter 7: Summary and Future Directions	152
7.1 Summary	152
7.2 Contributions.....	160
7.3 Future Directions	160
Chapter 8: References	164

List of Tables

Table 2.1 Selection of Relevant ASTM Standards for Testing Biomaterials.....	17
Table 2.2 Mechanical Properties of Select ECM-Based Biomaterials.....	24
Table 6.1 Photoinitiator Concentrations.....	129
Table 6.2 Concentrations of Hybrid Hydrogels.....	131
Table 6.3 Hydrogel Scaffolds for Co-Culture	135

List of Figures

- Figure 2. 1 Methods of Fabricating ECM-Based Biohybrid Materials.** (A) Materials are fabricated with interwoven fibers, using either electrospinning, electrospaying, or a combination of the two. (B) Materials are fabricated by blending hydrogel components of ECM derived proteins and polymer chains. (C) Materials are built using a layering technique, with either a whole tissue or a polymer scaffold as a base. (D) Cell-built ECM layer fabrication, where cells are cultured on a polymer scaffold, and then removed, leaving an ECM layer on the polymer surface. 15
- Figure 3. 1 PPF Thin Film Analysis.** The compositions of Various Thin Films Tested, listed as mass to mass ratios of PPF to DEF (A), were crosslinked into thin films from the same total volume (B). Resulting thin films were 0.25 mm thick and weighed 0.15 grams. The image in B shows a thin film composed of 2g PPF to 1g DEF (2:1). Elastic modulus and 1% yield strength of thin films (C) were tested on an INSTRON mechanical tester, and extended at 10mm/min by a 50 N load cell. $n \geq 7$ for all groups, ANOVA statistical test shows significant difference, ($p < 0.05$), and Tukey's Post Hoc results are shown on graph. Groups that do not share a letter are significantly different. 58
- Figure 3. 2 In vitro Analysis of PPF Reinforced Pericardium.** The graph displays the physical properties of pericardium from 3 different donors ($n=8$ per donor) (A). Yield strength and modulus were evaluated from samples over an in vitro degradation simulation using collagenase ($n=8$ per time point) (C). ANOVA statistical tests showed significant difference in the elastic modulus and in the thicknesses ($p < 0.05$), and results from a post hoc Tukey's Test are shown on the graphs. Groups that do not share a letter are significantly different. The control on Day 0 has no PPF reinforcement or collagenase exposure. Control groups on the following days are exposed to collagenase but not reinforced with PPF or treated GA. After degradation, samples were fixed and stained using hemotoxylin and eosin to display structure of collagen network (B). Control pericardium appears to have lost structural integrity after collagenase degradation (d), as did the EtOH dehydrated sample (c), while the sample with PPF reinforcement (b) appears unaltered from the natural pericardium (a). In vitro calcification was also simulated using a calcium phosphate buffer, and calcium deposition was quantified ($n=5$ per time point). A students T test shows significant difference between the calcium content for all time points, denoted “*”, ($p < 0.05$). 60
- Figure 3. 3 Calcification of Pericardium Samples from In vivo Subcutaneous Model.** Calcium content was quantified on samples explanted after 3 and 6 weeks, and compared to non-implanted controls ($n=8$ per time point) (C). Calcium content from each sample group was compared for each time point using an ANOVA test ($p < 0.01$). A post hoc Tukey's test showed significant difference in the GA-treated group, as denoted “*”, ($p < 0.05$). Samples were also fixed and prepared for histological analysis using Von Kossa stains. The dark black region indicates calcium phosphate deposits. This region is seen significantly darker in GA treated samples after 3 and 6 weeks of implantation, and not observed in PPF reinforced or untreated samples. Scale bars represent 100 μm 64

Figure 3. 4 Histological Analysis of Explanted Pericardium Samples. Cellular response to implanted samples was analyzed using Masson’s trichrome stain (A). Blue regions indicate collagen, pink indicates cell bodies. Staining shows local cell populations relative to implanted tissue. Cell populations in the region of the implanted tissues were also stained for F4/80, a macrophage surface marker (B). Staining shows a correlation between dense cell regions and the F4/80 stain, indicating an inflammatory response. A dense line of macrophages is seen near the edge of the GA treated tissue, while in the PPF reinforced and untreated samples, macrophages are seen in smaller regions throughout the sample. On the other hand, there was no significant F4/80 expression in Day 0 samples (B.A) and samples lacking the primary antigen from week 6 (B.B). A rat spleen stained by the same procedure is shown in B.C as a positive control. Macrophage population was investigated by examining 3 standardized images from each of n=5 samples per treatment group. Macrophage fraction was defined as the number of cells determined to have F4/80 staining divided by the total cells counted per image in a blinded study. Data is presented as an average of each of these fractions, and error was calculated as the standard deviation between all images in each group. Population fractions from the GA treated samples and the PPF reinforced samples are significantly different, as determined by a one way ANOVA test, followed by a post hoc Tukey’s test ($p < 0.05$). Groups that share the same letter are not statistically different. Scale bars represent 100 μm 65

Figure 4. 1 Subcutaneous Implants in Sprague Dawley Rats. Representative images (A) of the scaffolds before implantation are stained with H&E to show matrix organization and structure differences. The layer of PPF is visible in the top row using phase contrast microscopy. After 6 weeks of implantation, scaffolds are explanted and stained with H&E (B), showing cell infiltration (nuclei are purple) and matrix changes compared to the un-implanted images (A). Using immunohistochemical staining, cells near the scaffold were identified as macrophages using CD68, and further characterized using CD86 (an M1 marker) and CD206 (an M2 marker). Scale bar is 20 μm , unless otherwise indicated. These images are representative of n=5 implanted samples..... 81

Figure 4. 2 In vitro Independent Cell Activation. Splenocytes that positively express the macrophage marker CD68 after culture with PPF films are quantified in the first graph (A). Total activation from PPF is observed to be lower than the inflammatory control LPS. From the cells positive for CD68, samples were then evaluated for positive staining of CD163 and CD80 (B). Splenocytes determined to be positive for these markers are summarized in the graph in Figure 4.2 C. The percentages shown in A, B, and C are taken from 20,000 events per group. HUVECs cultured with PPF degraded for 3 or 5 days, or with the products of that degradation, were evaluated for changes to TNF α (D) and IL10 (E) gene expression. Standard deviation is displayed for technical triplicates from the RNA extracted from n=3 cell cultures. Groups that share letters are not statistically different as determined with an ANOVA followed by a post hoc Tukey’s test ($p < 0.05$). 84

Figure 4. 3 Subcutaneous Implants in Athymic Rats. After 6 weeks of implantation, scaffolds are explanted and stained with H&E (A), showing minimal cell infiltration (nuclei are purple) and matrix changes compared to the scaffolds in

Figure 4.1. Using immunohistochemical staining, cells near the scaffold were identified as macrophages using CD68, and further characterized using CD86 (an M1 marker) and CD206 (an M2 marker). Additionally, the scaffolds and surrounding tissue were homogenized and analyzed using an ELISA for TNF α (n=5 samples per group). Groups that share letters are not statistically different, ANOVA test & post hoc Tukey's test (p<0.05). Scale bar is 20 μ m, unless otherwise indicated. 88

Figure 5. 1 A Schematic Of The Biohybrid Material consisting of three layers shown in the illustration (A), and corresponding bright field images (B) from histological samples. In C, scanning electron microscopy shows the two polymer layers, and the surface from which pericardium was removed before imaging. 95

Figure 5. 2 Adhesion Testing Schematic This schematic demonstrates the approach to test adhesion between the polymer layer and the pericardium substrate. Briefly, samples of pericardium were coated in either PPF or the PPF+PLGA microsphere composite. A poly(propylene) mesh of equivalent size to the pericardium was gently pressed into the liquid phase of the PPF top layer. This mesh served as a "tab" to pull the polymer layer the opposite direction as the pericardium, and causing the polymer layer to shear off the pericardium substrate with a measurable amount of force. 100

Figure 5. 3 Dose Response for Established Bioassays. Data from XTT analysis confirming the expected result to metabolic activity when various concentrations of TNF α are added to the culture with L929 cells (A) and when VEGF is added to culture with HUVECS (B). 104

Figure 5. 4 Characterization of the Composite Polymer Layer. In A, degradation of PLGA microparticles with and without OVA encapsulated (loaded vs unloaded) as measured with GPC shows significant loss of molecular weight (Mn) over 20 days (n=3 per time point). This degradation is much faster than the degradation of PPF thin films (Figure 5.4 B), as measured by mass loss over 500 days (n=6 per time point). C shows bright field images of composite thin films with mass concentrations of PLGA microparticles embedded within them. D shows mechanical analysis of the composite thin films, including elastic modulus, 0.1% yield strength, and the maximum shear stress that can be applied to the biohybrid material before the composite polymer layer separates (n=5 per group). A Student's t-test shows no significant difference between PPF with or without PLGA. Figure 5.4 E shows the release of OVA from PLGA microparticles contained within the PPF film (composite films) (n=6 per time point). 108

Figure 5. 5 Release of Active Growth Factors from Composite Films. TGF β is released into cell culture from composite films (A) and supplemented into culture (B); the data are separated into panels (A) and (B) due to the significant differences in the ordinate's scale. TGF β released from composite films shows sustained presence in cell culture over 5 days that is significantly higher than both blank films and control cell cultures (n=3), as well as significantly higher than the supplemented media groups (B) after the media change between day 1 and day 2. This was confirmed using a one way ANOVA and post hoc Tukey's test to compare groups within the same time point from both panel (A) and panel (B). Groups that do not share a letter in this graph are significantly different (p<0.05). Figure 5.5 C shows fluorescently stained cell cultures after delivery of either TNF α , which is seen to kill L929s, or VEGF, which increases collagen and actin staining in HUVECS. The scale bar

represents 20 μm . Figure D corroborates this result with metabolic activity assay of the tested cell cultures (n=3). Groups that do not share a letter are significantly different ($p < 0.05$) as determined with a one way ANOVA and post hoc Tukey's test. 112

Figure 5. 6 Composite Polymers Effect on Viability. Confirmed viability of L929 cells in culture with the PPF/PLGA composite material for 2 points over 48 hours. Data is presented normalized to the positive, untreated control cells..... 116

Figure 5. 7 Directional Delivery from Composite Layer into Pericardium Substrate. Pericardium tissue samples coupled with OVA-loaded composite films PLGA/PPF or with just PPF layers were immunostained using an antibody for OVA, indicated with a localized blue stain. Staining shows OVA contained primarily in the polymer layer on day 0, moving into the pericardium tissue by day 5. There is very low blue fluorescence observed in the PPF and pericardium samples, corresponding to the absence of OVA. The scale bar in these images is 50 μm 117

Figure 6. 1 HPM Characterization. Protein quantification and colorimetric assays were used to determine the molecular concentrations in the HPM, and displayed as concentrations per mg of dry HPM (n=15) (A). HPM was analyzed using SDS-PAGE (B) and stained for total protein. HPM is compared to a standard of rat tail collagen I, and arrows indicate bands appearing in HPM that were further characterized using antibody specific staining on the right. The final characterization was completed using mass spectrometry, and proteins existing in significant quantities are displayed by total percent (C). The final product HPM is capable of forming a thermally crosslinked hydrogel, as compared to the same material stored at 4C (D). The hydrogel can maintain shape integrity, as shown from a cylindrical mold (E). 137

Figure 6. 2 HPM PEG Hydrogel Formation. A reduction in the total concentration of amines in the HPM PEG hydrogel compared to the uncrosslinked components demonstrates successful formation of the network (n=3) (A). In the FTIR spectra (B), a change near the 1600 wavenumber also indicates a change to the free amine group after crosslinking (n=6). Mass loss from hydrogels over 3 days with and without collagenase indicated the biodegradability of the hybrid hydrogels, as compared to PEG (-) hydrogels (n=5) (C). Compressive modulus was also evaluated in scaffolds formed with varying concentrations of HPM and PEG (n=5) (D). The greatest significance is seen as a result of PEG content, however, changes to modulus are also seen as a result of HPM concentration. Images display the 3D printing capability of this hydrogel, showing a 5mm hollow prism with 1 mm wall thickness (E), and a curved vascular model, with an inner diameter of 6mm and a wall thickness of 1.5mm (F). Significance between groups was determined using an ANOVA, with a post hoc Tukey's test. Groups that do not share a letter are significantly different ($p < 0.05$). 140

Figure 6. 3 Cell Response to Hybrid Hydrogel Components. L929 cells were found to maintain a metabolic activity of 70% or greater when TEA concentration was reduced to 0.5% or below (n=3 cell cultures) (A). When HUVECs were seeded on either hybrid hydrogels they lay more collagen matrix than on PEG (-) hydrogels (n=3) (B). HUVECs on HPM hydrogels are stained for actin (red) in Figure 6.3C, and show morphology changes compared to HUVECs on PEG(-). Similarly, RAECs on HPM gels show more staining for von Willebrand factor (purple) than RAECs on PEG or PEG +Collagen scaffolds (D). RMCs expression of inflammatory or healing

genes shows differences in response to HPM concentration (E). M1 and M2 control populations are shown after stimulation and polarization with soluble cytokines (represented as technical triplicates of RNA from 3 cell cultures). The gene profiles are summarized in Figure 6.3 F, showing a ratio of the expression of M1 genes over M2 genes for each group. Significance between groups was determined using an ANOVA, with a post hoc Tukey's test. Groups that do not share a letter are significantly different ($p < 0.05$)..... 146

Figure 6. 4 Co-Culture of RAECs and RMCs on Hybrid Hydrogels. RMCs expression of inflammatory or healing genes shows differences in response to HPM concentration including in the hybrid hydrogel (A). The gene profiles are summarized in Figure 6.4B, showing a ratio of the expression of M1 genes over M2 genes for each group. In this figure, we also show the change in gene expression as a result of the presence of RAECs. Cells in the co-culture on hybrid hydrogels were stained for macrophage phenotypic markers CD68 (green, all), CD86 (red, M1), and CD206 (purple, M2) (C)..... 149

Chapter 1: Introduction to Tissue Engineered Vascular Scaffolds

Surgical reconstruction of blood vessels and cardiac tissue is frequently required to repair or restore anatomic configuration following cardiovascular defects, disease or injury. Congenital cardiovascular disease, also known as congenital heart defects (CHD), describe cases in the pediatric population where structural problems arise from abnormal formation of the heart or major blood vessels. Of all population groups, pediatric patients have the longest potential demand for the replacement, thus it is especially essential that repairs are both appropriate and long lasting.

CHD is one of the most prevalent birth defects, affecting 1% of live births in the U.S. (1). A number of anomalies associated with this disease will require severe surgical vessel reconstruction, often with help from a prosthetic material (2).

Tetralogy of Fallot, pulmonary atresia with ventricular septal defect, and Loeys-Dietz syndrome (LDS) are just a few examples of disorders requiring different and custom surgical intervention and reconstruction of major arteries (3). In these diseases, major vessels are formed with extreme tortuosity, enlargement, occlusion, or mismatched origins. In addition to inefficient blood transport, there is high risk and occurrence of vascular aneurysm and dissection (4). Surgical repair approaches may combine cutting away obstructive tissue, adding occlusion elements, enlarging outflow pathways, or total replacement of the aortic arch (5).

Improvements in surgical technique and materials have significantly decreased mortality in the affected population in recent years, allowing many CHD patients to survive into adulthood (6, 7). A growing life expectancy further emphasizes the need for a versatile material that can grow and be maintained by the patient as part of the native body. Without a “grow-able” device, this population risks multiple re-intervention surgeries throughout their lifetime.

Successful vascular tissue replacements first and foremost must retain elasticity and strength over time, without risk of calcifications or other impediments to blood flow. A long lasting replacement intended to grow with the patient has the added criteria to develop appropriate cell organization at the injured site, and support the somatic growth of the patient’s tissue that can replace the scaffold as it degrades over time.

Current material options for use in cardiac surgeries include autologous or xenographic tissues, synthetic materials, and, more recently, tissue engineering based strategies. Autologous or xenographic tissues have been most widely utilized over the past 60 years (8). Historically, a common, xenographic material used for CHD as well as many other vascular prosthetic uses is glutaraldehyde (GA) crosslinked bovine pericardium (9-11). Pericardium is the fibrous membrane enclosing the heart muscle. Due to the unique composition of primarily collagen, elastin, and glycosaminoglycans, pericardium has a mechanical profile which resembles that of vascular tissue. In both tissues, the protein fibers make up a strong and elastic biomaterial that is well suited for the high stress environment of the cardiovascular system. In order to prevent immediate deterioration of these proteins post-

implantation, most xenographs are treated with GA, which chemically crosslinks the tissue's collagen molecules. This process is effective at stabilizing the tissue against chemical and enzymatic degradation, as well as lessening the display of antigenic determinants and inflammatory response (8, 12). However, by chemically crosslinking the proteins, the potential for viable cell inhabitation and remodeling is diminished (13), resulting in a material that can no longer maintain or repair itself. The crosslinked product has been associated with local inflammation and severe calcifications which can lead to subsequent matrix deterioration and compromised mechanical properties (10, 14, 15). These challenges are especially critical in pediatric cases, since this calcification and stenosis can occur within 10 years of implantation and would require re-intervention (11, 16, 17). Similar challenges related to stenosis and eventual loss of function are shared with most synthetic grafting material. Even though other commercially available textile materials are able to remain durable over long periods of time, there is still no growth potential and therefore limited durability in a pediatric patient.

Recent investigations and developments in engineered tissues have shown great progress in the vascular space. These approaches have the ability to grow, heal, and provide long-term durability to the vascular injury site. Methodologies following two main approaches have emerged: cell-based designs and acellular, material-based designs. On one hand, cell-seeded, biodegradable tissue engineered grafts provide a controlled cell population and can ensure adequate development of endothelial and smooth muscle layers before implantation. Both characteristics are essential to a successful vascular graft. Cell-seeded protein hydrogels, cell-seeded

biodegradable synthetic polymer scaffolds (18), and self-assembled cell sheets all have success in this area and have progressed to preclinical (19) and clinical (20) studies. A limitation of this approach is that to be used in humans, autologous cells would need to be isolated from the patient and expanded before implantation. This is typically costly and labor-intensive.

Acellular techniques, on the other hand, endeavor to build a more scalable and easily applied therapy. In this approach, bioactive materials are used to recruit host-cells, and then support both invasion and differentiation of endogenous cell populations to inhabit and maintain the graft site until complete degradation of the graft material. Smart design and selection of material for this approach is critical. Evidence shows that parameters such as slow-degradation of the material or dissimilar mechanical properties result in limited cell infiltration, poor remodeling, and improper restoration of function (18).

Naturally derived materials, such as extracellular matrix (ECM), have been shown in many applications to help define the microenvironment and signal the building of site appropriate functional tissue (21-23). ECM molecules represent a diverse set of structural and functional proteins as well as a variety of growth factors. Native binding sites from these molecules and the formation of chemotactic cryptic peptides from parent molecules can positively influence remodeling, recruit stem and progenitor cells, and modulate the immune response. These steps can ultimately contribute to the success of an implantable, acellular scaffold (22, 24, 25).

As described, ECM-derived proteins provide unmatched cellular recognition, and therefore influence cellular response toward predicted remodeling behaviors.

However, materials built with only these proteins can degrade rapidly or begin too weak to substitute for compliant, matrix-dense tissues, such as vasculature. Therefore, to achieve the characteristics required of a vascular scaffold, we propose a biohybrid material approach. A biohybrid material is able to incorporate polymer components with ECM-derived proteins to produce a substrate with desired mechanical and degradation properties that can actively guide tissue remodeling.

This dissertation work aims to provide an alternative approach to cardiac tissue repair through the development and characterization of pericardium based biohybrid materials. As previously mentioned, pericardium has the appropriate protein composition for matching mechanical strength of a vessel wall, as well as the bioactivity to recruit and attach native cells. To supplement durability and add support during remodeling, we have combined pericardium with biodegradable polymers. The objectives of this work are to successfully couple pericardium with a synthetic polymer and show retained strength and bioactivity provided by the scaffold to endothelial cells and key immune system responders. Specifically, the aims of this work are as follows:

- 1) Develop an ECM-based hybrid material for vascular wall repair that provides strength during remodeling and promotes functional tissue regrowth.
 - a. Examine the hybrid material combining a poly(propylene fumarate) (PPF) and pericardium tissue for reduced calcification and controlled

degradation compared to chemically crosslinked surgical standards in a subdermal implant

- b. Characterize the inflammatory response from macrophages to the PPF + pericardium hybrid and determine how to modulate material to promote a healing response
 - c. Utilize the developed material as a platform to directionally release pro-angiogenic factors to the tissue substrate to direct or further promote vascular regrowth and reduced inflammation
- 2) Establish a 3D printed hybrid hydrogel that promotes wound healing response and endothelial cell growth in vascular tissue.
- a. Develop a composition of hydrogel that is biodegradable and biocompatible with the high geometric control of a 3D printed scaffold
 - b. Demonstrate that the inclusion of bioactive peptides from the pericardium promotes the functional regrowth of endothelial cells
 - c. Demonstrate the positive, pro-healing response of macrophages in response to the hybrid hydrogel

In this dissertation, we have successfully developed two distinct hybrid materials that increase the strength of natural ECM without diminishing the potential to promote regrowth at the injured site. Scaffolds that combine unaltered structural proteins from the native ECM with sustained support from the polymer component result in more moderate inflammation and degradation compared to untreated ECM tissue or synthetic alternatives. This dynamic creates a scaffold that can be slowly replaced

with living tissue, leaving a functional vessel in its place. The availability of a readily available grafting material that supports the re-growth of a pediatric patient's own tissue can eliminate multiple operations and morbidities associated with CHD and other vascular disease (26).

Chapter 2: ECM-Based Biohybrid Materials for Engineering Compliant, Matrix-Dense Tissues¹

This review will discuss biohybrid materials, or materials with both a synthetic and natural component, being developed to rebuild compliant, matrix-dense tissues. These materials have great potential for tissue engineering strategies since they combine the advantage of a natural substrate, to aid in site specific tissue regrowth, as well as a synthetic polymer component, to provide strength to withstand the force from environment while the material is remodeled. The applications for these materials include skin wound healing, vascular repair and grafts, tendon replacement, and intestinal wall reconstruction. We describe the materials fitting this description by dividing them into four groups based on fabrication techniques, and then report on biological and mechanical property progress in subsequent sections. We conclude with a summary of the current work evaluating immune response to the biohybrid material, and suggest the need for a more in depth investigation into the relationship.

2.1 Role of ECM in Engineering Tissue

No longer casted with a merely supportive role, the extracellular matrix (ECM) is now considered to play a major part in tissue morphology and function, defining the microenvironment through controlling migration, behavior, and phenotype of resident cells (27). The dynamic interaction between ECM and local cells is responsible for

¹ Adapted and reprinted with permission from: L.G. Bracaglia and J.P. Fisher. ECM-Based Biohybrid Materials for Engineering Compliant, Matrix-Dense Tissues. *Advanced Healthcare Materials*, 2015. (2192-2640).

mechanical, chemical and physical changes in the tissue (24, 28). As such, the ECM must be in constant state of deconstruction and specific rebuilding, based on cellular secretions, physical and chemical cues.

An ideal scaffold for tissue engineering would not only promote but take active part in this constructive remodeling and formation of site appropriate tissue. Material choice can be very influential in the overall success and incorporation of an implantable scaffold into the rebuilding process. Many implantable materials have been engineered to prioritize one of two main characteristics: biological relevancy or mechanical consistency to the tissue they are intended to replace.

Biologically relevant materials, such as naturally produced ECM structures, have been shown to help define the microenvironment and signal the building of site appropriate functional tissue. Matrix molecules represent a diverse set of structural and functional proteins, glycoproteins, and glycosaminoglycans that are arranged in an ultrastructure that is unique to each anatomic location. A variety of growth factors and binding sites have been described in nearly every tissue, specific to the environment and contained or transported through the ECM, as well. As described, the ECM provides a naturally occurring and highly conserved substrate for cell viability and growth through biological and chemical cues. Fragments of parent molecules, including collagen and fibronectin, have been shown to promote activities including angiogenesis, anti-angiogenesis, antimicrobial effects, and chemotactic effects. It is hypothesized that the specialized composition including structural and functional proteins and growth factors, together with the formation of chemotactic

cryptic peptides, can recruit stem and progenitor cells and contribute to modulating the immune response. Successful stem and progenitor cell recruitment together with a moderate immune response have significant influence when determining the success of an implantable scaffold (22, 24, 25, 29).

Due to this highly specified nature, ECM-based materials have great and perhaps unparalleled potential to control the biological activities of cellular recognition and colonization. In addition to, or in fact because of, the particular composition of material, mechanical and physical characteristics of ECM are unique and highly specific. In fact, many of the ECM-based implantables that are commercially available today are utilized only for mechanical properties, intentionally blocking any chemical or biological identifiers (9, 30).

The complexity of ECM makes identifying and understanding the minute components challenging, and because the constitution is only partially understood, it becomes a difficult material to replicate. ECM protein identification was pursued by Hansen et al, who used a novel combination of rapid ultrasonication and surfactant assisted digestion to aid in proteomic analysis of tissue derived ECM (31). Their results reveal hundreds of previously unidentified proteins in rat mammary glands that were substantially different from those in matrigel alternatives. Human mammary epithelial cells cultured in each of the two mediums demonstrate significantly different behavior, indicating that inaccuracies of mimicking cellular ECM constitution could significantly alter the nature of the resultant tissue (31). The physical presentation of

ECM derived tissue has been implicated in cellular behavior influences as well. In a study conducted by Xu et al. to mimic the ECM using a synthetic component, they found that minor changes in fiber diameters (1.28-1.50 μm), fiber density (22.2-46.1 # of fibers/100 μm^2), and fiber alignment (0.45-0.60 angular distribution), as well as resulting changes to the construct modulus, had significant effects on cardiac cell differentiation and growth (32). This study agrees with many, that the precise composition and physical appearance of cell substrate, natural ECM or synthetic scaffold, can drastically direct cell and therefore tissue function (33).

Considering the unique advantages of ECM-based materials, and the complexity to replicating the naturally composed tissue, a hypothetical ideal tissue engineering scaffold would utilize ECM already produced, on a site and person specific basis. Unfortunately, ECM if left untreated has several challenges to consider before including it in an implantable scaffold material.

ECM-based material is observed to degrade rapidly when implanted in a foreign body. It has been reported to have degraded significantly in 2-3 weeks *in vivo* in a subdermal implant,(34) 60% in 30 days and 100% at 90 days in an *in vivo* tendon repair model.(35) The incorporation into self-sustained material through constructive remodeling can be a long process, and the material needs to retain designed physical properties until that time. A synthetic material, on the other hand, is much less vulnerable to proteolytic enzymes and degradation tactics, and can be tuned to retain certain physical parameters.

As pointed out by Zhu et al, synthetic polymer constituents allow for manipulation of a scaffold on a molecular level by controlling polymerization, crosslinking and functionalization (36). These are important considerations when engineering soft tissue components, as the physical properties of the bulk tissue determine its ability to carry out its main function. There has been much development in polymer manufacturing techniques to produce materials that can mimic ECM in strength, elasticity, and structure of interconnected networks. However, synthetic polymers are usually utilized as passive scaffolds, and do not naturally create active cell interactions.

By combining blocks of natural tissue ECM with synthetic polymer components, the best of both materials can be included in one scaffold. This combination will be termed an ECM-based biohybrid material. A biohybrid material for the purpose of this review must contain significant blocks of both natural ECM-based material as well as synthetic fibers, for the purpose of influencing the biology of the microenvironment or providing strength and resistance to degradation. Small-scale natural components such as growth factors and small adherent proteins are excluded from the natural material category, since they do not play a major role in ECM material bulk or mechanical properties.

2.2 Methods

In order to prepare a comprehensive review of this topic, a search was conducted through Thompson Reuters Web of Science and PubMed to compile recent and relevant publications. Searches covered 10 years, and the following search terms were

used to conduct three independent searches of title, abstract, author key words, and key words plus®: “*extracellular matrix*” near *scaffold and poly**, *biohybrid and polymer and material*, and *biohybrid and scaffold*. Each search yielded 800, 108, and 85 publications, respectively. Searches were designed to include any material containing physiologically built components that was used in combination with a polymer as a scaffold. The term biohybrid can be applied in the literature to a material that has any part of a biologically created material, including components as small as functional molecular groups and growth factors. The search terms were kept intentionally broad, and publications that did not involve large ECM-based structural proteins were excluded by hand. From the remaining pool, publications were selected for review that matched the above definition of an ECM-based biohybrid material, and were used for a compliant, matrix-dense tissue application. Relevant citations from or of said papers were reviewed as well.

2.3 Types of Biohybrid Materials

Upon review, we see four classes that can describe ECM-based biohybrid materials, separated by fabrication and ultimate landscape of the material. Selection of fabrication technique is in part dictated by the choice of both polymer and natural constituent. The fabrication techniques covered in this review are illustrated in Figure 2.1.

- Materials composed primarily of intermingled fibers of both the polymer and natural component: The first technique covered in this report is the building of a composite by interweaving fibers. Typically, this is achieved by electrospinning or electrospraying one or both components although other

methods like co-extrusion can produce this effect as well. Even though electrodeposition is capable of producing independent fibers on a micro and nano level, the deposition can be random, and cannot account for organized bioactive factor incorporation or placement (37, 38).

- Materials fabricated using the layering technique: The next method covered results in a bilayered scaffold, with distinct layers or regions of polymer and natural constituents. Regions of each constituent must be large enough to locally retain physical properties of the independent constituent. Fabricating this way can incorporate whole, decellularized tissue, which allows for the inclusion of many (even many unidentified) proteins and minerals.
- Cell-built ECM layer fabrication method: The third method covered utilizes a cell layer to build a matrix on the surface of a polymer scaffold, leaving behind a biologically active interface when the cells are removed. This cell laid matrix is the primary biological contribution to the scaffold. This is also an effective means to ensure complete inclusion of proteins. For some tissue applications, this method is perhaps the closest to reality, if site appropriate cells can be cultured. Although, the resources and time to culture could prevent this method from being a scalable procedure.
- Materials fabricated by blending hydrogel components: The approach is to blend together homogenized tissue or ECM components with a soluble polymer phase, in order to create one cohesive hydrogel. The blending in this method mostly occurs on a molecular level. This method allows for a high

level of user control, but eliminates natural structure and organization of the tissue components.

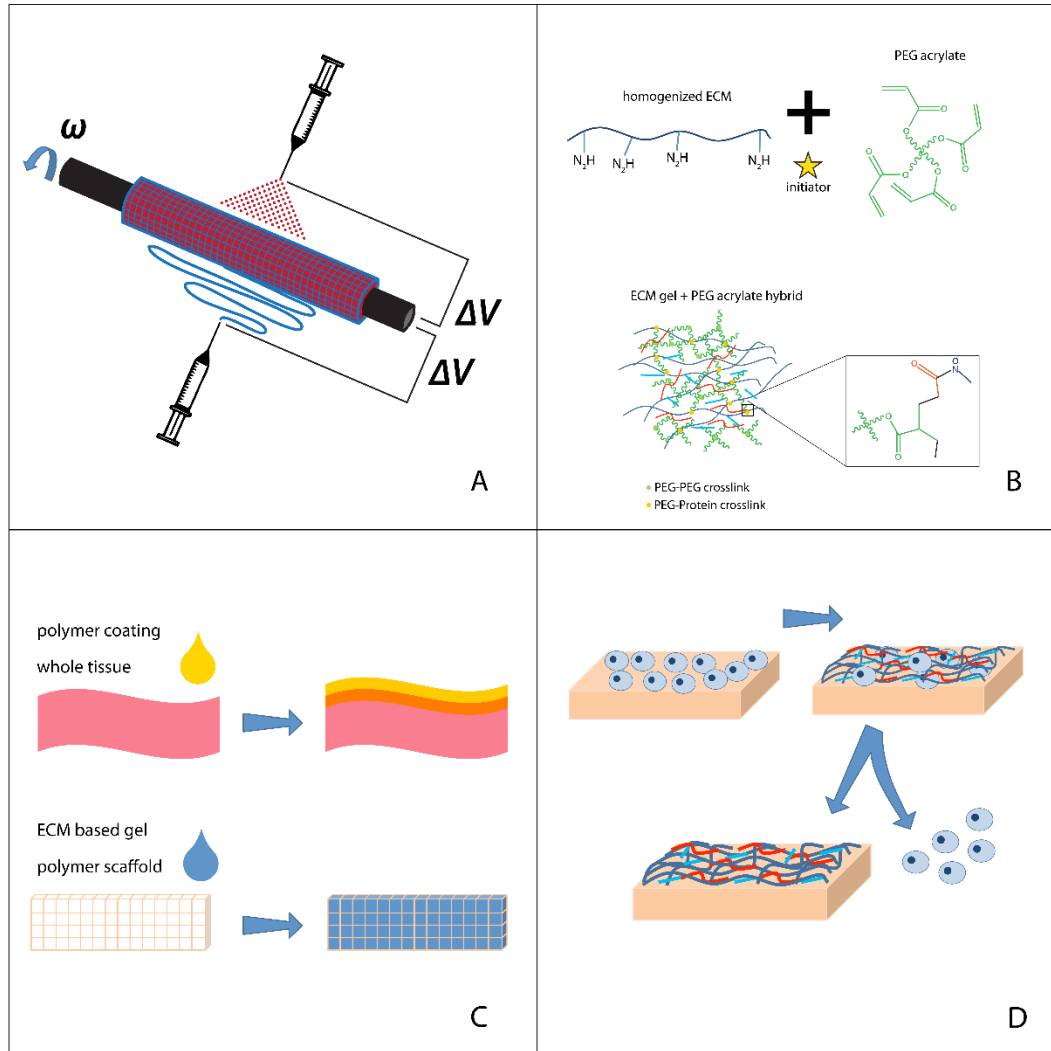


Figure 2. 1 Methods of Fabricating ECM-Based Biohybrid Materials. (A) Materials are fabricated with interwoven fibers, using either electrospinning, electrospraying, or a combination of the two. (B) Materials are fabricated by blending hydrogel components of ECM derived proteins and polymer chains. (C) Materials are built using a layering technique, with either a whole tissue or a polymer scaffold as a base. (D) Cell-built ECM layer fabrication, where cells are cultured on a polymer scaffold, and then removed, leaving an ECM layer on the polymer surface.

Based on the variety of material components, and in cases of significant contribution from biological material, it can be difficult to define biohybrid material scaffolds within traditional categories for standardized surgical implants. With regard to mechanical assessment, appropriate testing and measurement protocols to represent the most important characteristics of the material could be unavailable. ASTM International describes this problem for new biomaterials of tissue engineering scaffolds for growth, support, or delivery of cells and/or biomolecules in standard F2027. The standard explains that although there are no specific protocols set for novel materials, important properties that should be specified include elastic modulus, ultimate tensile strength and compressive modulus, among other physical properties such as viscosity, density and contact angles when appropriate. In standard F2150, Standard Guide for Characterization and Testing of Biomaterial Scaffolds Used in Tissue-Engineered Medical Products, a list is compiled of standards to consult for methodology that would be perhaps appropriate based on material characteristics. These recommendations are included in Table 2.1. Most of the protocols are designed for plastics, which neglects the natural tissue component.

Table 2.1 Selection of Relevant ASTM Standards for Testing Biomaterials

	Standard	Title	Test Notes
Tensile Testing	D412	Standard Test Methods for Vulcanized Rubber and Thermoplastic Elastomers—Tension	<ul style="list-style-type: none"> • Suggests a uniform rate of grip separation of 500 ± 50 mm/min • Material can be in either a dumbbell shape, straight line, or ring shape
	D638	Standard Test Method for Tensile Properties of Plastics	<ul style="list-style-type: none"> • Determination of the tensile properties of unreinforced and reinforced plastics • Material can be in standard dumbbell-shaped test specimens • Preferred testing method for materials between 1 and 14 mm thick
	D882	Standard Test Method for Tensile Properties of Thin Plastic Sheeting	<ul style="list-style-type: none"> • Determination of the tensile properties of thin sheeting and films (less than 1.0 mm (0.04 in.) in thickness) • Specimens should be of uniform width (between 5.0 and 25.4 mm) and be at least 50 mm longer than the grip separation used. • Specimens must have width-thickness ratio of at least eight shall be used
	D1623	Standard Test Method for Tensile and Tensile Adhesion Properties of Rigid Cellular Plastics	<ul style="list-style-type: none"> • Specimens should be rectangular, round or square and shall have a minimum cross-sectional area of 645 mm^2 • When testing materials that are suspected to be anisotropic, prepare duplicate sets of specimens having their long axes parallel and perpendicular to the direction of the cell orientation
	D1708	Tensile Properties of Plastics microtensile specimens	<ul style="list-style-type: none"> • Specimens can be rectangular, round or square and should have a minimum cross-sectional area of 645 mm^2
	D3039	Standard Test Method for Tensile Properties of Polymer Matrix Composite Materials	<ul style="list-style-type: none"> • Determination of the in-plane tensile properties of polymer matrix composite materials reinforced by high-modulus fibers. • Specimens shape is suggested, but

			remains up to the user to determine ideal gripping surface
Compressive Testing	D695	Standard Test Method for Compressive Properties of Rigid Plastics	<ul style="list-style-type: none"> • Specimens should be either a right cylinder or prism whose length is twice its principal width or diameter • Preferred specimen sizes are 12.7 by 12.7 by 25.4 mm (prism), or 12.7 mm in diameter by 25.4 mm (cylinder)
	D1621	Standard Test Method for Compressive Properties of Rigid Cellular Plastics	<ul style="list-style-type: none"> • Specimens should be either square or circular in cross section with a minimum of 25.8 cm² and a maximum of 232 cm² in area. • Minimum height should be 25.4 mm (1 in.) and the maximum height shall be no greater than the width or diameter of the specimen.
	F2977	Standard Test Method for Small Punch Testing of Polymeric Biomaterials Used in Surgical Implant	<ul style="list-style-type: none"> • Specimens should be miniature disks of 0.5 mm in thickness and 6.4 mm in diameter • Test method has been established for characterizing surgical materials after ram extrusion or compression molding • Test parameters provide metrics of the yielding, ultimate strength, ductility, and toughness under multiaxial loading conditions

Following a standard protocol to test these new biohybrid materials would help identify the effect of various constituents and fabrication techniques to create material physically suited for several compliant tissue applications. To summarize the current mechanical data on biohybrid materials, mechanical properties, if reported, are often under testing conditions unique to the specific application of the study. For example, the elastic modulus of a polypropylene and collagen mesh from a tracheal implant was evaluated using compressive testing after 6 months implanted (39). It is possible, however, that this combination of materials would be well suited for another tissue as

well if evaluated using tension or in a different sample shape. In a discussion on the mechanical properties of a polypropylene mesh with dermal ECM for hernia repair, one group suggests that a standard should include an analysis of planar biaxial mechanics, instead of merely stretching a sample until failure (40). Protocols that may have been originally designed for plastics and metals expose tissue to super-physiological conditions, which may not record the most relevant behavior. To design materials for compliant tissue engineering, a portrayal of stress and strain in a multi-axis relationship could be the closest to realistic physiological challenges.

2.3.1 Materials Fabricated with Interwoven Fibers

Building a scaffold by weaving or spinning together various compositions of fibers and polymer chains is a popular technique for creating hybrid scaffolds.

Electrospinning and electrospraying provide a controlled way to deposit fibers in a designed shape. By controlling the speed and charge of material as it is deposited, the resulting woven material can resemble the structure of natural ECM, by producing single strand diameters between 50 and 500 nm (37). Additionally, scaffolds manufactured on an individual fiber basis can have an open and interconnected porous architecture, which can help cells easily penetrate to the inner part of the scaffold. The single fiber identity can also provide cell attachment points at each fiber junction, similar to collagen fibrous strands *in vivo* structures (41). This ease of infiltration, migration and adherence results in homogenous cell distribution and tissue formation in these types of grafts (42).

By incorporating both synthetic and natural components into interpenetrating networks, each region of the scaffold has identical cell attachment and signaling opportunities, and at the same time provides equal stiffness or strength at each point of the scaffold. There are typically few to no concentrations of either component, which could create a polar or nonbioactive side of the scaffold. As a result, scaffolds built in this manner often see uniform degradation and infiltration, as well as uniform remodeling (43).

2.3.1.1 Material Selection

The primary determinant in selecting materials for this fabrication technique is the potential for electric deposition. Common materials include poly(ϵ -caprolactone) (PCL), poly(lactic acid) (PLA), or poly(lactic-co-glycolic acid) (PLGA), which have been extensively developed to electrically deposit, and are biocompatible, strong, and biodegradable. Using an electro-spun fiber as a base building block, the biological components can be incorporated with either casting, electrospraying, or in some cases electrospinning along with the synthetic component. Casting methods have been used to incorporate water-soluble collagen nanofibers (44) and ECM-based polysaccharides and proteins (45) into PCL electrospun meshes. Since casting methods can avoid harsh solvents and conditions, they can be adapted to transport cellular constituents to the scaffold. In a study by Koch et al., we see the development of vascular grafts by casting fibrin gel with resident cells in a mold around a poly(D,L-lactide) mesh cylinder (43).

To prioritize an organized, fiber-based deposition, ECM components can be incorporated into the polymer phase before it is electrospun. In a study by Hong et al, porcine small intestine mucosa (SIS) powder was blended with PCL before it was co-electrospun with silk fibroin. This method of incorporation improved hydrophilicity of the polymer, and effectively incorporated the biological component (46). Other successful applications that rely solely on electrospinning include a blend of poly(vinyl alcohol), (PVA), with type I collagen into a single fiber constituent (47), and a blend solution of PLGA, gelatin and elastin that was electrospun into vascular grafts (48).

In contrast, using electrospraying techniques in combination with electrospinning can maintain the single fiber integrity of the polymer phase, but can apply the control of deposition more broadly to the collection of water based biological components. In one study, a complete tissue ECM is homogenized and then sprayed onto a poly(ester urethane) urea (PEUU) mesh scaffold resulting in interconnected fibrous layers embedded in a ECM gel (49). Similarly, by developing a dual head, co-electrospinning device, a human-like collagen/chitosan blend was able to be co-spun into a vascular graft with PLA (36), demonstrating the feasibility of using two different solutions to construct a scaffold for blood vessel tissue engineering. Finally, by combining the above mentioned methods, a hyaluronic acid (HA) hydrogel (HeprasilTM) was added via a dual electrodeposition system to PCL-collagen blend (PCL/Col), mesh. Collagen was blended with PCL prior to deposition, resulting in an apparent surface coating of the deposited fibers, with obvious collagen domains and

segregations. Simultaneous deposition of HA and PCL/Col allowed HA gel to be electrospayed onto the mesh of electrospun PCL/Col, creating a mesh with hydrogel pockets interspersed within a matrix of polymer microfibers (50). This double-team of electrospaying and electrospinning is conceivably capable of producing the closest replica of the ECM in vasculature and barrier tissues compared to an independent technique, since it combines fibers with softer gel pockets for a heterogeneous but consistent material.

2.3.1.2 Mechanical and Physical Properties

The geometric properties of scaffolds formed using this fabrication method are highly similar to the fibrous network of ECM. The thinly sprayed woven fibers can resemble specific components of ECM through intentional size-control by altering composition and deposition parameters. As shown by Hong et al., among others, increasing the concentration of the SIS powder in the PCL/silk fibroin solution resulted in a diameter reduction of the fibers due to increased electrical conductivity (46). The increased electrical conductivity appeared to improve the size uniformity as well, compared to that of pure PCL fibers (46). Results from incorporating human-like collagen/chitosan blend to PCL agree; Zhu et al found the electrospun collagen/chitosan/PCL had a more biomimetic structure than pure PLA, as the fiber diameters approached the size of the extracellular matrix (36).

The deliberate deposition of fibers in the manufacturing process makes this method well suited to form highly defined cylindrical, or other self-supporting shapes. Since most methods contain a polymer phase that solidifies after deposition, fibers can usually support themselves. Woven fibers that possess strength individually, when

combined and held together at junction points in a mesh, form materials with noted high flexibility and strength. In one case, blended fibers of PVA and collagen type I are gathered into a bundle and three bundles were twisted into a braid with the diameter of ~4.5 mm, building a flexible rope (47). It is as a result of this strength in a variety of formations that we see many free standing scaffolds where structural integrity is crucial. This high structural integrity is an indicator of success in applications such as vascular grafts, intestinal lining, skin and even tendon or ligament grafts (36, 43, 47, 48).

The mechanical strength is usually determined by the contents polymer phase, not the components contained in the hydrogel or biological fibers. As such, maximum mechanical strength of the composite can be attributed to the choice of polymer component and configuration. In some cases, the nature of the polymer phase can be altered by incorporation of biological or other components (46). A table comparing mechanical strength of scaffolds fabricated using the woven fibers methods, as well as other methods, is shown in Table 2. While it is by no means to draw specific comparisons between the scaffolds, as they are all tested in their own specific shapes and thicknesses under different parameters, it can provide a vision of the broad range of parameters achieved by various materials and fabrication methods.

Table 2.2 Mechanical Properties of Select ECM-Based Biomaterials

		Variety	Tensile Strength	Young's Modulus
Fibers Woven	Composite of poly(ester urethane) urea (PEUU) and ECM gel (electrospun/sprayed in cylindrical conduits) (47)	67 PEUU/33 ECM	80 kPa longitudinal axis, 41 kPa circumferential	
		80 PEUU/20 ECM	187 kPa longitudinal axis, 91 kPa circumferential	
	Collagen type 1 (Col-1) and polyvinyl alcohol (PVA) scaffold (braided fibers 4.5mm diameter) (51)	Col-1/PVA scaffold	33.63 ± 3.10 MPa	0.26 ± 0.05 GPa
		Regenerated ligament	29.71 ± 0.96 MPa	0.25 ± 0.02 GPa
		Native ACL	37.43 ± 2.13 MPa	0.01 ± 0 GPa
	Small intestine submuscosa (SIS) powder blended with poly(ϵ -caprolactone) (PCL), co-electrospun with silk fibroin (SF) (46)	PCL	13 MPa	11 MPa
		PCL/SF	13.5 MPa	12.5 MPa
		PCL/SF/SIS	14 MPa	14 MPa
	Poly(lactic-co-glycolic acid) (PLGA), gelatin, and elastin electrospun fiber mats, (PGE) (52)	1 PLGA : 2 gelatin : 1 elastin	16 ± 7 kPa	134 ± 51 kPa
		2 PLGA : 2 gelatin : 1 elastin	102 ± 26 kPa	427 ± 41 kPa
		3 PLGA : 2 gelatin : 1 elastin	130 ± 7 kPa	770 ± 131 kPa
	Electrospun PCL/collagen nanofiber meshes (tested parallel to fibers) (53)	Random fiber orientation	4.01 ± 0.29 MPa	4.33 ± 0.57 MPa
Aligned fiber orientation		4.88 ± 0.18 MPa	4.43 ± 0.37 MPa	
Layer Method	Poly-L-lactide (PLLA) mesh and collagen (28)	PLLA mesh	33.8 ± 0.7 MPa warp ^a , 32.3 ± 0.1 MPa weft ^a	212 ± 11 MPa warp, 177 ± 28 MPa weft
		PLLA-collagen	5.0 ± 0.4 MPa warp, 4.9 ± 0.8 MPa weft	55 ± 12 MPa warp, 43 ± 4 MPa weft
		PLLA-gelatin	5.8 ± 0.4 MPa	43 ± 5 MPa

			warp, 4.7 ± 1.7 MPa weft	warp, 41 ± 3 MPa weft
		Collagen sponge	0.01 ± 0.00 MPa	0.11 ± 0.05 MPa
	Poly(propylene fumarate) (PPF) and bovine pericardium (54)	PPF reinforced pericardium	14.17 ± 4.59 MPa	54.00 ± 12.67 MPa
		GA-crosslinked pericardium	11.51 ± 3.42 MPa	67.87 ± 18.48 MPa
		Untreated pericardium	12.34 ± 1.49 MPa	58.79 ± 10.17 MPa
	Poly(L-lactic acid)-co-poly-(ε-caprolactone (PLACL) nanofibers and GA-bovine pericardium (55)	PLACL and GA-pericardium	2.39 ± 0.17 MPa	
		PLACL-Gel and GA-pericardium	1.22 ± 0.17 MPa	
		GA-pericardium	7.04 ± 0.51 MPa	
ECM Polymer Hydrogel			Compressive Modulus	
	Carbon nanotube (CNT)-gelatin methacrylate (GelMA) hydrogels (56)	GelMA, no CNT	10 kPa	
		CNT-GelMA	32 kPa	
	Myocardial Matrix poly(ethylene glycol) (PEG) hydrogels (57)	ECM gel	5 Pa	
		ECM- PEG NHS	5-30 Pa	
		ECM- PEG diacrylate	5-30 Pa	
		ECM-StarPEG acrylate	719 Pa	
	Gelatin methacrylamide (GelMA) polymerized within a PEG framework (57)	GelMA(5%) PEG (5%)	10.8 kPa	
		GelMA (20%) PEG (20%)	327.7 kPa	
		Gelatin (5%) physically mixed with PEG (5%)	8.2 kPa	
		Gelatin (20%) physically mixed with PEG (20%)	66.3 kPa	

2.3.1.3 Biological Properties

While the woven polymer addition to biological components can improve strength of the scaffold, the incorporation of biological elements has a positive impact on the biocompatibility of the material. Electrospun pure polymer scaffolds alone have been plagued by low cell infiltration, cell adhesion, proliferation, and differentiation, due to minimal porosity, hydrophobicity acidic degrading sections, among other problems. By increasing the presence of a biological component, these problems can be mitigated (50, 53, 58, 59). Improved cell adhesion, infiltration and migration are seen as a result of incorporating both natural and synthetic components in many of these studies.

By incorporating a significant biological component, cell viability and metabolism are seen to improve over the pure polymer control in several studies (36, 60). As an example, a biohybrid composite of a ratio of 72 PEUU: 28 ECM gel and a control mesh of PEUU were implanted into Lewis rats, replacing a full-thickness abdominal wall defect. After 4 weeks of implantation, histological staining showed extensive cellular infiltration into the biohybrid scaffold. The newly developed tissue was well integrated with the native periphery, while minimal cellular ingress into the electrospun PEUU scaffold was observed (49). Similarly, by increasing the SIS concentration in the PCL/SF/SIS polymer blend, a high level of initial cell attachment was achieved. The result of incorporating the ECM-based material SIS was compared to plain PCL/SF fibers, which showed a low level of initial cell attachment compared to that of even the pure PCL fibers (46).

Histological evidence from scaffolds extracted from *in vivo* experiments in trachea , arteries (49), abdominal wall (49), and ligaments (47), all show increased number of recruited cells over the polymer scaffold alone. The speed and numbers of migrating cells can help determine the success of the implant, especially in cases of trachea, vessels, and abdominal wall, where a complete lining is essential to success. PCL grafts electrospun and then cast with collagen nanofiber gel showed significantly higher cell number stained for nuclei and f actin than PCL alone in a tracheal wall implant. In contrast to the control PCL group, the PCL- collagen fiber group showed complete regeneration of the tracheal wall, with the mucosal epithelium of the trachea completely covered (44).

In addition to cell infiltration and cell attachment, many studies cite an improvement in ECM production when ECM-based materials are included. Improved cell attachment and ECM production usually results in beneficial remodeling of the construct. Specifically, a study by Hong et al. discovered in their *in vivo* assessment of an abdominal wall that biohybrid material started to remodel so significantly that its mechanical properties mimicked those of the native abdominal wall. Histological methods revealed dense homogenous cell layers, extensive collagen formation, no calcification, absence of thrombus, and no evidence of aneurysm. These results were compared to polytetrafluoroethylene grafts (that have no ECM-based material component), which were occluded with thrombus formation (49). The ability of the biohybrid graft to create rapid endothelium is an important success indicator in other applications as well, particularly in vascular grafts (43). Vascular grafts electrospun

from a blend solution of PLGA, gelatin, and elastin (PGE), were seen to support human aortic endothelial cells (HAECs) in forming a confluent, nonthrombogenic, and physiologically competent monolayer, as assessed by tissue factor gene expression and protein activity assays. The levels of mRNA/protein activity in HAECs grown on PGE scaffolds were similar to those on gelatin or collagen IV-coated 2-D surfaces. However, analysis of a microarray containing 84 ECM-related cDNA probes demonstrated that HAECs on PGE scaffolds expressed an ECM-related “transcriptome”, where cells were less activated on 2-D gelatin. This study highlights the important role of substrate composition, and suggests that that substrate composition plays a greater role than surface topography in affecting the endothelial ECM-related “transcriptome” (48). Comparatively, in a study on the hybrid mesh PCL/collagen and HA hydrogel loaded with two potent angiogenic growth factors (VEGF165 and PDGF-BB) the growth factor-loaded hybrid meshes were shown to not only support cellular attachment, but also their infiltration and the recapitulation of primitive capillary network in the scaffold’s architecture (50).

It is apparent that PCL is a popular choice for electrospun polymers, used in biohybrid material scaffolds for muscular (53), nervous (59), dermal (58), and vascular tissue repair (50). Certainly through this frequent review, protocols to electrospin the polymer have been optimized, and use of the polymer in biomedical implantables has been well accepted. It is possible however, that the popularity and progress is reinforcing the repeated selection of PCL, as it may appear as a well-established go-to scaffold material. In fact, as a linear hydrophobic polymer, it’s

degradation rate through hydrolysis is fairly slow, cited at longer than 24 months (61). This timeline is not ideal for most soft tissue engineering applications.

Degradation, as well as wettability can be improved through the mixing with ECM-based proteins (gelatin and collagen) (53, 58), but the rate is still slower than other hydrophilic, electrospinnable polymers, such as PVA and polyurethane (61). It may be beneficial to continue to develop electrospinning techniques with these polymers, or investigate the use of others with alternate physical properties.

2.3.2 Materials Fabricated Using the Layering Technique

In this fabrication technique, two components are considered as distinct entities that are combined in a layered fashion to create one composite material. Because the components are not integrated on fiber by fiber basis, the outcomes are evaluated as two separate materials. In some cases, the materials are defined by a hierarchy of influence, one material as the main focus, and the other material as a support of the primary constituent. As such, the primary material often has an outstanding intrinsic quality that makes it well suited for the application, such as elasticity or strength, but requires additional support in the form of biocompatibility or resistance to degradation. Material fabricated in this way is being developed for skin (62), cardiac and vascular tissue (10, 63), and abdominal muscle injury (49).

2.3.1.1 Material Selection

As the biological component, in some cases, it is beneficial to use an already intact tissue. Some tissues, like pericardium, dermis, and intestinal submucosa have very unique mechanical properties that are unmimicable by manmade techniques. In these

applications, the synthetic component is layered on top of or around the tissue to add strength to the composite and to prevent against degradation.

Pericardium, one unique material, is well suited for use in a layering application. It is clinically used in a chemically fixed form, usually with glutaraldehyde, in heart valves, vascular and intestinal patches (11). However, it is a tissue primarily composed of extracellular matrix proteins, with few resident cells, and unmatched mechanical properties which make it an ideal candidate for an ECM-based biohybrid material. In chapter 3, we describe in depth the coupling of a thin layer of poly(propylene fumarate) (PPF) and bovine pericardium. We show that the polymer layer can provide initial physical protection from proteolytic enzymes and degradation, but leaves the original collagen and elastin matrix unaltered (63).

Porcine pericardium has also been investigated by other groups, using a polyurethane oligomer coating layer, which is found to crosslink with the top surface of pericardial tissue. This protective layer is predicted to also prevent against degradation, similar to chemical fixation agent, but with less alteration of the underlying tissue (64). Other coatings have been investigated with bovine pericardium, including titanium (10), polyurethane prepolymer (55), and chitosan or silk fibroin film (65). In one study, 3D nanofibers of poly(L-lactic acid)-co-poly-(ε-caprolactone) (PLACL) were coated on the surface of bovine pericardium. This method introduced valuable porosity and cell attachment points, as covered earlier. However, the tissue was also treated with glutaraldehyde to crosslink the constituents, which would severely mask biological components and alter cell interaction with the tissue⁽⁶⁶⁾. In a final example, equine

pericardium that is surface-crosslinked with woven polymer (commercially, orthADAPT PR Bioimplant) has FDA clearance for rotator cuff repair ⁽⁶⁷⁾, and is reported to have performed better than its pure pericardium predecessor in *in vivo* studies. This tissue source can provide rich amounts of organized ECM around 0.5mm thick as a substrate for infiltrating and recruited cells to an injury site ⁽⁶³⁾. The thickness provides a substantial reservoir for hosting cells, but can take time to remodel, and requires support through remodeling. Methods that crosslink the tissue reduce the space for cell recognition and habitation, as well as alter the time to remodel, since crosslinked tissues do not break down. To fully utilize the benefits of the tissue, techniques should be pursued to use pericardium in a way that keeps it as close to unaltered as possible.

In other applications, the polymer is the base component, and a weaker natural component gel is layered on top or through the pre-formed polymer scaffold. PLGA scaffolds filled with a layer of fibrin gel (45), or modified with a layer coating of artificial extracellular matrices (aECM) consisting of collagen type I, chondroitin sulphate, and sulphated hyaluronan ⁽⁶⁸⁾, and laminin, fibronectin, vitronectin, collagen type IV and poly(lysine) are examples of this type of combination ⁽⁶⁹⁾. Other polymer components reported use porous elastomeric scaffolds filled with self-assembling peptide gel ^(70, 71).

Utilizing more of a traditional layer technique, some scaffolds are first formed in a mesh, and then a hydrogel component is gelled on top. In one study, a

poly(caprolactone-co-lactide)/Poloxamer nanofiber membrane was made using electrospinning, and then a hydrogel of gelatin (20%) and dextran (10%) was layered on the bottom of the fiber mesh to create a bilayer scaffold ⁽⁶²⁾. In other studies, hybrid scaffolds were constructed by forming funnel-like collagen or gelatin sponges on one side of a poly-L-lactide (PLLA) woven mesh (28), or layered around a PCL electrospun mesh (33). Neutralized dermal ECM digest has also been used in this method, forming a layer to coat a polypropylene mesh ⁽⁷²⁾. This method is particularly adaptable to 3D printing techniques, since the two layers can be formed separately with reconciling potentially complex printing parameters. For example, materials that are not conducive self-supporting structures can be extrusion printed directly on the surface of polymer meshes that would be created using stereolithography, extrusion under harsher conditions, or a method separate from 3D printing altogether (73).

2.3.2.2 Mechanical and Physical Properties

Investigations of mechanical properties are often conducted in comparison to the individual components of the layered material. Hydrogels such as collagen, gelatin and HA are considered weak independently, but show improved mechanical strength with the addition of the polymer layer. This relationship highlights the benefit of the fabrication method. For example, when collagen or gelatin is gelled within a PLLA scaffold with interconnected pore structures, mechanical strength is increased by the presence of PLLA, but interconnected regions of the hydrogel remain unaltered if examined in isolation (28). Using a similar fabrication technique, PLGA–collagen hybrid scaffold formed from collagen microsponges in the openings of a PLGA knitted mesh were evaluated in a tracheal wall reconstruction. The elastic modulus of

engineered tissues was tested after 6 months of implantation. Incorporating collagen, gelatin, and basic fibroblast growth factor resulted in a significantly higher modulus than the pure polymer ($7.52 \pm 1.60 \times 10^{-2}$ and $3.00 \pm 1.60 \times 10^{-2}$), although was still significantly less than that of the native trachea ($10.79 \pm 1.49 \times 10^{-2}$) (39).

With similar conclusions, some have investigated PCL porous scaffolds fabricated using a salt leaching technique, and injected with HA hydrogel. As expected, the storage modulus of the composite is greater than the hydrogel, and reduced when compared to the PCL porous scaffold alone. However, the composite does not show major changes in Young's modulus over the 6 week testing period from plain PCL scaffolds (74). The results from this study suggest that the hybrid scaffolds provide the potential for high stiffness properties in tension and compression, (presumably from the PCL component), while exhibiting the viscoelastic response found in hydrogels (HA) and native cartilage tissue. For softer tissue applications however, regional mechanical characteristics from a horizontal layered technique appear to accurately approximate target tissue. If skin, for example, was approximated as a bilayer consisting of the epidermis (modulus, 140 to 600 kPa; thickness, 0.05 to 1.5 mm) and the dermis (modulus, 2 to 80 kPa; thickness, 0.3 to 3 mm), then a bilayer scaffold of PLCL/Ploxamer nanofibers with dextran/gelatin hydrogel was found to be a suitable substitute when both constituents were mechanically tested as independent layers⁽⁶²⁾.

2.3.2.3 Biological Properties

Parallel to the mechanical analysis of these constructs, cellular response is often investigated in comparison with the individual components of the layered material. It is important to show that since this method could involve incorporating a polymer with a biological scaffold there is no statistically significant difference between the bilayer composite and a control group of pure biological component. As seen in a comparison between PLCL/Poloxamer nanofibers with dextran/gelatin hydrogel and plain dextran/gelatin hydrogel, there was no significant difference when the polymer was incorporated, indicating that the bilayer scaffold has no detriment on cell viability⁽⁶²⁾. Fortunately, several studies show improved cell viability, cell adhesion and proliferation, compared to polymer alternatives or control collagen sponges^(28, 74). The porous nature of some composites, supported by an overall porous, or funnel like structure of the polymer base (28), is suggested to aid in the improved adhesion and proliferation⁽⁶⁶⁾.

Perhaps more convincing of a scaffold's benefit than unaffected viability is the potential to promote cell behavior towards reconstruction. In an *in vivo* comparison after 180 days post implantation in a rat abdominal muscle injury, the ECM-coated polypropylene mesh showed decreased density of collagen and amount of mature type I collagen deposited between mesh fibers when compared to the uncoated mesh devices. This study confirmed and extends previous findings that an ECM coating supports healing and reconstruction of the injury site, and mitigates associated scar tissue deposition characteristic of polypropylene expected when used for ventral hernia repair (72). In another example, the combination of PLLA and collagen for

skin wound healing, resulted in better regeneration of dermal tissue and epidermis than either of the materials independently when evaluated in a nude mouse subdermal study (28). Other studies support this finding, citing the production of increased amount and specificity of matrix proteins by recruited cells on biohybrid materials when compared to the plain polymer alternative ^(45, 66, 68).

2.3.3 Cell-Built ECM Layer Fabrication Method

This method describes utilizing a cell population to lay down a tissue specific matrix on a polymer scaffold. When the cells are removed, the polymer scaffold is left with a bioactive ECM layer, prepared to host recruited cells. As described, this method could be an effective means to ensure complete inclusion of proteins based on cellular production, assuming the physiological niche can be appropriately simulated.

This method appears to be more frequently used in bone and cartilage engineering applications ⁽⁷⁵⁾, which are beyond the scope of this report. However, there has been promising results in soft tissue engineering applications as well. In a study by Shtrichman et al, an electrospun PCL/PLGA mesh served as mechanical support for cell seeding and ECM generation. By decellularizing the composite after a fixed time, the result is self termed an available "off-the-shelf" implantable product. This composite demonstrated biodegradability and biocompatibility in a rat subcutaneous model, and supported advanced cellular infiltration and habitation compared to uncoated PCL/PLGA scaffolds ⁽⁷⁶⁾. Along similar lines, another study utilized a Vicryl knitted mesh made of polyglactin 910 (a 90:10 copolymer of glycolic acid and lactic acid (PLGA)), and cultured either mesenchymal stem cells, normal human articular chondrocytes, or normal human dermal fibroblasts onto both sides of the

PLGA mesh. When these discs were decellularized, they also showed promising results for supporting cell viability and ingrowth (28). In an *in vivo* study, a similar approach utilizing hMSCs to build a cell derived matrix within a collagen/HA scaffold showed excellent results in mimicking the bone marrow niche. ECM-Col/HA scaffolds formed less bone than Col/HA with or without hMSCs, suggesting the appropriate environment for bone marrow cells ⁽⁷⁷⁾.

For some tissue applications, this method is perhaps the closest to reality if site-appropriate cells can be cultured. However, the resources and time required to culture these cells could prevent this method from being a scalable procedure, and so far, success appears mostly in 2-dimensional constructs. Relying on cells to build an amount of ECM that would produce a significant, 3-dimensional layer could be challenging. It may be more feasible to obtain 3-dimensional scaffolds by designing the polymer base to support a 3D culture structure with pores or mesh. If a decellularizing technique could be developed that effectively removed cell fragments and other possible inflammatory debris, this method has the potential to add very specific ECM to geometrically relevant soft tissue implants.

2.3.4 Materials Fabricated By Blending Hydrogel Components

In this approach, presentation of site-specific proteins and extracellular matrix components are the main focus for the material. The objective of most design plans is to improve mechanical properties of biologically based matrices, and ensure retained cytocompatibility. In order to alter mechanical properties, yet leave the natural portion bioactive and retain cellular recognition, inert polymers are doped into the

material as structural components. Inert polymers are often chosen over the addition of other proteins to avoid disruption of the tissue specific composition of the ECM.

2.3.4.1 Material Selection

To create a cohesive and consistent material, a synthetic polymer network can physically and covalently incorporate a protein phase. In this way, ECM proteins are secured in 3D space without modification while the biological inert polymer serves to maintain consistent mechanical integrity and transport properties. As a bioinert and biodegradable material, the source of polymer component is most commonly poly(ethylene glycol) (PEG), or PEG with some modifications. PEG gels are often selected due to high water solubility, nontoxicity, low protein adhesion, and non immunogenic properties⁽⁷⁸⁾. If modified through common techniques, PEG molecules can be functionalized using NHS and acrylate groups, for example, making them suited to chemically crosslink with side amine groups in ECM proteins.

The source of the biological component in this fabrication technique is often either non-purified ECM homogenate, or artificially constructed ECM-like gel made from individual purified components. Non-purified ECM homogenate may more accurately emulate the microscale heterogeneity of natural ECM⁽⁵⁷⁾. As we have described, using regionally specific tissue has great effects on the incorporation of the tissue, and the inclusion of possibly unknown structural and chemical components could aid in tissue regeneration. It follows that the choice of tissue for this ECM homogenate should reflect the ultimate cite for the material. Popular choices include myocardial matrix (heart tissue homogenized), alternative ECM tissue derived from the umbilical

cord (Wharton's jelly), homogenized intestinal lining, and homogenized dermal tissue (60, 79, 80).

On the other hand, creating an ECM-based hydrogel from scratch by using building blocks with known concentration and composition can create a consistent material. These building blocks include collagen, elastin, glycosaminoglycan, as well as gelatin and chitosan. Gelatin, the partially hydrolyzed form of collagen, is not naturally present active ECM. However, in many respects including chemical structure, degradation mechanisms, and byproducts, can closely resemble its parent molecule collagen. Modified gelatin (gelatin methacrylate) hydrogels are a popular choice for the biological component in these scaffolds, combined with silk (81), PEG (82), PEG diacrylate (PEGDA) (32), chondroitin sulfate (83), and cellulose (84).

Blending of the materials requires optimization techniques based on unique properties of the hydrogels. In addition to the chemical crosslinking referred to above that utilizes functionalized PEG or gelatin, physical entrapment or freeze-thaw cycles to form cryogels are also possible techniques shown to produce evenly dispersed materials (84). By incorporating fibrillar type I collagen and reticular laminin, Jung et al were able to physically entrap these two ECM proteins within chemoselectively crosslinked PEG. The interpenetrating networks of these molecules were confirmed, and it was determined that the PEG component is capable of slowing degradation of the bulk material without chemically altering the proteins (60). In another example, silk fibroin protein and chitosan hydrogels are formed using physical entrapment through

ultrasonication to avoid harsh solvents or chemical crosslinking. The ultrasonication of silk and chitosan induce a conformational change of the silk from random coil to beta sheet. This results in the self-assembly of the hydrophobic peptide segments in the protein, entrapping chitosan chains in the silk networks ⁽⁵⁶⁾. Freeze thaw cycles were employed by several groups to form cryogels of glycosaminoglycan-PEG ⁽⁸⁵⁾, and ECM/PVA hydrogel. In this technique, scaffolds were created in a mold, with a thin ECM layer on top of the polymer solution. Freeze-thaw cycles are then introduced to physically cross-link the hydrogel and to embed the lyophilized matrix upon it ⁽⁷⁹⁾.

A unique inclusion by Shin et al. highlights the possibility of one additional material characteristic, electroconductivity, otherwise unmentioned in the research compiled here. In this study, carbon nanotubes (CNT) were incorporated into gelatin methacrylate (GelMA) hydrogels. The composite material resulted in cardiac tissue constructs that showed excellent mechanical integrity, as well as advanced electrophysiological functions. Specifically, myocardial tissues cultured on 50 μm thick CNT-GelMA showed 3 times higher spontaneous synchronous beating rates and 85% lower excitation threshold, compared to cells cultured on plain GelMA hydrogel. This parameter, it is discussed, is important when engineering tissues with particularly important conductive ability, such as heart muscle and nervous tissue ⁽⁸⁶⁾.

2.3.4.2 Mechanical Properties

The driving reason to alter an ECM-based hydrogel is to incorporate additional strength, shape integrity, or resistance to rapid degradation. Softness of hydrogels

made from matrix materials have been reported around 5-10 Pa at 1Hz (specifically from a gel formed from myocardial matrix)⁽⁸⁰⁾. The significant decrease from native heart muscle, in this particular example, can negatively affect cell adhesion, cell migration and signal transport. Mechanical comparisons, conducted by Christman et al., found that the addition of PEG to the hydrogel with either NHS, star PEG acrylate, or PEG diacrylate, significantly increased the storage modulus of the gel (5-30 Pa in PEG NHS or PEG diacrylate, 719 Pa in the star PEG acrylate system) over the ECM gel alone (5 Pa). The incorporation of PEG variations allowed for tunable degradation, with the ECM gel degrading two to three times faster than all of the hybrid variations. Cell studies indicate that adhesion and migration through myocardial matrix-PEG-NHS and acrylate hydrogels was possible, and that cells could be efficiently encapsulated, a process impossible in the weaker pure ECM gel⁽⁸⁰⁾.

These results are echoed in studies investigating other combinations of materials. An interpenetrating network of gelatin methacrylimide polymerized within a tetrafunctional PEG framework resulted in unique properties. Crosslinking ECM proteins within a synthetic matrix created a stable scaffold with tunable properties and with long term cell anchorage points supporting cell attachment and proliferation in the 3D environment⁽⁵⁷⁾. Cryogels of glycosaminoglycan-PEG were determined to have varied stiffness between the struts of the scaffold and the less stiff corresponding bulk hydrogel, suggesting this method can be utilized in design goals⁽⁸⁵⁾. This control over mechanical properties is useful; however applications for hydrogel based

material in compliant tissues may be limited. If the polymer component could be incorporated to a point that made it possible to attain tensile and elastic properties from the material, the composite could be used more broadly.

2.3.4.3 Biological Properties

In several studies, cell viability and function was seen to increase over the plain polymer controls. Cardiac cells improved cellular adhesion, organization, and cell-cell coupling on CNT-GelMA compared to GelMA alone ⁽⁸⁶⁾. Chondrocytes exhibited improved colonization and adhesion on ECM-PVA scaffolds compared with plain PVA as well as plain articular cartilage derived matrix, suggesting it is the combination of two materials that is most beneficial ⁽⁷⁹⁾.

Jung et al noted that hMSC viability was enhanced by the addition of exogenous ECM to PEG frameworks. In addition to viability, a glimpse of cell behavioral changes was observed in direct response to scaffold composition. For example, In the presence of exogenous laminin, hMSCs produced reticulate structures, as opposed to fibrillar masses in the presence of collagen I. In addition, miPSCs were able to form beating areas in composites containing no ECM, but to a lesser extent in composites containing either collagen I or laminin. Thus, the PEG-NCL approach provides an opportunity to independently examine the biochemical impact of ECM on stem cell differentiation in 3D environments ⁽⁶⁰⁾.

2.4 Other Considerations: Inflammatory Response

As ECM-based biohybrid materials continue to be designed, an in depth analysis of immune response to the materials could provide illuminating information on the mechanisms that contribute to successful reconstruction. Moving beyond basic cell viability and material biodegradability, advanced studies can start to investigate and learn the complex role of the immune response to these scaffolds, and how that plays a role in long term functionality and constructive remodeling.

Considering the complexity of the interaction between the immune response and other physiological systems, initial studies that have begun to look at this are providing a small taste of available knowledge. The majority of biohybrid materials investigated in this report are tested in animal models at their furthest point of investigation. Some earlier reports use histological techniques to identify “immune” cells from these sort of experiments. Although this gives some measure of immune activation, it does not give any insights into the complicated and dynamic interactions. Additionally, evaluating the materials in immunosuppressed animals artificially removes elements that could significantly change the course of remodeling of the tissue (28).

A large presence of foreign material can cause a foreign body response resulting from overlapping acute and chronic inflammation, and subsequent fibrotic and collagen encapsulation ⁽⁸⁷⁾, which has historically been the assessment for “success” or “failure” of an implant. However, before that severe endpoint, there exists several mechanisms that can determine the fate of an implanted material. Although the initial

events are not confirmed, one theory suggests that the foreign material will activate inflammasomes, which recruit macrophages as well as other leukocytes to the region to secrete additional signal and activate successive pathways (87, 88). Soon after arrival at the injured site, macrophages are expected to polarize, into a classic (M1) or an alternate (M2) phenotype (89). The classic phenotype is associated with inflammatory related events, including tissue destruction and activation of Th1 T cells. The alternate phenotype, on the other hand, stimulates healing events, including tissue remodeling and inflammatory cytokine suppression (89-91). Although it seems clear that activation towards an M2 phenotype in macrophages together with Th2 T cell activation would be desired, the interaction between the two activation pathways and local signaling events needs to be further investigated. An outline by Faulk suggests three mechanisms to include when studying this interaction. First to consider are the signals and environment created by the bioactive peptide fragments generated through scaffold degradation. Second, the recruitment of endogenous stem and progenitor stem cells to the site for ECM remodeling. And third, the modulation of the host macrophage response away from a proinflammatory phenotype, and towards an M2-TH2, pro-healing phenotype (72).

Without intervention, ECM-based materials are most often degraded *in vivo*, and are associated with constructive tissue remodeling and minimal fibrosis (87, 89). As of yet, the specific cell signaling events by which ECM biomaterials modulate the host macrophage population toward a more constructive remodeling phenotype are not fully understood (76). In several examples, the presence of ECM components was

shown to influence the initial response of the immune system to prohealing, despite the polymer components that would be expected to individually illicit an inflammatory response (28, 44, 49, 92). The abdominal wall injury model comparing ECM-coated and uncoated polypropylene mesh devices showed that ECM coating decreased the inflammatory response as characterized by the number and distribution of M1 macrophages (CD86+/CD68+) around mesh fibers when compared to the uncoated mesh devices at 14 days post implantation (72). Furthermore, the local response was characterized as having less scar tissue, resulting from the ECM mitigated immune response. Interestingly, other studies reference reduced fibrotic capsule (28), an indicator of reduced inflammation, and production of functional ECM (43, 49). Although these results do not provide insights into the intermediate steps, the end results do compel future studies on the material. Expanding the understanding of how the immune system interacts with the implants can provide tools to assure or even manipulate healing of the implant.

As an example, other studies investigating materials in subdermal implants have had success comparing the local cytokines belonging to either a Th1 (interleukin (IL) 2, interferon- γ) or Th2 (IL-4, IL-10, IL-13) profile. In a study comparing porcine dermal collagenous membranes to PTFE in Sprague Dawley rats, a higher ratio of Th1 cytokines was found surrounding the porcine dermal tissue, where an increase in Th2 cytokines was measured surrounding PTFE implants. This result agrees with the inverse relationship of the Th1/Th2 cell mediated and humoral immune response (90). Although this study did not involve biohybrid materials, a similar protocol would

provide new information regarding the intermediate steps in response to these materials.

Crosslinking, or other altering steps to the natural tissue component, threatens to negatively impact this positive remodeling. Crosslinking or otherwise altering the tissue affects the functional design, manifested in changes to rigidity, porosity, insolubility and topography of the matrix. These characteristics determine the mechanical profile of each individual tissue (93, 94). Scaffold materials with chemical crosslinking agents may delay or prevent macrophage mediated degradation, but they also inhibit the formation of the M2-type response. The altered characteristics caused by crosslinking fibers result in decreased hydrophilicity and recognition of the scaffold, which can result in slowed cellular adhesion and proliferation in or near the scaffold. In fact, some crosslinked tissue shows resistance to cellular infiltration, and is characterized by a dense cell lining around the surface (63). The lack of healing and remodeling can result in downstream scar tissue formation and a persistent foreign body response (72).

In a less drastic way, the choice to use gelatin instead of collagen could also affect the matrix presentation to cells. Gelatin, being chemically similar, but structurally different from collagen, does partially contribute towards unfamiliar environments in the form of physical recognition. In some cases, the comparison between gelatin and collagen in the same biohybrid scaffold shows significant differences in cellular response. In the development of funnel-like collagen or gelatin sponges on one side of

a PLLA woven mesh, the PLLA–collagen scaffolds supported cells that more strongly promoted rebuilding ECM than did the PLLA–gelatin scaffolds (28).

2.5. Conclusion

A significant struggle in the development of tissue engineered constructs is remodeling and permanent maintenance by the body. This review considered the use of ECM-based biohybrid materials as tools to promote constructive remodeling through natural physiological functions. Keeping the scaffold as close as possible to the natural environment has been shown to significantly improve cellular infiltration, inhabitation, and constructive remodeling. Using natural tissue components is a direct way to incorporate natural signaling domains, recognition, attachment points to a scaffold. Incorporating polymer components can help recapitulate the bulk environment, which is also an important indicator of lasting success. Expanding the understanding of how the immune response interacts with the implants will help us determine how to use those systems to encourage success and integration of the scaffold. The quick recognition by native cells has been shown to be important in modulating immune response and contributing to lasting mechanical properties of the constructs.

2.6 Acknowledgments

This work was supported by American Heart Association Grant # 14PRE20380374 (Laura Bracaglia), as well as the National Institutes of Health under the Award Number R01 AR061460.

Chapter 3: PPF Reinforced Pericardium as a Hybrid Material for Cardiovascular Applications²

3.1 Introduction

For more than 50 years, a method to replace malfunctioning or diseased tissue in the cardiovascular system has been an important area of development. Each year, over 275,000 replacement valves and 600,000 vascular grafts are implanted to correct damaged native structures (17, 95). Complex pediatric and general cardiac surgeries also utilize tissue or synthetic patch material in reconstruction and repair. When considering materials for prosthetic applications, biological tissues offer some clear advantages over synthetic substitutes. Aside from the inherent biocompatibility, biological tissues possess “intelligent” elastic and mechanical properties that are unable to be mimicked by manmade material (96, 97).

One biological tissue commonly used is pericardium. Pericardial tissue has historically been selected for cardiovascular devices due to its availability, inherent strength, and elastic properties. In addition to the desirable mechanical behavior described, natural tissue often demonstrates superior fluid dynamic properties, and when compared to synthetic materials, requires less anticoagulation therapy (97).

² Adapted from: L.G. Bracaglia, L. Yu, N. Hibino, and J.P. Fisher. Reinforced pericardium as a hybrid material for cardiovascular applications. *Tissue Eng Part A*, 2014. 20(21-22): p. 2807-16. Reprinted with permission from *TISSUE ENGINEERING Part A*, Volume 20, Issue 21/22, 2014, published by Mary Ann Liebert, Inc., New Rochelle, NY

In order to capitalize on and maintain the natural properties of pericardium, previous research has focused on improving the durability and biocompatibility of the material upon implantation. However, and despite significant advances, clinical experience continues to highlight the challenges of the prolonged use of pericardium implants in the cardiovascular system(17).

All natural tissue, including pericardium, can elicit an inflammatory and immune response from the host. To combat these inevitable events, pericardial tissue is commonly preserved in glutaraldehyde (GA), which chemically crosslinks the tissue's collagen molecules. This crosslinking process is effective at stabilizing the tissue against chemical and enzymatic degradation, as well as lessening the display of antigenic determinants (8, 12, 98). However, the crosslinked product has been associated with local cytotoxicity and, more importantly, severe calcification of the material that can over time lead to subsequent matrix deterioration and compromised mechanical properties (10, 99, 100).

The detailed pathways controlling calcification of cardiovascular tissue, both natural and prosthetic, are not explicitly understood, but as the most common pathology recorded in heart valve failures (16, 101), it is certainly a process under high investigation. It is observed that chemically crosslinking pericardium damages and distorts the natural structure, destroys interstitial cells, and diminishes potential for viable cell inhabitation (102). The specialized matrix consisting of collagen, elastin and glycosaminoglycans (GAGs) that composes pericardium is responsible for

allowing the tissue to accommodate the constant changes in shape and stress transfer (102, 103), and is therefore essential to maintain. Damaging this natural structure and removing native cells results in a tissue that can no longer maintain or repair itself. It has been suggested in literature that calcification and eventual ossification is the result of insufficient or irregular repair of the tissue network. In culture, myofibroblasts have been shown to undergo phenotypic differentiation into the osteoblast like cells seen in calcified cardiac tissue, promoting calcification and bone type remodeling (16). Others suggest that the origin of bone cells in ossified valves is unknown, but their presence is confirmed in observation of excised heart valves and tissue (104).

Original damage leading to the irregular repair of the implanted tissue can be a result of mechanical stress, immune cell infiltration, or other pathologies, which complicates the investigation of the process. In one theory, responding immune cells are reported to secrete collagenase, among other proteolytic enzymes, which immediately begin to degrade the collagen network (99). It is further hypothesized by some that this initial proteolysis of crosslinked collagen debris creates foci for calcium deposition to initialize (30, 95, 100). Studies have shown a cooperative relationship between calcification of this type of tissue and the inflammatory response, enzymatic degradation, and microstructural failure (both independent failures and those associated with calcium deposits.)

Regardless of the mechanism directly controlling the calcium deposits, GA treatment has been shown through both *in vivo* and *in vitro* accelerated testing to destroy the surface endothelium of the tissue, autolytically disrupt interstitial cells, alter natural collagen bundles, and destroy native GAGS (15). Despite the discrepancies in origin of the deterioration, a strong correlation between GA treated tissue and increased calcification suggests that the chemical fixation of the tissue further inhibits the appropriate remodeling.

The theory of calcification above suggests that if an alternative to GA can be developed that is effective at blocking enzymes and other immune activators, but avoids crosslinking of the tissue, then subsequent calcification of the material will be reduced. Our principal hypothesis is that applying a paintable polymer to the surface of pericardium tissue will provide the physical support and biological block to natural degradation, while leaving the original tissue unaltered. This will result in a hybrid material that will retain mechanical integrity but will not accumulate calcium deposits. For this purpose, the synthetic polymer poly(propylene fumarate) (PPF), was selected for its demonstrated biocompatibility, biodegradability, and strength in other biomedical applications (105, 106).

Poly(propylene fumarate), (PPF), is an unsaturated linear polyester that is crosslinkable through UV radiation with itself or with other compatible crosslinkers through the double bonds in fumarate. PPF is biodegradable by hydrolysis of ester bonds, and forms the naturally occurring byproducts fumaric acid and propylene

glycol upon degradation (107). The degradation time is largely dependent on polymer characteristics such as molecular weight, crosslinker, and crosslinked density (107). The uncrosslinked polymer is viscous at room temperature, allowing it to be easily “painted” onto a surface. In addition, PPF viscosity can be reduced, without significantly altering the components of the system, with the addition of diethyl fumarate (DEF), the monomer from which PPF is synthesized. The addition of DEF to PPF can also cause variations in the crosslinked biomaterial’s mechanical strength, and can be utilized as a parameter to tune the characteristics of the hybrid biomaterial (108).

To address our overall hypothesis, the first aim was to identify measurable mechanical properties of natural pericardium and develop a composition of PPF to mirror those properties. The designed composition of the polymer was then married to the pericardium tissue, and the hybrid material was evaluated on two fronts. The first evaluation of the hybrid material was to test if PPF reinforcement was an effective support for natural pericardium enzymatic degradation. The second evaluation of the hybrid material was to investigate if PPF reinforced pericardium would cause minimal calcification when compared to the GA treated standard. Performance in these two areas will support the hypothesis that a topically applied polymer can biologically and mechanically support pericardium for use in cardiovascular applications.

3.2 Methods

3.2.1 Polymer Synthesis and Composition

PPF was synthesized by a two-step process as previously described (109). Briefly, propylene glycol and diethyl fumarate were combined in a 3:1 molar ratio. Zinc chloride, acting as a catalyst, and hydroquinone, as a radical inhibitor, were added in a 0.01:0.002 molar ratio. The reaction was carried out under nitrogen flow, producing ethanol as a byproduct and bis(hydroxypropyl) as the intermediate. Next, under vacuum, transesterification of the intermediate produces PPF with propylene glycol as a byproduct. Gel permeation chromatography was used to calculate the number average molecular weight (M_n) and polydispersity index (PDI) of the purified PPF. For use in this study, PPF (M_n 1150 and PDI 1.6) was mixed with the monomer DEF, and then mixed with the photoinitiator bis(2,4,6-trimethylbenzoyl) phenylphosphine oxide (BAPO), to create a UV sensitive reaction.

To select the ratio of polymer to monomer that would be a suitable match for pericardium material, a set of weight to weight ratios of PPF to DEF was tested in thin-film formation, as shown in Figure 3.1A. Soluble fraction of the crosslinked composite was measured comparing the dry mass of the film to the dry mass after soluble components were dissolved in acetone for 12 hours, using the following equation:

$$\text{Soluble Fraction \%} = \frac{m_{\text{initial}} - m_{\text{final}}}{m_{\text{initial}}} \times 100$$

3.2.2 Mechanical Testing of Polymer Compositions

PPF composite films as previously described were tested on an Instron for mechanical analysis using ASTM D638 to obtain 0.1% yield strength and elastic modulus. Thin-films were formed between two 2x2 cm square glass plates, and resulted in 0.25 mm thick, 0.15 g films (Figure 3.1B). This geometry is similar to the weight per surface area approximated for coating pericardium, as well as a suitable shape for testing according to ASTM D882. Extension rate was set at 10mm/min, and extension and corresponding load was recorded at a frequency of 10 Hz. A preload of 5 N was considered. Elastic modulus for each sample was calculated using MATLAB to determine the slope of the linear region of the stress-strain curve reported by the Instron. The linear region of the curve was systematically calculated using linear line fit command based on the first 10 data points. The program then continued to add data points in steps of 10 until the $R^2 < 0.97$. The slope of this region was determined to be the modulus of the sample. Strength at 0.1% yield was calculated as the intersection of the stress-strain curve with a line drawn parallel to the linear slope, whose x-axis intercept is shifted 0.01 mm/mm strain.

3.2.3 Sample Preparation

Throughout this study, PPF reinforced pericardium was compared to GA treated pericardium and untreated pericardium as controls. All pericardium was obtained 2 days after harvest from Innovative Research, Inc. and stored at 4 °C in physiological saline. Experiments were conducted within 2 days of receiving the pericardium, and because the properties of pericardium are thought to vary among individual donors, all samples for each test were taken from the same donor.

Glutaraldehyde treated samples were prepared by immersing small strips of pericardium (2 x 6 cm) in a 0.625% GA solution for 6 hours at room temperature. Samples were then washed twice and stored in saline at 4 °C. PPF reinforced samples were also cut into 2 x 6 cm strips, and were lightly stretched onto wooden frames to maintain spatial conformation. The tissue was then dehydrated in ethanol dilutions, in order to facilitate the interaction and integration of hydrophobic PPF with pericardium and remove antigenic determinants. Dehydrated pericardium was then coated with a thin and uniform layer of PPF to completely cover the tissue strip. The coated tissue strip was then exposed to UVa light for 90 minutes (3.5 mW/cm^2) to crosslink the polymer. After crosslinking, tissue and polymer composite were rehydrated in physiological buffer at room temperature for 2 hours, and then stored in 4 °C. Pericardium samples from each group were mechanically tested using the method described previously as controls.

3.2.4 *In vitro* Evaluation- Degradation Test

An *in vitro* degradation model was designed to investigate the added strength and resiliency of the PPF reinforcement as compared to untreated pericardium and GA treated pericardium as controls. Pericardium samples were exposed to 0.4 U/mL of collagenase, and shaken at 60 RPM in 37 °C. The test was run over a period of 12 days, with mechanical analysis testing performed every 4 days (n=8 per day), as described previously. Samples were preserved at various time points for histological analysis.

3.2.5 *In vitro* Evaluation- Calcification Test

To compare *in vitro* calcification between PPF reinforced and GA treated pericardium, samples from these groups were exposed to physiological calcium buffer (2.6 mM calcium/1.6 mM phosphate) at 37 °C, for a total period of 45 days. At each time point (5, 12, 21 days), 15 samples from each treatment group were isolated for analysis. For each treatment group, eight of the isolated samples were reserved for mechanical analysis, which was performed as previously described. Two of the samples were preserved for histological study. The final 5 samples were used to quantify calcium deposition. These samples were first triple washed in deionized water to remove loosely attached calcium, and then oven dried at 80 °C for 6 hours to measure dry mass. Samples were then hydrolyzed in 2M HCl for 48 hours to dissolve calcium deposits on the tissue. Solutions were then measured for calcium concentration using a colorimetric assay. Calcium concentration at each time point was statistically compared using a student's T test.

3.2.6 *In vivo* Evaluation

Calcification rate and material integrity of the hybrid material were evaluated in a subdermal rat model. The Institutional Animal Care and Use Committee of the University of Maryland approved the study, and all animals were treated in accordance with the "Guide for the Care and Use of Laboratory Animals". The experiment was conducted in n=16 male Sprague Dawley (SD) rats, as determined by a power analysis. As seen in literature for material analysis (110), a small incision is made in the dorsal dermal layer, and a material patch (1 x 1 cm) from each of the three groups is sutured by the corners to the underlying tissue (Figure 3.3A). At time

points of 3 weeks and 6 weeks, n=8 animals were euthanized and the pericardium patches and surrounding tissue were explanted. Each explanted tissue sample was carefully sliced in half. One half of each sample was preserved in paraformaldehyde (4%) and embedded in paraffin for histological analysis to determine calcium deposition, cellular population and resulting tissue morphology, and inflammatory response.

Inflammatory response in particular was investigated using immunohistochemistry to stain for the presence of the macrophage cell surface antigen F4/80. Slides were incubated with PEROXIDAZED1 (Biocare, Concord, CA), an endogenous peroxidase blocker, and BackgroundSNIPER1 (Biocare), a broad spectrum blocking reagent. The samples were then incubated with anti-F4/80 (rabbit polyclonal to F4/80, abcam ab74384) as the primary antibody, followed by a biotinylated anti-rabbit IgG as the secondary antibody (Vector laboratories). Using a horseradish peroxidase-streptavidin system, followed by a 3,3'-diaminobenzidine tetrahydrochloride chromagen, the presence of the F4/80 molecule was detected. All samples were then counterstained with hematoxylin. Macrophage population was determined through examining 3 standardized images from each of n=5 samples per treatment group. Macrophage fraction was defined as the number of cells determined to have F4/80 staining divided by the total cells counted per image in a blinded study. Data is presented as an average of each of these fractions, and error was calculated as the standard deviation between all images in each group.

The other half of each sample was dried in a 60 °C oven 18 hours, and then hydrolyzed in 2M HCl for 48 hours. A colorimetric assay was used to determine calcium concentration of each sample.

3.2.7 Statistical Analysis

All quantitative assessments were statistically compared using a one-way ANOVA test, ($p < 0.05$), followed by a post hoc Tukey's test, unless otherwise noted.

3.3 Results

We have developed a biohybrid material that consists of a polymer reinforcement later painted on the natural biomaterial pericardium. The mechanical characteristics of the polymer directly affect those of the hybrid material, and were therefore the determining factor in selecting a polymer composite. Following mechanical analysis of the thin-films composed of different formations of PPF: DEF ratios, the 2:1 dilution was selected for future work. The yield strength of this composition (5.48 ± 2.27 MPa) was found to be the greatest, and therefore the closest to the tested values for untreated and GA fixed pericardium (11.32 ± 4.24 and 13.01 ± 4.35 MPa, respectively). A comparison of yield strength and modulus of the thin-films is shown in Figure 3.1C. The modulus of elasticity and yield stress of pericardium is known to vary between donors based on age and other physiological features, but the values exhibited by the 2:1 films in elasticity measurements are sufficiently high to support the pericardium within the range tested.

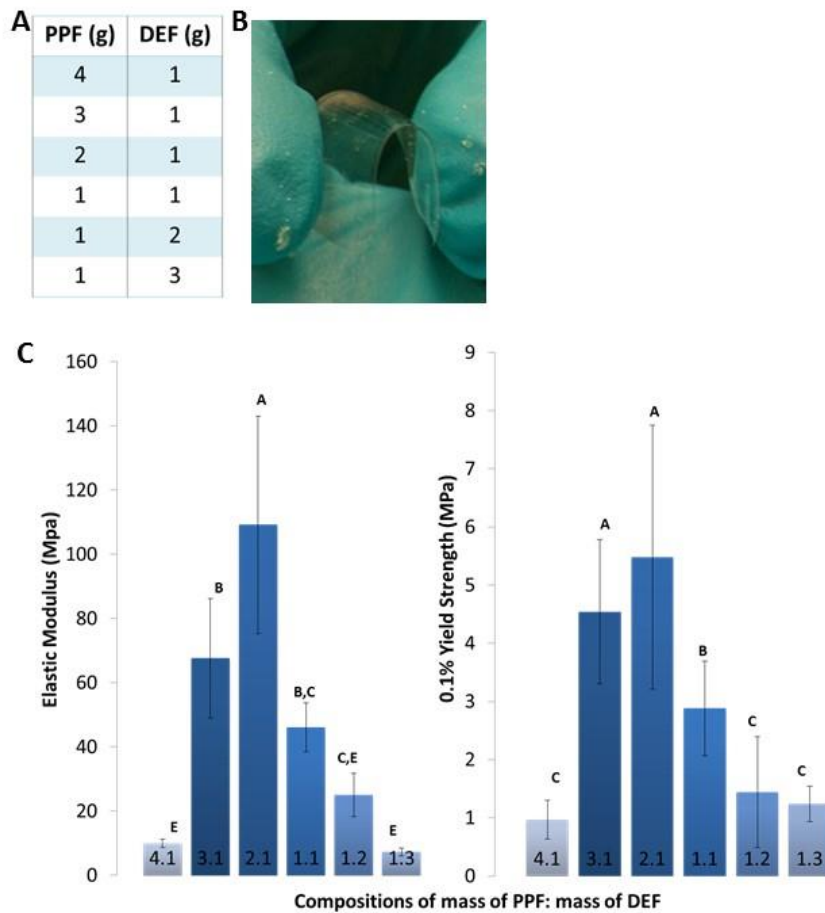


Figure 3. 1 PPF Thin Film Analysis. The compositions of Various Thin Films Tested, listed as mass to mass ratios of PPF to DEF (A), were crosslinked into thin films from the same total volume (B). Resulting thin films were 0.25 mm thick and weighed 0.15 grams. The image in B shows a thin film composed of 2g PPF to 1g DEF (2:1). Elastic modulus and 1% yield strength of thin films (C) were tested on an INSTRON mechanical tester, and extended at 10mm/min by a 50 N load cell. $n \geq 7$ for all groups, ANOVA statistical test shows significant difference, ($p < 0.05$), and Tukey's Post Hoc results are shown on graph. Groups that do not share a letter are significantly different.

Figure 3.2A displays mechanical analysis data from untreated pericardium from three separate donors, as a reference. The soluble fraction of thin sheets of 2:1 PPF to DEF was calculated as $13.3 \% \pm 2.7\%$, (n=9).

As mentioned, the 2 PPF: 1 DEF composition was selected for further evaluation in the hybrid material model. After physiological degradation *in vitro*, mechanical yield strength and elastic modulus of PPF reinforced pericardium are not significantly different than the gold standard GA treated pericardium, ($\alpha=0.05$), (Figure 3.2C). By day 8, the strength and elasticity of both of these materials still remains above 11.5 ± 3.42 MPa 0.1% yield strength and 54.00 ± 12.67 MPa elastic modulus. These values are comparable to the untreated control on day 0, measured at 12.34 ± 1.49 and 58.80 ± 10.17 MPa, respectively. However, by day 8, the untreated sample has fallen as low as 2.91 ± 0.80 MPa and 20.29 ± 7.76 MPa. These results of reduced or maintained material strength are supported by observations from histological photographs of the pericardium samples, which contrast a highly disordered fresh pericardium fiber network with a more ordered and dense PPF reinforced pericardium sample (Figure 3.2B).

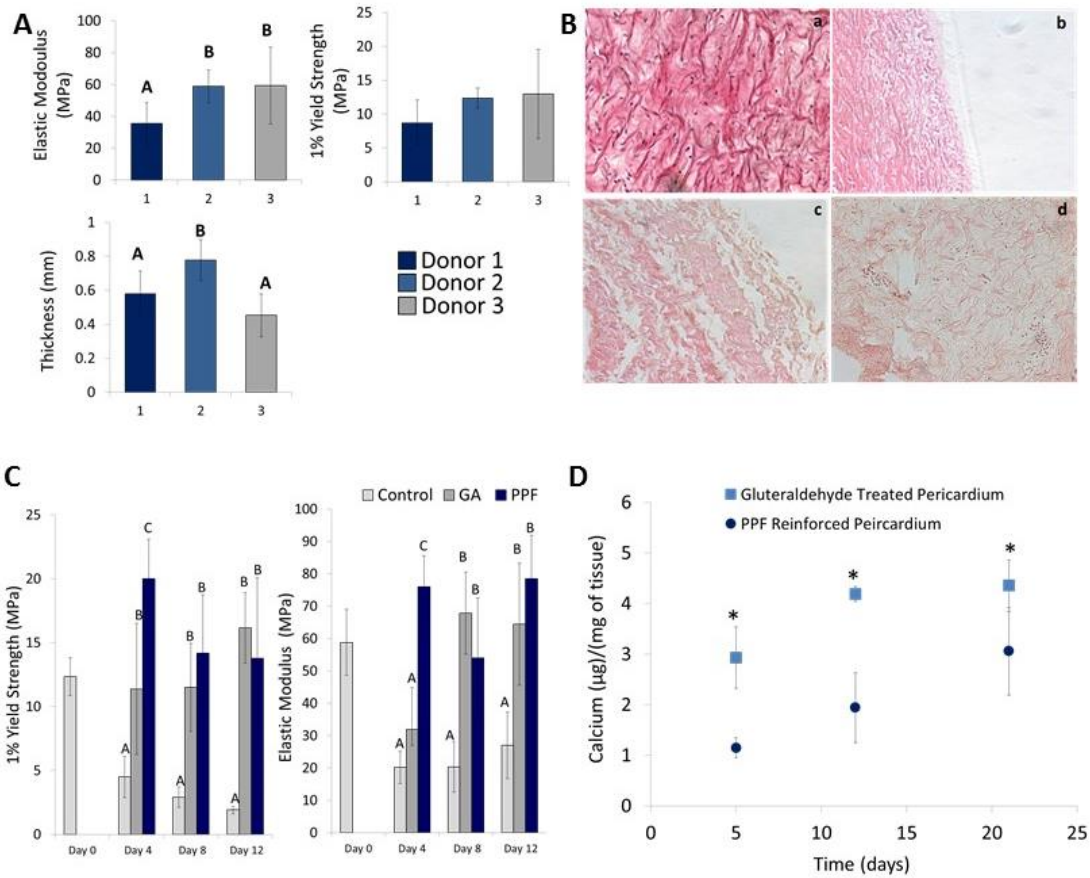


Figure 3. 2 *In vitro* Analysis of PPF Reinforced Pericardium. The graph displays the physical properties of pericardium from 3 different donors (n=8 per donor) (A). Yield strength and modulus were evaluated from samples over an *in vitro* degradation simulation using collagenase (n=8 per time point) (C). ANOVA statistical tests showed significant difference in the elastic modulus and in the thicknesses ($p < 0.05$), and results from a post hoc Tukey's Test are shown on the graphs. Groups that do not share a letter are significantly different. The control on Day 0 has no PPF reinforcement or collagenase exposure. Control groups on the following days are exposed to collagenase but not reinforced with PPF or treated GA. After degradation, samples were fixed and stained using hemotoxylin and eosin to display structure of collagen network (B). Control pericardium appears to have lost structural integrity after collagenase degradation (d), as did the EtOH dehydrated sample (c), while the sample with PPF reinforcement (b) appears unaltered from the natural pericardium (a). *In vitro* calcification was also simulated using a calcium phosphate buffer, and calcium deposition was

quantified (n=5 per time point). A students T test shows significant difference between the calcium content for all time points, denoted “*”, (p<0.05).

In addition to mechanical property retention, calcium deposition was also evaluated *in vitro*. The time dependent graph in Figure 3.2D displays calcium deposition onto GA treated and PPF reinforced tissue from an *in vitro* calcification model. The level of calcification of GA treated tissue is significantly higher than the level of calcification of PPF reinforced tissue at each time point (except day 0), ($p < 0.05$). Mechanical data did not show any distinct differences between groups.

Calcification was next further evaluated in the *in vivo* model. Calcification of PPF reinforced pericardium was significantly less than GA treated samples in the quantitative assessment ($p < 0.05$) at each time point. The graph in Figure 3.3B shows calcium deposition per mass of dried tissue weight compared between the three experimental groups. These results were confirmed by the Von Kossa histological stain (Figure 3.3C), in which calcium phosphate depositions are observed in GA treated samples on week 3 and 6, but little to no staining is observed on PPF reinforced samples or on untreated samples. The staining in these last two groups appears unchanged from the un-implanted controls (day 0), a result that is confirmed by the maximum variance of $\pm 1 \mu\text{g}$ of calcium /mg of tissue from the day 0 level over the 6 week period.

In histological samples stained with Masson's trichrome (Figure 3.4A), we observe that PPF reinforced tissue remain intact up to 6 weeks, with regions of cellular infiltration. GA treated tissue appears to have limited cell movement into the implanted tissue, but instead has a line of cells near the surface of the implant.

Furthermore, GA treated pericardium is observed to exist in a dense network. We further observed untreated tissue was difficult to identify as a distinct material within the surrounding tissue.

Using immunohistological staining techniques, it was confirmed that cells expressing the F4/80 surface molecule, a known marker of macrophages, are present at or near the implanted tissue in all treatment groups (Figure 3.4B). Regions of tissue with dense cell packing also present high amounts of F4/80 stain. In particular, it was observed that the dense cell line seen near the edge of the GA treated tissue has a high presence of F4/80 stain. This is also observed in the other tissue samples, but in small pockets and dispersed throughout the implanted region and neighboring soft tissue. Macrophage fraction of the total cell population in each sample is displayed in Figure 3.4C. This fraction is greatest in GA treated samples, $36.3 \pm 18.7\%$ of the population, and is followed by the untreated samples at $29.0 \pm 12.4\%$, and finally by the PPF reinforced samples at $18.2 \pm 8.0\%$.

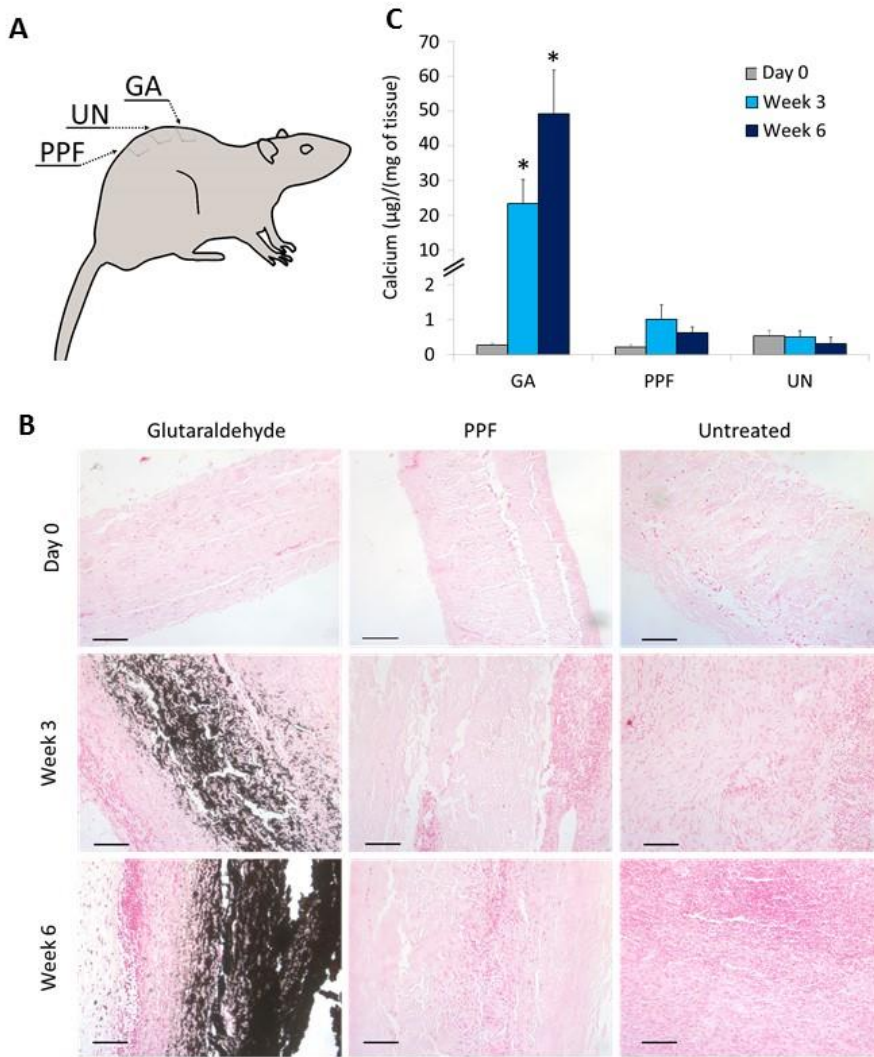


Figure 3.3 Calcification of Pericardium Samples from *In vivo* Subcutaneous Model. Calcium content was quantified on samples explanted after 3 and 6 weeks, and compared to non-implanted controls (n=8 per time point) (C). Calcium content from each sample group was compared for each time point using an ANOVA test ($p < 0.01$). A post hoc Tukey’s test showed significant difference in the GA-treated group, as denoted “*”, ($p < 0.05$). Samples were also fixed and prepared for histological analysis using Von Kossa stains. The dark black region indicates calcium phosphate deposits. This region is seen significantly darker in GA treated samples after 3 and 6 weeks of implantation, and not observed in PPF reinforced or untreated samples. Scale bars represent 100 μm .

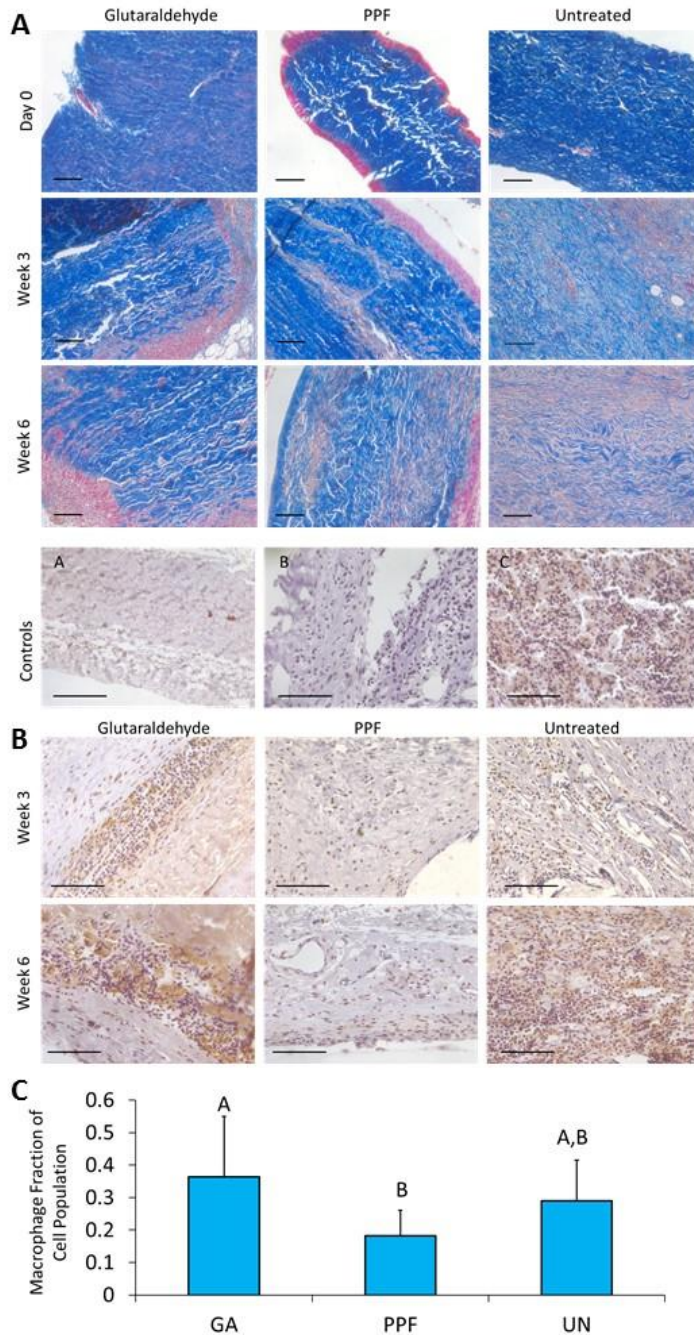


Figure 3. 4 Histological Analysis of Explanted Pericardium Samples. Cellular response to implanted samples was analyzed using Masson's trichrome stain (A). Blue regions indicate collagen, pink indicates cell bodies. Staining shows local cell populations relative to implanted tissue. Cell populations in the region of the implanted tissues were also stained for F4/80, a macrophage surface marker (B). Staining shows a correlation between dense cell regions and the F4/80 stain, indicating an inflammatory response. A dense line of macrophages is seen near the edge of the GA treated tissue,

while in the PPF reinforced and untreated samples, macrophages are seen in smaller regions throughout the sample. On the other hand, there was no significant F4/80 expression in Day 0 samples (B.A) and samples lacking the primary antigen from week 6 (B.B). A rat spleen stained by the same procedure is shown in B.C as a positive control. Macrophage population was investigated by examining 3 standardized images from each of n=5 samples per treatment group. Macrophage fraction was defined as the number of cells determined to have F4/80 staining divided by the total cells counted per image in a blinded study. Data is presented as an average of each of these fractions, and error was calculated as the standard deviation between all images in each group. Population fractions from the GA treated samples and the PPF reinforced samples are significantly different, as determined by a one way ANOVA test, followed by a post hoc Tukey's test ($p < 0.05$). Groups that share the same letter are not statistically different. Scale bars represent 100 μm .

3.4 Discussion

Utilizing pericardium as a naturally strong and elastic biomaterial offers clear benefits for building cardiovascular devices. In order to utilize pericardium's strengths for a cardiovascular implant, steps need to be taken to preserve the tissue in a foreign body environment. Glutaraldehyde treatment is effective at preventing degradation of the collagen network and preventing immune cell infiltration by crosslinking the collagen fibers. However, this process renders the tissue non-viable, which forces the body to resort to unnatural healing mechanisms to repair inevitable fractures and defects in the tissue. In this process, the natural mechanical properties and hemodynamic capabilities are lost or altered.

To combat the issues caused by GA fixation, strategies that target either therapy with anticalcification agents or biomaterial modifications are among approaches commonly investigated. Biomaterial modifications focus on improving or modifying the GA fixation through altering the reactivity or concentration of the chemical, or using an altogether different chemical process. This last route has included options such as epoxy compounds, carbodiimides, and acyl azides, which all eliminate the use of GA, but still hinge on a chemical crosslink of the tissue. Some of those methods have shown successful results in the laboratory, but have had little translation into clinical practice (17).

In this study, it was hypothesized in this study that a thin coating of PPF would sufficiently prevent enzymatic degradation of the pericardium tissue, and yet by

completely avoiding alteration of the tissue though the use of chemical crosslinker, result in a less calcium deposits.

As demonstrated initially in *in vitro* degradation, PPF reinforced pericardium did not lose mechanical strength (yield strength or elastic modulus) after collagenase exposure. In fact, the retained elastic modulus and yield strength was not significantly different from the gold standard control (GA treated). This retained strength as demonstrated in mechanical testing and retained physical structure observed in histological images support the superior durability of PPF reinforced pericardium when compared to the untreated control in a physiological model. This indicates a thin layer of PPF is successful at protecting pericardium from structural deformation due to enzyme activity. This claim is supported further by results from the sub dermal model. The rapid loss in strength and observed loss in organization of natural pericardium is visually and statistically distinct from the PPF reinforced and GA treated pericardium after enzymatic degradation.

Furthermore, the inflammatory response characteristics differ between the PPF reinforced and GA treated cases, as observed with immunohistochemical staining for macrophage presence. In addition to overall lower total macrophage density in PPF reinforced samples; macrophages are homogenously spread throughout the implant. In GA treated samples macrophages are seen in a distinct and dense cell line surrounding the exterior.

More importantly, the calcium deposition in the reinforced pericardium was significantly less than the GA treated samples in both the *in vitro* and *in vivo* models. The accumulated calcium on the PPF reinforced samples was in fact so low that it was not significantly higher than either the untreated samples or any of the unimplanted day 0 samples. This result suggests that the calcium deposits are not necessarily related to implanting xenographic tissue, but agrees with the theory that detrimental calcium deposition seen on GA treated implants is related directly to the crosslinking of the tissue. By eliminating the crosslinking component, we have demonstrated an approach that could block calcification of implants before the unnatural healing mechanism starts.

As we have shown here, the process of dehydrating and coating the pericardium with the biocompatible polymer PPF interacts with the extracellular matrix in a physical and not chemical or otherwise transformative way. Histological images in Figure 10 display cellular infiltration from the edges of the samples, indicating that PPF reinforcement leaves the protein matrix suitable for cell viability. These observations can be directly compared to GA treated samples, where little to no cells have migrated into the tissue. This difference suggests that PPF crosslinks into a network on the surface of the pericardium that is mechanically linked in the surface network of proteins, and does not disturb the natural composition. This alternate outcome from the processing of pericardium may explain why the PPF reinforced pericardium appears to retain more original structure (Figure 3.4A), as compared to the dense protein packing in GA treated tissue, as well as why it does not accumulate

significant calcium deposits. Overall, the results presented support that the innovative and unprecedented combination of a synthetic polymer with a natural biomaterial may avoid the detrimental end points of GA treated pericardium.

3.5 Conclusion

We have established for the first time a hybrid material that preserves the natural properties of pericardium and adds support with a biocompatible polymer, while avoiding crosslinking of the tissue. We have shown that the pericardium composite is protected against enzymatic degradation by the paintable application of the polymer, and that the addition of this polymer causes less calcification than the GA treated pericardium. Calcification of cardiovascular devices remains a forefront of concerns. The lower amount of calcium deposition on PPF reinforced pericardium is an important improvement when compared the GA treated calcium accumulation. These results suggest that PPF can be applied to reinforce pericardium instead of glutaraldehyde treated tissue, which is habitually used despite its dangerous and inevitable failure. By eliminating crosslinking with GA, not only would this fate be avoided, but the probability of improved healing and maintenance of the injured or diseased state would be gained. A material with lowered calcification rate would significantly improve the material options and revolutionize expectations for extent of cardiovascular repair.

3.6 Acknowledgements

This work was supported by Sheikh Zayed Institute for Pediatric Surgical Innovation at Children's National Medical Center, The Clark School of Engineering Seed Grant, and the National Institutes of Health under the Award Number R01 AR061460.

Chapter 4: Inflammatory Response to PPF Reinforced Pericardium in a Rat Model

4.1 Introduction

Materials for vascular grafts and patches are essential tools for aneurysm repair, vascular reconstruction, and congenital heart disease treatment (18, 111). Tissue engineering strategies applied to vascular material development strive to create an implant that will support ingrowth and maintenance from a patient's own tissue, leaving behind functional vasculature when the implanted scaffold slowly degrades away. To be successful in this application, scaffolds need to fulfill a number of broad functions, both in mechanical behavior as well as complex biological remodeling. New approaches to vascular grafts and patches attempt to utilize the inherent immune reaction to implanted material to harness the patient's natural healing capabilities, and then ultimately use those capabilities to develop the new tissue (112).

Extracellular matrix (ECM) based scaffolds are being developed to harness the immune reaction and natural healing capabilities (113). The constituents of ECM make it biologically active, with the potential to provide tissue specific environmental cues (23, 114). Specifically for vascular tissue, unique ratios of collagen types, elastin, and other proteins can stimulate distinct cell populations such as endothelial cells and smooth muscle cells that are required in the functional development of vascular tissue (21, 115). In addition, many applications of ECM-based scaffolds have demonstrated favorable healing phenotypes (M2) in arriving macrophages,

compared to synthetic scaffold controls. The temporal polarization of arriving macrophages could be a significant determinant of the healing path followed by other cells (116, 117). An M1 phenotype is often involved in phagocytosis of debris, recruitment of other immune cells, and signaling for new matrix production and proliferation of fibroblasts and other cells (118). These actions are beneficial in initial wound repair, but can become pathogenic if they continue to propagate, leading to fibrous capsule formation, rapid deterioration of the scaffold, and stenosis in the vicinity. On the other side of the spectrum are M2 macrophages, which are responsible for cytokines that can stabilize new endothelial layers, reduce inflammatory cytokines, and support endothelial cell proliferation (119).

The effect of ECM on the activation and polarization of macrophages can have immense benefits as the new vascular tissue develops, either in propagating inflammation or stabilizing new tissue formation (120). Creating a scaffold that induces the right balance of macrophages and ratio of scaffold destruction to tissue rebuilding could have a big impact on outcome of the injured site. The macrophage activation in response to a hybrid biomaterial is an important indicator of the potential outcome both in terms of endothelialization and chronic inflammation (118, 121). Macrophages that sustain an M1 phenotype may impede the initiation of the remodeling phase. An M1 phenotype after 6 weeks may indicate the formation of a fibrotic capsule or a generally pathogenic environment (122).

In Chapter 3, we reported on the biohybrid material, poly(propylene fumarate) (PPF) reinforced pericardium, as a scaffold for vascular wall repair (63). This material combines the bioactivity of pericardium, a matrix-dense tissue found surrounding the heart muscle, with the strength of the polymer PPF. In this previous chapter, we demonstrate that the polymer reinforcement is as effective as the chemically crosslinked alternative (glutaraldehyde, (GA)) at preventing detrimental weakening due to enzymatic degradation upon implantation (Figure 3.2). More importantly, the polymer reinforcement results in significantly lower calcification of the pericardium than chemical crosslinking in a rat subdermal implant after only 3 weeks (Figure 3.3). Changes in calcification could be explained by unnatural healing in response to eliminated or masked active components of the pericardium due to chemical crosslinking (63). Furthermore, immunohistochemical staining for the F4/80 surface antigen showed significantly less macrophages ($p < 0.05$), quantified as a percent of total cell population, surrounding the PPF reinforced pericardium ($18.2 \pm 8.0\%$ of the population) compared to GA ($36.3 \pm 18.7\%$) or untreated pericardium (UN) ($29.0 \pm 12.4\%$) (Figure 3.4) (63).

In addition to macrophage presence, the PPF reinforced tissue caused moderate cell infiltration, indicating a “middle road” between rapid scaffold deterioration in the untreated case, and capsule formation around the GA pericardium. These results suggest that the PPF layer could be responsible for controlling the presentation of the potent ECM molecules to the system, allowing for the benefits of bioactive

components, but eliminating the risk of rapid degradation and propagation of inflammatory cycles.

The work presented in this chapter aims to understand and capitalize on the addition of a synthetic component to control the inflammatory response and eventual rebuilding of the tissue implant. The objectives of this study are to first characterize the immune response in terms of extent (number of responders) and macrophage phenotype after 6 weeks of implantation from the pericardium scaffolds in immunocompetent rats. Second, in order to use PPF as a tool to leverage presentation of the ECM molecules, the isolated effect of an incremental increase in amount of polymer and degradation products in relevant cell groups, leukocytes and endothelial cells. Finally, the polymer:ECM ratio is repeated in a subdermal study in athymic rats. This experiment will target a macrophage dominated response, and provide an isolated look at the macrophage population. We hypothesize that increasing the amount of polymer, and therefore decreasing the concentration of ECM that is exposed without complete masking with chemical crosslinking, will reflect a healing and anti-inflammatory environment from responding macrophages.

4.2 Methods

4.2.1 Material Synthesis

The polymer PPF was synthesized following previously published methods (109). Briefly, propylene glycol and diethyl fumarate were combined in a 3:1 molar ratio. Zinc chloride (catalyst) and hydroquinone (radical inhibitor) were incorporated in a 0.01:0.002 molar ratio. Under nitrogen flow, the reaction produces ethanol as a

byproduct and bis(hydroxypropyl) as the intermediate. Transesterification under vacuum of the intermediate produces PPF with propylene glycol as a byproduct. Gel permeation chromatography was used to calculate the number average molecular weight (M_n) and polydispersity index (PDI) of the purified PPF. For use in this study, PPF (M_n 1150 and PDI 1.6) was mixed with the monomer DEF in a 3:1 ratio and then mixed with the photoinitiator bis(2,4,6-trimethylbenzoyl) phenylphosphine oxide (BAPO), to create a UV sensitive reaction. The polymer at this phase can be crosslinked to a solid, thin film with UV light (3.5 mW/cm^2) for 45 minutes.

The PPF pericardium hybrid was created as developed as described in Chapter 3 (63). Briefly, fresh bovine pericardium was obtained 2 days after harvest from Innovative Research, Inc. and cut into strips 2x6 cm for dehydration. A liquid layer of PPF:DEF as described above was applied either as a single layer on the surface or on both sides of the tissue, and the combined material was exposed to UV radiation for 45 minutes (3.5 mW/cm^2) to crosslink the polymer. This method was used to create samples for PPF_{SD} (both sides), 2PPF_{Athymic(AT)} (both sides), and 1PPF_{AT} (one side). The hybrid material is then cut to 1x1 cm squares, washed in sterile 70% ethanol for 6 hours, and then rehydrated fully in sterile PBS for 12 hours.

4.2.2 *In vitro* Studies

Primary splenocytes were isolated from the spleens of male Sprague Dawley (SD) rats. Spleens were aseptically removed from the animal and pressed through a 60- μm nylon mesh in RPMI-1640 medium. The cells washed and re-suspended in RPMI-1640 medium containing 10% fetal bovine serum, 100 U/mL penicillin and

100 µg/mL streptomycin. PPF thin films were added to the splenocyte culture on the day of isolation (day 0). Control groups were created using 100ng/mL lipopolysaccharide (LPS) as an activator. After 3 days, cells were collected via cell scraping and stained for surface marker analysis.

Splenocytes were fixed and permeabilized following procedures recommended for antibody use from BioRad. Briefly, cells were fixed with 0.1% PFA for 15 minutes, and then permeabilized using 0.5% Tween. Cells were stained with anti-CD68 (a general macrophage marker), anti CD163 (expressed intracellularly on M2 macrophages) and anti CD80 (expressed intracellularly on M1 macrophages). For each cell sample, 20,000 events per test were analyzed using a BD FACSCanto II flow cytometer.

Human umbilical vein endothelial cells (HUVECs) were cultured in endothelial basal media (EBM) supplemented with EGM SingleQuot Kit Supplements and Growth Factors (Lonza, Walkersville, MD). All cells were used at or below the 4th passage. To determine behavior changes to HUVECs in response to the PPF, PPF thin films were created as described, and washed to remove uncrosslinked polymers. Films were combined with EGM media, and incubated for 0, 3 and 5 days to create 3 stages of hydrolytically degraded states. The films or media containing the degraded products were added to HUVEC culture for 6 hours. RNA was isolated from HUVECs using an RNeasy Mini Plus Kit (Qiagen, Valencia, CA) following standard procedures. Isolated RNA was then reverse transcribed to cDNA using a High Capacity cDNA

Reverse Transcription Kit (Applied Biosystems). Glyceraldehyde-3-phosphatase dehydrogenase (GAPDH) was used as an endogenous control gene for all samples.

Gene expression assays were combined with the cDNA from each sample and TaqMan PCR Master Mix II (Applied Biosystems). The reaction was conducted on a 7900HT real-time PCR system (Applied Biosystems) using thermal conditions of 2 min at 50 °C, 10 min at 95, and 40 cycles of 15 seconds at 95 and 1 min at 60. The relative gene expression level of each target was normalized to the mean of the GAPDH level, and then fold change was calculated using the $\Delta\Delta CT$ method. Samples were completed in triplicate and the standard deviations are reported.

4.2.3 *In vivo* Studies

In vivo analysis was conducted in both SD and athymic adult, male rats. The protocol was approved by the Institutional Animal Care and Use Committee of the University of Maryland, and all animals were treated in accordance with the “Guide for the Care and Use of Laboratory Animals”. The first experiment was conducted in n=5 SD rats, as determined by a power analysis. A small incision is made in the dorsal dermal layer, and a material patch (1 x 1 cm) from each of the following three groups was sutured by the corners to the underlying tissue: GA crosslinked pericardium (GA_{SD}), untreated pericardium (UN_{SD}), and PPF reinforced pericardium (PPF_{SD}). After 6 weeks animals were euthanized and the pericardium patches and surrounding tissue were explanted, preserved in paraformaldehyde (4%), and embedded in paraffin for histological analysis.

The second study was conducted in n=5 athymic rats. Following a similar procedure, one material patch from each of the following groups was implanted subdermally in the dorsal dermal layer: untreated pericardium (UN_{AT}), pericardium with PPF on both sides (2PPF_{AT}) and pericardium with PPF on one side (PPF_{AT}). Material was explanted after 6 weeks. Half of each explant was fixed in paraformaldehyde (4%) and embedded in paraffin for histochemical analysis. The other half of each material was homogenized and analyzed using a TNF α ELISA (Qiagen).

Paraffin embedded samples were sectioned into 5 μ m slides and stained using hematoxylin and eosin (H&E) to assess remodeling and total cell infiltration. To quantify the cell density near the implanted material, a midline was drawn down the center of the original material volume using Image J. Parallel lines were placed at 100 μ m intervals from the center. Macrophages were identified using following antibody and fluorophore pairs: a mouse anti-CD68 antibody (Abcam, 1:100) and goat anti-mouse FITC conjugated secondary antibody (Abcam, 1:200), a rabbit anti-CD206 antibody (Abcam, 1:600) and a donkey anti-rabbit Alexa Fluor®647 secondary (Abcam, 1:200), a goat anti-CD86 antibody (Novus Biologics, 1:200) and donkey anti-goat Alexa Fluor®555 secondary (Abcam, 1:200), and a cell nucleus stain VectaSheild® plus 4',6-diamidino-2-phenylindole, dihydrochloride (DAPI) (Vector Laboratories).

4.3 Results and Discussion

Biomaterial implantation into SD, immunocompetent rats results in distinct differences in number of cell infiltrations, organization of that population, and cell

mediated remodeling of the pericardium. In Figure 4.1A, we can see initial differences in the material due to treatment methods. GA_{SD} treated tissue is tightly ordered, and exists in dense waves. PPF_{SD} reinforced pericardium is less tightly packed, resembling more the flexible structure of untreated pericardium. After 6 weeks *in vivo*, representative images with H &E staining highlight host cells that have moved into or near the implant (Figure 4.1B).

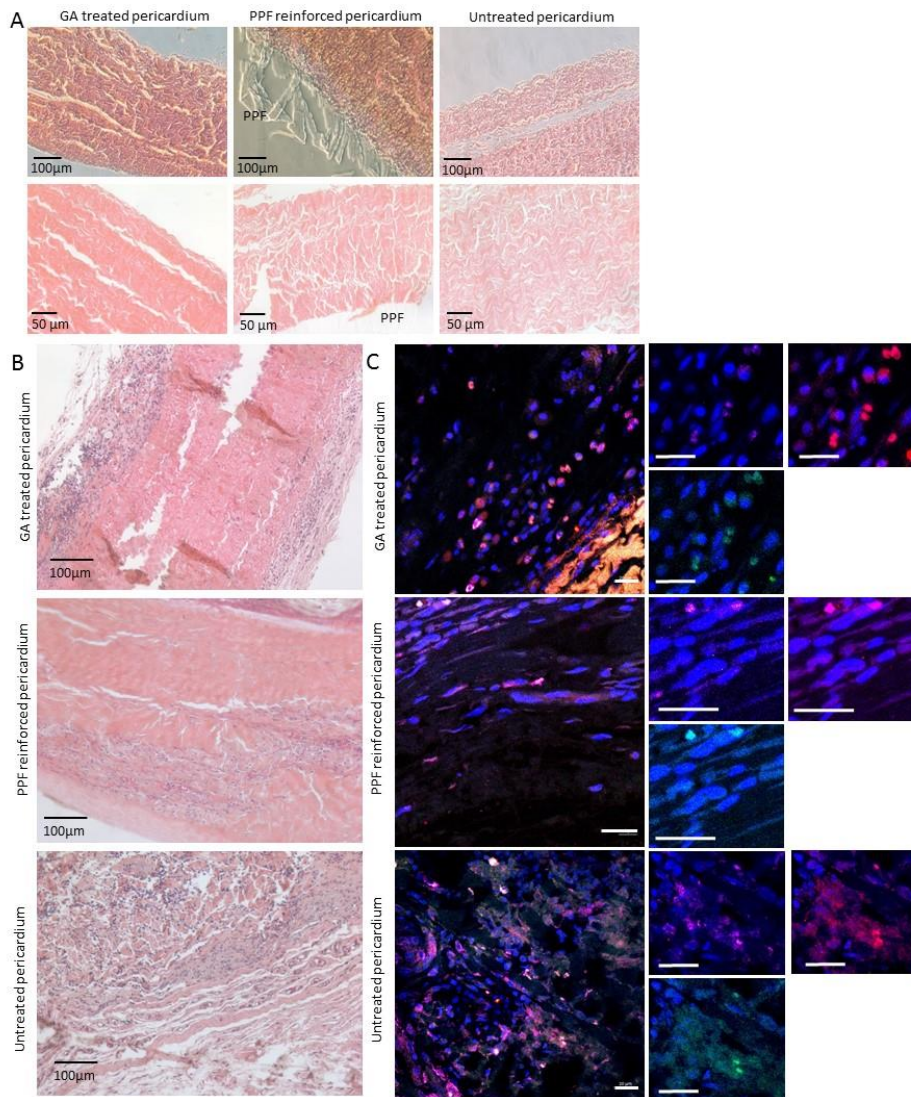


Figure 4. 1 Subcutaneous Implants in Sprague Dawley Rats. Representative images (A) of the scaffolds before implantation are stained with H&E to show matrix organization and structure differences. The layer of PPF is visible in the top row using phase contrast microscopy. After 6 weeks of implantation, scaffolds are explanted and stained with H&E (B), showing cell infiltration (nuclei are purple) and matrix changes compared to the un-implanted images (A). Using immunohistochemical staining, cells near the scaffold were identified as macrophages using CD68, and further characterized using CD86 (an M1 marker) and CD206 (an M2 marker). Scale bar is 20 μm, unless otherwise indicated. These images are representative of n=5 implanted samples.

Cell nuclei are stained purple, and are counterstained with pink to observe collagen structure and other matrix proteins. In our previous investigation, we reported dense cell bands near the edge of GA_{SD} treated pericardium. We also noted moderate cell infiltration into the PPF_{SD} reinforced case, as compared with the immense cell infiltration into the untreated pericardium case. Very densely packed cells persisting after 6 weeks in implantation could indicate a chronic inflammation and has characteristics of a foreign body response (123, 124).

To further investigate this result, we stained cells for surface markers to indicate macrophage phenotype at or near each implant. Macrophages bare the surface marker CD68 regardless of phenotype, and can be classified further as M1 (CD86) and M2 (CD206). The M1 phenotype, which is associated with host defense and pro-inflammatory functions, is observed in higher frequency on both the UN_{SD} and GA_{SD} samples than the PPF_{SD}. M2 (CD163) phenotype, which is associated with tissue remodeling and constructive functions, is observed in all scaffolds, but appears to account for a greater portion of the total cells in the PPF reinforced samples. An M2 weighted M2:M1 ratio can describe the host-material relationship and indicate remodeling. Looking closely at the representative images in Figure 4.1C, there is a high prevalence of the M1 stain among many macrophages in the dense cell band surrounding the GA_{SD} sample. We also observe high quantities of macrophages (identified with CD68) in the UN_{SD}, with noticeable presence of both M1 and M2 phenotypes. The PPF_{SD} reinforced pericardium does have macrophages in the vicinity, but appears to have more M2 phenotypes at this stage than the GA_{SD} sample.

As previously described, some macrophage presence, even inflammatory, can be an important step in the vascular healing process. A carefully balanced population of M1 and M2 could direct appropriate healing. Sustained presence after 6 weeks of the inflammatory phenotype M1 in the GA_{SD} and UN_{SD} samples supports the observation of chronic inflammation and foreign body response at the injured site. Less cells involved in the PPF_{SD} reinforced sample could mean fewer MMPs and matrix breakdown pathways, slowing the process of remodeling. This observation is supported by comparing the lack of original organization of matrix seen in the UN_{SD} sample compared to the PPF_{SD} reinforced sample (Figure 4.1B).

Macrophages are expected to be important in determining the response to this tissue, as has been seen in other ECM-based implants. To investigate if PPF plays an active role in macrophage activation or polarization it was investigated independently of pericardium on the activation of splenocytes. Splenocytes represent a diverse population of leukocytes and were harvested from untreated SD rats. After 24 hours of culture with PPF, we see between 30 and 40% of splenocytes become activated macrophages, displaying the CD68 marker (Figure 4.2A). Further classification of that population in Figure 4.2B and quantified in Figure 4.2C shows a percentage of the population that is positive for both CD80 and CD163. Macrophage phenotype exists on a spectrum, and thus the positive staining of one surface marker is not a definitive indicator of phenotype. In the presence of high PPF, the population of activated macrophages shifts to relatively higher positive staining of all 3 markers. However, a large portion of this increase is positive for CD 163, an M2 marker.

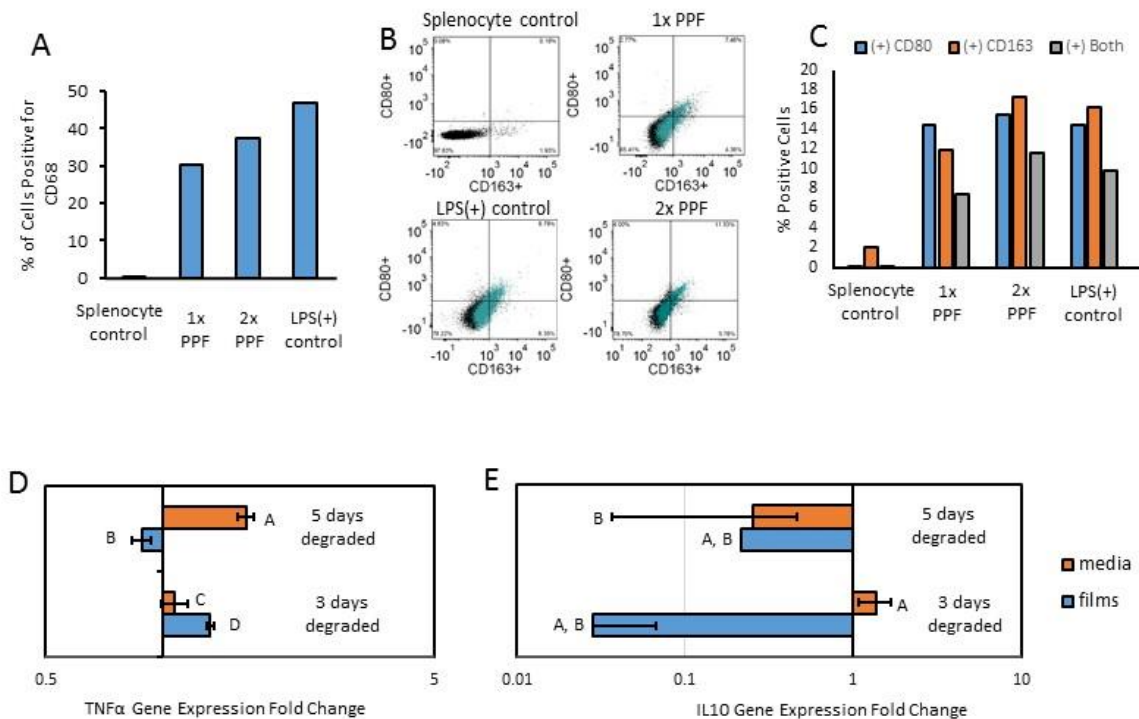


Figure 4.2 *In vitro* Independent Cell Activation. Splenocytes that positively express the macrophage marker CD68 after culture with PPF films are quantified in the first graph (A). Total activation from PPF is observed to be lower than the inflammatory control LPS. From the cells positive for CD68, samples were then evaluated for positive staining of CD163 and CD80 (B). Splenocytes determined to be positive for these markers are summarized in the graph in Figure 4.2 C. The percentages shown in A, B, and C are taken from 20,000 events per group. HUVECs cultured with PPF degraded for 3 or 5 days, or with the products of that degradation, were evaluated for changes to TNF α (D) and IL10 (E) gene expression. Standard deviation is displayed for technical triplicates from the RNA extracted from n=3 cell cultures. Groups that share letters are not statistically different as determined with an ANOVA followed by a post hoc Tukey's test ($p < 0.05$).

The activation of splenocytes in response to PPF is less pronounced than activation to LPS, an established stimulatory molecule. This result suggests that PPF, if added in the concentrations tested, may act as an inert polymer, with slight differences based on the mass of foreign material in the cell environment.

In addition to macrophage polarization, initial endothelial cell response could be an important factor determining the fate of a PPF pericardium patch implanted in the vasculature. In this setting, the relationship between macrophages and endothelial cells is reciprocal. Macrophages secrete growth factors VEGF, FGF, TGF β , and PDGF that act on endothelial cells to contribute to and stimulate angiogenesis and tissue repair. For example, endothelial cells can contribute to M1 stimulation with danger associated antigen TNF α , or can provide signals that promote expansion of M2 macrophages and M_R macrophages, which inhibit the proliferation of M1 macrophages, by upregulating IL10.

HUVECs were cultured together either with PPF or with the products of hydrolytic degradation of the polymer, since realistically these smaller components may enter HUVECs and have different modes of action. Using gene expression analysis, an upregulation of TNF α was measured in response to both the 3 day polymer and the 3 day degraded products. However, only the degraded products of 5 day degradation caused an upregulation of TNF α . The down regulation of TNF α in response to 5 day degraded films is especially interesting, since some TNF α can be expected when any foreign environment is encountered. The results from IL10 gene expression show a down regulation compared to normal HUVEC cells, indicating that PPF films or

degradation products do not stimulate this cytokine. Independently, PPF does not appear to induce major macrophage or endothelial cell changes. We therefore conclude that changes observed in Figure 4.1 are the result of various exposures of the pericardium to the host.

Based on the significant macrophage activation in both the subdermal study and the *in vitro* analysis, the final study was conducted in athymic rats, to isolate the role of the innate immune system. This final study compares pericardium with either PPF on both sides of the tissue (2PPF_{AT}), pericardium with PPF on one side (PPF_{AT}), and pericardium untreated (UN_{AT}) as a control. This design controls the degree to which pericardium is exposed to the host. The first observation, shown with an H&E stain in Figure 4.3A, is the overall number of macrophages and other cells is lower in the athymic implants than in the SD implants. In immunocompetent systems, NK cells, T cells and DCs all interact with macrophage cells to suppress or propagate the inflammatory response (125). The lack of T cells in athymic rats could substantially decrease the propagation of the immune signals in response to the implant. Looking at the cell infiltration in H&E staining (Figure 4.3A), a distinct, one-sided infiltration of cells into the 1PPF_{AT}. However, this density is only slightly less than a single side of the untreated control. This similarity could indicate the overall lowered amount of signals that recruit cells, as it is markedly different from the PPF_{SD} and UN_{SD}. There are the least number of cells in the 2PPF_{AT}. Immunohistochemical staining was used to identify the cell population further. The 2PPF_{AT} has the least amount of positive macrophage stain, even in the dense pocket of cells near the edge, as shown in Figure

4.3B. There is distinct CD206 stain in both the 2PPFAT and 1PPFAT, and less so in the untreated pericardium. At this late, 6 week time point, this could indicate a pro-healing shift of macrophages in both the PPF reinforced cases.

In the graph in Figure 4.3C, TNF α is quantified from homogenized samples of the implants at the 6 week time point. The sample 2PPF_{AT} has significantly less TNF α than the UN_{AT} sample. The PPF_{AT} sample TNF α concentration is also less than UN_{AT}, but greater than 2PPF_{AT}. This result suggests that with increased PPF, less ECM is presented to the host, resulting in less TNF α . Although TNF α is a relevant molecule in tissue regrowth, high levels at this stage (6 weeks), can recruit and stimulate more M1 macrophages, leading to over production of matrix, proliferation of fibroblasts, and maintenance of the inflamed state.

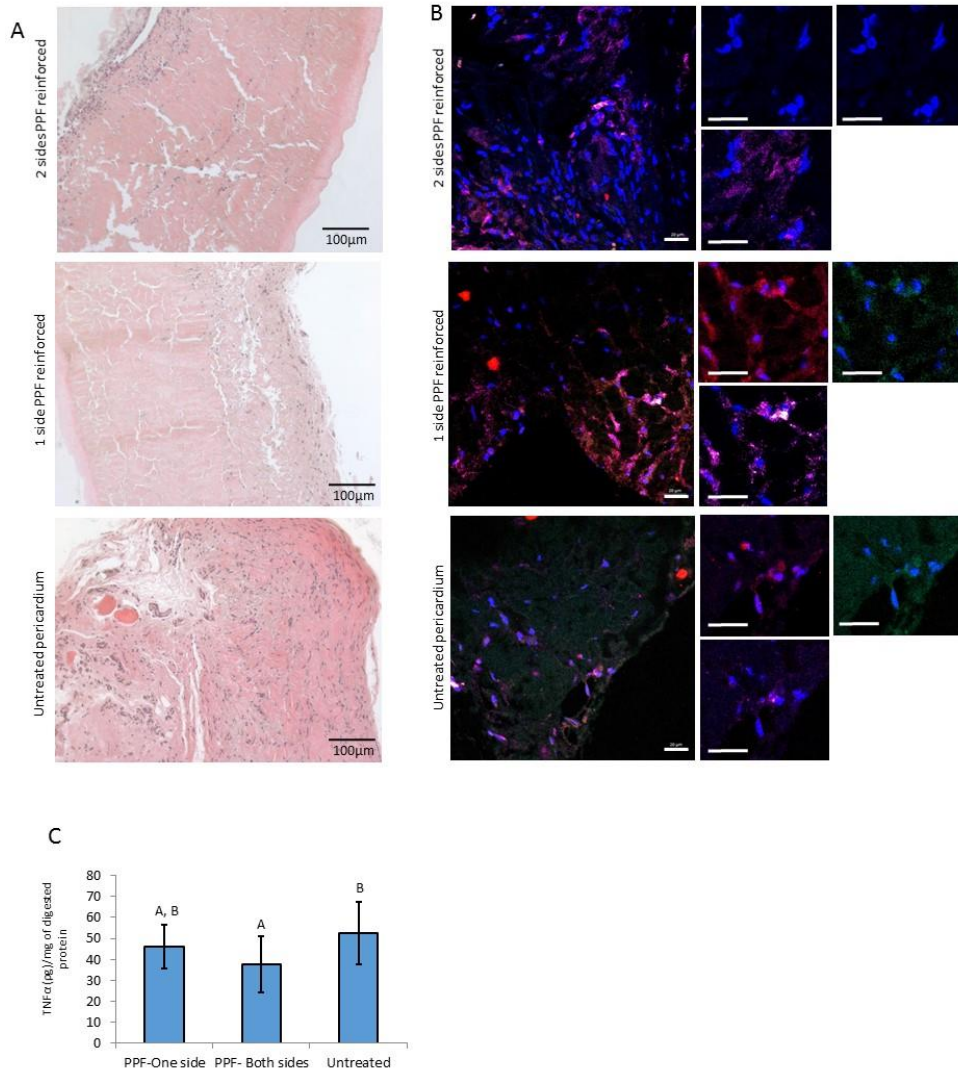


Figure 4.3 Subcutaneous Implants in Athymic Rats. After 6 weeks of implantation, scaffolds are explanted and stained with H&E (A), showing minimal cell infiltration (nuclei are purple) and matrix changes compared to the scaffolds in Figure 4.1. Using immunohistochemical staining, cells near the scaffold were identified as macrophages using CD68, and further characterized using CD86 (an M1 marker) and CD206 (an M2 marker). Additionally, the scaffolds and surrounding tissue were homogenized and analyzed using an ELISA for TNF α (n=5 samples per group). Groups that share letters are not statistically different, ANOVA test & post hoc Tukey's test (p<0.05). Scale bar is 20 μ m, unless otherwise indicated.

To continue to explore this relationship, more analysis should be conducted in immunocompetent systems. There are other cell types that are relevant to host-material interactions that are not considered in this study including the innate immune system as indicated by the difference in macrophage presence between athymic and SD rats (112). Never the less, the results from this study indicate that PPF presence does not increase inflammatory metrics significantly *in vivo*, and in fact may reduce the propagation of inflammatory pathways resulting from a substantial amount of natural and degradable material. Increasing the presentation of pericardium and therefore recognizable cues as the scaffolds move from low polymer ratio to high polymer ratio and finally reach untreated pericardium, the expected result is that cell infiltration and resulting matrix remodeling should increase. This relationship can be leveraged to direct the appropriate timing, governed by the relationship of macrophages and endothelial cells, of scaffold degradation and new tissue formation.

Chapter 5: Controlled Delivery of Tissue Inductive

Factors in a Cardiovascular Hybrid Biomaterial Scaffold³

5.1 Introduction

Rebuilding and maintenance of an implantable tissue construct is an essential consideration in designing materials for vascular grafts. Maintenance of the implant relies on controlled cell infiltration and production of new extracellular matrix (ECM), which is in part governed by the initial immune response. One method to initiate this process is to start with a biologically relevant material, such as native ECM. Implantable devices that incorporate natural ECM often result in constructive tissue remodeling and minimal fibrosis (68, 70), with reduced inflammation and favorable macrophage polarization around the implant (29, 40, 72, 126). This result has been linked to providing bioactive peptide fragments as the materials degrade, which contribute to the recruitment of endogenous stem and progenitor cells to the site for ECM remodeling, and ultimately guide the invading macrophages toward a remodeling phenotype and attenuate the proinflammatory phenotype (55, 89, 126). By controlling the initial cues provided by the material design, we can influence cellular signaling pathways, immune response and long term fate of the vascular graft or implant. A material engineered to replace vessels, as complex, compliant tissues,

³ Adapted and reprinted with permission from: L.G. Bracaglia, M. J. Messina, C.E. Vantucci, H.B.Baker, A. Pandit, and J.P. Fisher. Controlled Delivery of Tissue Inductive Factors in A Cardiovascular Hybrid Biomaterial Scaffold. ACS Biomaterials Science & Engineering. Copyright 2016 American Chemical Society

would strive to both mimic the native mechanical properties as well as encourage native regrowth, remodeling and maintenance of the tissue site as fast as possible. Hybrid biomaterials offer a platform to pursue these two goals in parallel, by providing initial mechanical support from a synthetic biomaterial, and including a viable, bioactive substrate to support native cell infiltration and remodeling. Hybrid biomaterials designed to mimic compliant tissue such as vessels, skin, and tendons have been successfully developed using a layering approach, where a distinct synthetic polymer component is bound to a layer of a biological material to create one composite material. Fabricating a material in this way can incorporate whole, decellularized tissue, which allows for the inclusion of many (including some unidentified) proteins and minerals. In several examples of biohybrid materials, the presence of ECM components was shown to influence the initial response of the immune system to promote healing, despite the polymer components that would be expected to individually illicit an inflammatory response (58, 64, 72).

As described, cell behavior in response to the implant ultimately determines the fate of the injured site. In the specific cardiovascular space, studies have shown that an immediate development of a pure endothelial layer can significantly reduce occlusion of vascular grafts (127). Polymers can be selected to encourage the growth of site-specific cells (49), but a layered biohybrid technique also provides a platform to further influence the local environment and control cellular response. For example, delivering vascular endothelial growth factor (VEGF) to sites of vascular injury has shown significant improvements in endothelial wall formation and matrix production

(128, 129). In this chapter, we describe the development of a vascular graft platform that can be utilized for further control through local delivery of growth factors to enhance cell infiltration, migration and matrix production. This system is built using three layers: The bottom layer consists of an ECM biomaterial which provides cell attachment points and biological cues. The top layer consists of a biodegradable polymer which can retain strength in the composite as the bottom layer is remodeled. The middle layer consists of quickly degrading polymer microspheres embedded within the slower degrading polymer used in the top layer. These microspheres can be utilized in the delivery of critical growth factors such as VEGF and transforming growth factor-beta 3 (TGF β 3) to cardiovascular tissue engineering sites.

The goal of this work was to develop a directional delivery system for bioactive molecules that can be coupled with a hybrid biomaterial. In this chapter, we have designed this structure using bovine pericardium as the natural biomaterial, poly(propylene fumarate) (PPF) as the slower degrading polymer, and poly(lactic-co-glycolic acid) (PLGA) for the faster degrading microspheres.

The biocompatible and biodegradable polymer, PPF, was originally selected to blend with pericardium for the strength the polymer would lend through remodeling, as seen in other biomedical applications (105, 107, 130). PPF is an unsaturated, linear polyester that is crosslinkable through UV radiation with itself or with other compatible crosslinkers through the double bonds in fumarate (108). It is biodegradable by hydrolysis of ester bonds, and forms the naturally occurring

byproducts fumaric acid and propylene glycol upon degradation (131). The degradation time is largely dependent on polymer characteristics such as molecular weight, crosslinker and crosslinking density (132). The uncrosslinked polymer is viscous at room temperature, allowing it to be easily “painted” onto a surface. In addition, PPF viscosity can be reduced, without significantly altering the components of the system, with the addition of diethyl fumarate (DEF), the monomer from which PPF is synthesized. The addition of DEF to PPF can also cause variations in the crosslinked biomaterial’s mechanical strength, and can be utilized as a parameter to tune the characteristics of the hybrid biomaterial (133).

We have shown in Chapter 3 that a composite of PPF and pericardium demonstrates not only reduced macrophage infiltration and calcium deposition compared to chemically crosslinked vascular material alternatives, but that this composite also maintains the mechanical integrity and supports cell infiltration through degradation (63). In particular, when challenged with enzymatic degradation, the composite PPF pericardium material was not statistically different from GA crosslinked pericardium (typically used surgical material) in either elastic modulus or yield strength (Figure 3.2) (63). Furthermore, drug delivery from PLGA microparticles coupled with PPF (134) as well as other polymers (135, 136) has been successfully used in previous research. The system described herein includes a layer of PPF with embedded PLGA particles adhered to pericardium and is depicted in Figure 5.1.

In this current development, it was hypothesized that by using PPF as a scaffold to encapsulate PLGA microparticles as well as the top, slower degrading layer, a tunable and directional release can be achieved from the intact scaffold into the bioactive substrate. Release will occur as PLGA microparticles degrade hydrolytically into biocompatible molecules, leaving the PPF scaffold unchanged within the release time frame and able to support the pericardium substrate through remodeling. This chapter examines this platform through three objectives. First, the mechanical properties of the composite material, as well as the release of proteins as the polymer components degrade were assessed. Next, the bioactivity of encapsulated cargo was confirmed, to ensure that molecules are not altered in the encapsulation or release process. Finally, the location of released proteins is confirmed in an *in vitro* analysis of the biohybrid material.

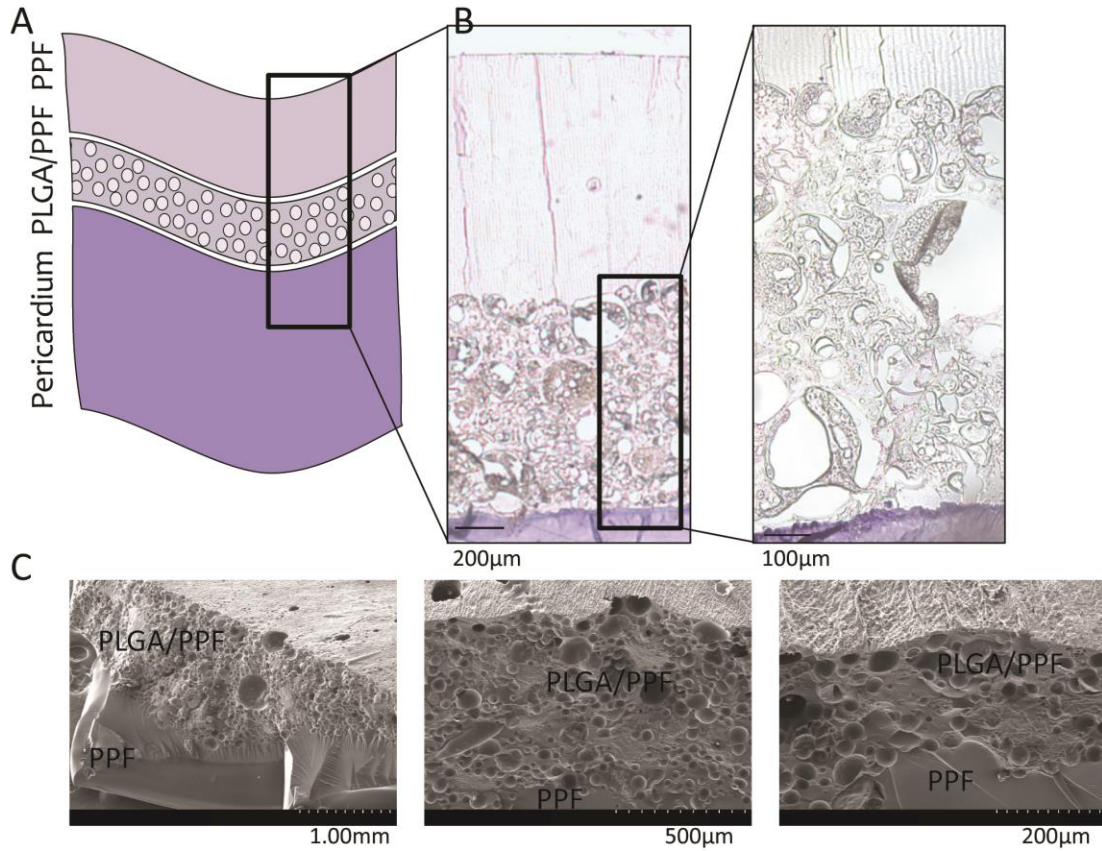


Figure 5. 1 A Schematic Of The Biohybrid Material consisting of three layers shown in the illustration (A), and corresponding bright field images (B) from histological samples. In C, scanning electron microscopy shows the two polymer layers, and the surface from which pericardium was removed before imaging.

5.2 Methods

5.2.1 Preparation of the Microspheres

Microparticles were produced using a double emulsion technique by first dissolving 100 mg of PLGA (Polysciences 50:50, Mw 150,000) in 1 mL of dichloromethane (DCM). The encapsulated protein or growth factor was dissolved in phosphate buffered saline (PBS), and 200 μ L of this aqueous phase was emulsified in the PLGA/DCM solution using high speed vortexing. The homogeneous PLGA/DCM/protein solution was then poured into 3 mL of 1% polyvinyl alcohol (PVA) with constant vortexing, followed by alternating vortexing and ultrasonication for approximately five minutes. This solution was then poured into 50 mL of stirring 1% PVA. The solution was left stirring for four hours, after which the PVA was removed and the remaining microparticles were washed with deionized water and centrifuged at 1000 x g for 10 minutes. This process was repeated twice, and the spheres were then lyophilized and stored at 4°C.

5.2.2 Polymer Synthesis and Composite Film Assembly

PPF was synthesized by a two-step process as previously described and initiated using phenylbis (2,4,6-trimethylbenzoyl)-phosphine oxide (BAPO) to create a UV light sensitive reaction (108, 109). Lyophilized PLGA microparticles were then mixed with the PPF solution with mass ratios of 1:20, 1:4, and 1:2 (PPF:PLGA). This mixture was then placed between square, glass microscope cover slips and compressed to a uniform thickness of 200 μ m. The films were exposed to UV light (3.5 mW/cm²) for 90 minutes in order to initiate photocrosslinking.

The films were embedded in paraffin and sliced into 5 μm sections for optical microscopy imaging (Figure 5.4 C). Image analysis measurements were taken to determine the relative volume ratios of each polymer component in the composite thin film. ImageJ (U. S. National Institutes of Health, Bethesda, Maryland) was used to create a binary mask in order to differentiate PLGA from PPF. Relative volumes were then calculated based on pixel quantity.

Upon visualization of the polymer/microparticle composites (Figure 5.4 C), the 1:2 PLGA:PPF mass ratio presented the most tightly packed microsphere organization among the visualized ratios. It was anticipated that degradation of the microspheres in this composite would allow for the most extensive interconnected network compared with the other investigated ratios. As such, the 1:2 PLGA:PPF mass ratio was ultimately selected for additional evaluation within this study. The 1:2 mass ratio yields a PLGA:PPF volume ratio of 1:1.01 and approximately 50 mg of microparticles per film.

5.2.3 Degradation Assessment

To assess PLGA particle degradation, microspheres were manufactured as described, using either PBS or a 200 mg/mL solution of ovalbumin (OVA) as a representative antigen in the aqueous phase. Samples of PLGA microspheres were placed in PBS solution (4 mg/5 mL) and incubated at 37°C while shaking for 21 days. At predetermined time points 3 groups of 4 mg of spheres from each set were stopped and lyophilized. After 21 days, all groups were analyzed using a gel permeation chromatography system (GPC) (Waters) to assess number averaged molecular weight

(Mn) of PLGA. A Student's t-test was conducted to assess statistical difference between unloaded and loaded microspheres at each time point.

Mass loss was used to assess PPF film degradation independently from PLGA, since the crosslinked products are not suitable for GPC analysis. Films of PPF were created by crosslinking the polymer in between 2 glass coverslips as previously described in Chapter 2. The films were cut into quarters and massed, and incubated in PBS at 37°C while shaking. At predetermined time points, six films were oven dried for 24 hours before measuring final mass. Mass loss was calculated following:

$$\textit{Thin Film Mass Loss} = \frac{\textit{Mass after crosslinking} - \textit{Mass after degradation}}{\textit{Mass after crosslinking}}$$

5.2.4 Release from Films and Free Microspheres

Two individual studies were performed in order to measure the rate at which OVA molecules would be released from freestanding microparticles in an aqueous environment, and from microparticles embedded within a PPF thin film.

Microparticles in solution were prepared in 25 mg samples, and incubated at 1 mg/mL, shaking at 37°C. At each predetermined time interval, 200 µL of solution was removed from the vial and flash frozen for later analysis. 200 µL of PBS was replaced in each vial in order to maintain constant volume. This same procedure was repeated for composite films, where one film is immersed in 25 mL of PBS. After the collection of samples from all time points, the extracted PBS was analyzed using a Bradford protein assay to determine OVA concentration.

5.2.5 Construction and Assessment of Hybrid Material

Although the composite of pericardium and PPF has been previously described, the incorporation of the PLGA microparticles could alter relevant mechanical characteristics, namely the elastic modulus of the composite and the adhesion between the PPF layer and the pericardium. Samples of pericardium coated with PPF with and without PLGA microparticles, and then crosslinked using UV light (63). All samples were then rehydrated in PBS. Using a universal testing machine (Model 1185, Instron, USA) eight samples were subjected to tensile testing, with a set extension rate of 10 mm/min. Extension and corresponding load was recorded at a frequency of 10 Hz, and a preload of 5 N was applied. The elastic modulus and 0.1% yield strength for each sample was calculated using MATLAB to determine the slope of the linear region of the stress–strain curve reported by the Instron software. A Student’s t-test was conducted to assess the significance between PPF with and without the PLGA.

To test adhesion, following an adaptation from ASTM standard D5868, samples of pericardium were prepared through the described dehydration method before coating in either PPF or the PPF+PLGA microsphere composite (63). Poly(propylene) mesh of equivalent size to the pericardium was gently pressed into the liquid phase of the polymer (Figure 5.2). The pericardium/mesh/PPF sample was then crosslinked with UV light, allowing the PPF polymer to solidify and crosslink with itself around the mesh. This creates a “tab” that is physically integrated with the polymer layer, and allows the pericardium layer and the PPF layer to be pulled in opposite directions

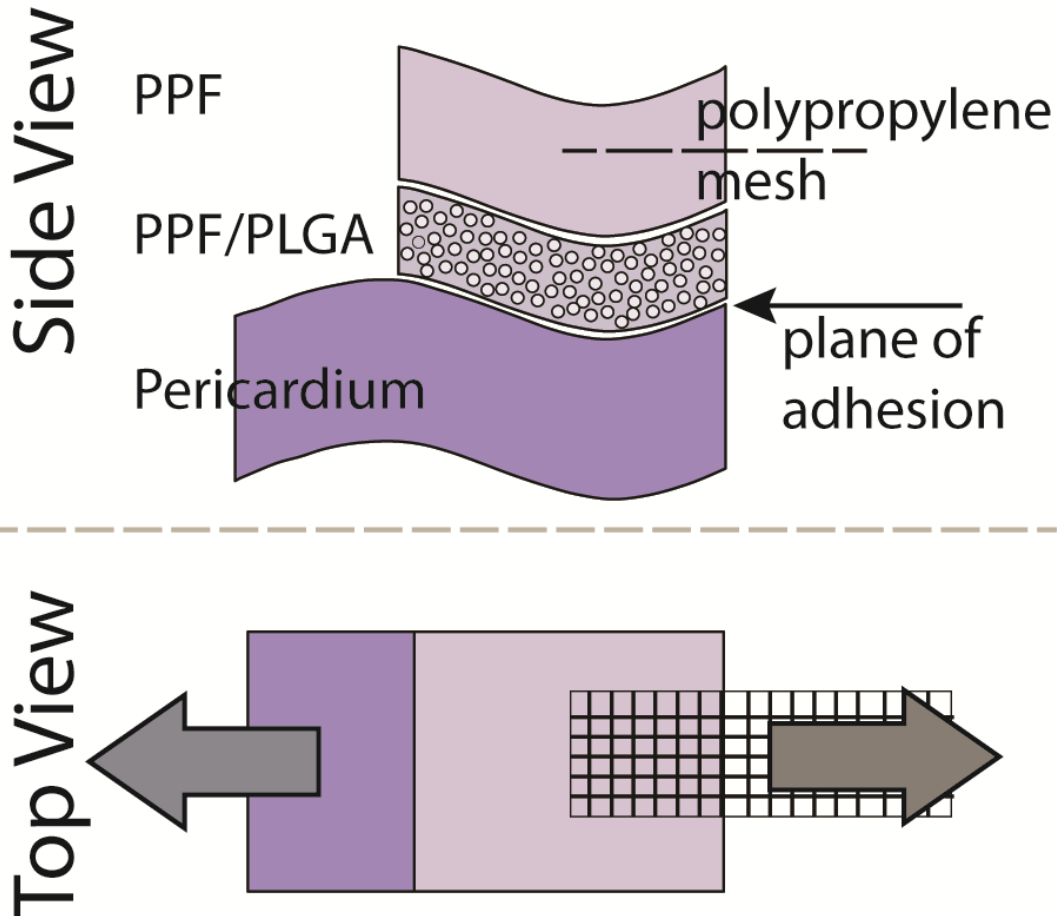


Figure 5. 2 Adhesion Testing Schematic This schematic demonstrates the approach to test adhesion between the polymer layer and the pericardium substrate. Briefly, samples of pericardium were coated in either PPF or the PPF+PLGA microsphere composite. A poly(propylene) mesh of equivalent size to the pericardium was gently pressed into the liquid phase of the PPF top layer. This mesh served as a “tab” to pull the polymer layer the opposite direction as the pericardium, and causing the polymer layer to shear off the pericardium substrate with a measurable amount of force.

during the testing. The whole material was then rehydrated overnight in PBS. Each sample was pulled to failure, by pulling the mesh tab and the pericardium in parallel but opposite directions, on an Instron testing frame, at an extension speed of 10 mm/min, with a sample size of eight per group. Failure is defined when the PPF has separated from the pericardium. Again, a Student's t-test was conducted to assess the difference in adhesion between PPF with and without the PLGA.

5.2.6 Demonstration of Effect on Cells *In vitro*

Release of bioactive factors was first investigated using PLGA microparticles with encapsulated TGF β 3 as a large representative bioactive molecule. These PLGA microparticles were made as previously described, by incorporating 100 ng/mL of recombinant human TGF β 3 (R&D Systems, Minneapolis, MN) into the aqueous phase of particle manufacture. The microparticles were embedded within PPF thin films, and crosslinked with UV light. The composite thin films were then added to human umbilical vein endothelial cell (HUVEC) culture. Over five days, media samples were collected from cell cultures containing the composite thin films and tested for TGF β 3 concentration using an enzyme-linked immunosorbent assay (ELISA). These samples were compared to media samples from cell culture supplemented with soluble TGF β 3, cell culture with blank PPF films, and unaltered cells as control groups. Within each time point, a one-way ANOVA was conducted to compare the TGF β 3 concentration between the samples, followed with a post hoc Tukey's Test.

Delivery of bioactive factors to cells was next assessed through two established bioassays. To confirm that the release of the factor from the composite thin film evoked changes in cell behavior, both a proliferative (VEGF to HUVECs) and a cytotoxic molecule (tumor necrosis factor-alpha (TNF α) to the NCTC clone 929 [L cell, L-929, derivative of Strain L] (ATCC® CCL-1™) (L929)) were released separately, and compared to control cultures with blank PLGA microspheres, both free and embedded in PPF, as well as to pure PPF thin films.

PLGA microspheres were manufactured as previously described. Into the initial aqueous phase, either 40 ng of human recombinant VEGF₁₆₅ (Sigma-Aldrich, St. Louis, MO), or 50 ng/mL of recombinant human TNF α (R&D Systems, Minneapolis, MN) were incorporated per mg of PLGA. Resulting PLGA microspheres were embedded within PPF thin films.

The following assays were carried out using these bioactive films. First, in agreement with previously published results (137, 138), human TNF α composite films were added to L929 cell culture (corresponding to 4 mg of PLGA microspheres, or 6.5 ng/mL of TNF α culture media). Cells were sensitized using actinomycin-D (4 μ g/mL), and metabolic activity was evaluated after 24 hours using an XTT assay. Adequate doses of TNF α are reported to cause apoptotic cell death in L929s when sensitized with actinomycin-D. A dose dependent response of L929s to soluble TNF α was also confirmed with the XTT metabolic assay (Figure 5.3). Absorbance readings from this assay are normalized to the same density of untreated cells, which are

considered to be at 100% metabolic activity. In parallel, VEGF containing films were added to culture of HUVECs (corresponding to 4 mg of PLGA microspheres, or 60 ng/mL culture media). After 72 hours, HUVECs were evaluated using the XTT metabolic assay. Results from each assay were compared to each other using a one-way ANOVA with a post hoc Tukey's test.

Results from these studies were confirmed with fluorescent stains, both Live/Dead and immunohistochemical staining. In the Live/Dead stain, cells are washed with PBS, and then incubated for 45 min with a solution of 4 μ M of calcein AM (Invitrogen, Carlsbad, CA) and 2 μ M of ethidium homodimer (Invitrogen, Carlsbad, CA). For immunohistochemistry, cells were fixed in 4% para-formaldehyde, permeabilized, and blocked following recommendations for the primary antibodies. Cells were stained using the following antibody set and stains: an anti-Collagen I antibody (ab21286, 1:200) followed by a goat anti-rabbit fluorescein isothiocyanate (FITC) conjugated secondary antibody (1:200), an actin stain Alexa Fluor® 594 Phalloidin (2.5%), and a cell nucleus stain VectaShield® plus 4',6-diamidino-2-phenylindole, dihydrochloride (DAPI) (Vector Laboratories).

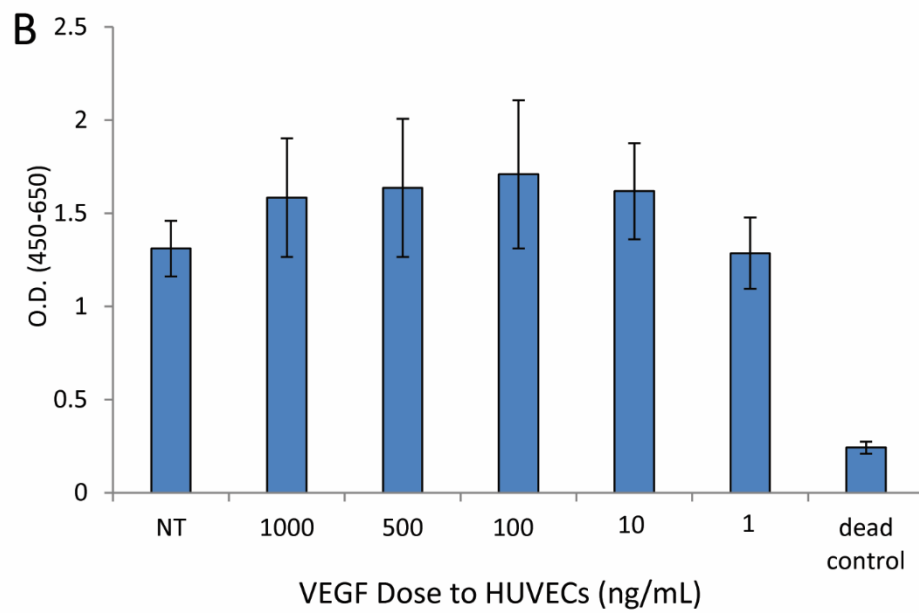
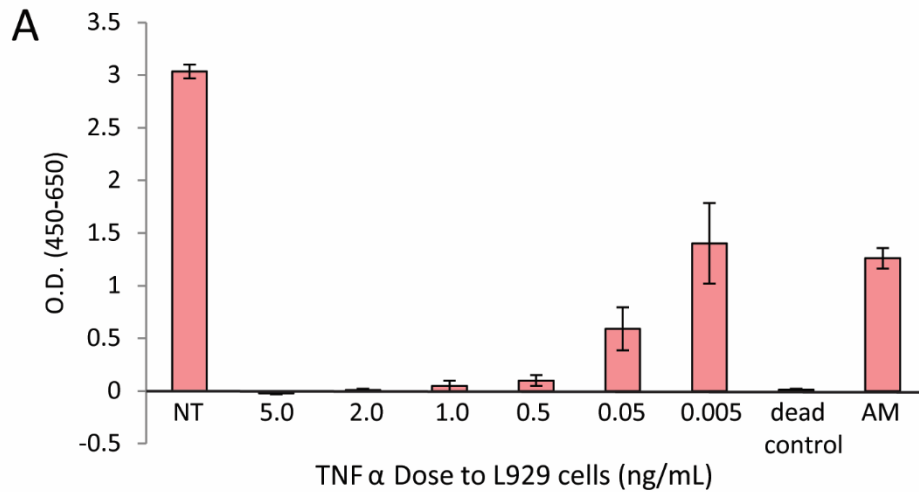


Figure 5. 3 Dose Response for Established Bioassays. Data from XTT analysis confirming the expected result to metabolic activity when various concentrations of TNF α are added to the culture with L929 cells (A) and when VEGF is added to culture with HUVECS (B).

5.2.7 Demonstration of Directional Release

PLGA microspheres with OVA encapsulation were used in this experiment. Pericardium/PPF/PLGA composite samples as well as PPF/pericardium samples were individually submerged in 20 mL of PBS and incubated while shaking at 37°C. At time points of 0, 1, 3, 5, and 7 days, samples from both groups were removed from the study, fixed in 4% paraformaldehyde, and embedded in paraffin for histological examination. PBS solution containing the sample was tested using a Bradford assay for available OVA concentration in the solution.

OVA presence in the pericardium tissue resulting from directed release from PPF/PLGA composite was investigated using immunohistochemistry. Slices of the composite (5 µm) were incubated with BackgroundSNIPER1 (Biocare), a broad spectrum blocking reagent, and then incubated with anti-OVA primary antibody (rabbit polyclonal to OVA, Abcam ab74384, 1:500). This antibody was detected with a biotinylated anti-rabbit IgG (Vector Laboratories, 1:200), and an aminomethylcoumarin (AMCA) conjugated streptavidin (1:200). Fluorescent images were merged with phase contrast images of the construct.

5.3 Results and Discussion

The first objective of this study was to confirm that the mechanical properties of the composite material, specifically elastic modulus, yield strength, and adhesion between the layers, are suitable for use as a graft in the cardiovascular space. Typically, human vessels are reported to have an elastic modulus between 4-12 MPa (femoral artery, saphenous vein) with an ultimate tensile strength between 1-3 MPa

(96, 97, 139-141). Materials used as grafts are reported to have elastic moduli between 5-30 MPa with ultimate tensile strength of 2-10 MPa (54, 63, 98, 142-144), placing these previously developed materials in the same range as the native vessel. It is important to match characteristics such as mechanical strength and compliance with the native tissue, as pointed out in a recent review, since poorly matched mechanical properties can affect remodeling of the site, blood flow dynamics, and cause issues such as bursting or fraying at the sutures (145). Evaluation of the elastic modulus and 0.1% yield strength of our composite material show that the inclusion of PLGA microparticles does not significantly alter the modulus and yield strength of the composite when crosslinked in a thin film, as shown with a Student's t-test ($p > 0.05$) (Figure 5.4 D). Elastic modulus in particular was found to be between 40 and 65 MPa for these materials, both placing it at the high end of the range of moduli from previous engineered vascular graft material, and aligning it with reported values of GA treated pericardium (the surgical gold standard for vascular repair) (63). Furthermore, the adhesion between the PPF and the pericardium layer again are not significantly altered when PLGA microparticles are included in the material (Student's t-test ($p > 0.05$)). In this assessment, both combinations (PPF/pericardium and PPF/PLGA/pericardium) were found to remain adhered until 0.05 MPa of stress. These results suggest that the layered biohybrid material is still within a suitable range for compliant tissue approximation, and will resist delamination at a similar strength to other adhesive surgical glues. In Chapter 2, we found the modulus of unaltered pericardium to be between 20-60 MPa, placing the modulus of the

pericardium/PPF/PLGA material within an appropriate range to interact with the tissue (63).

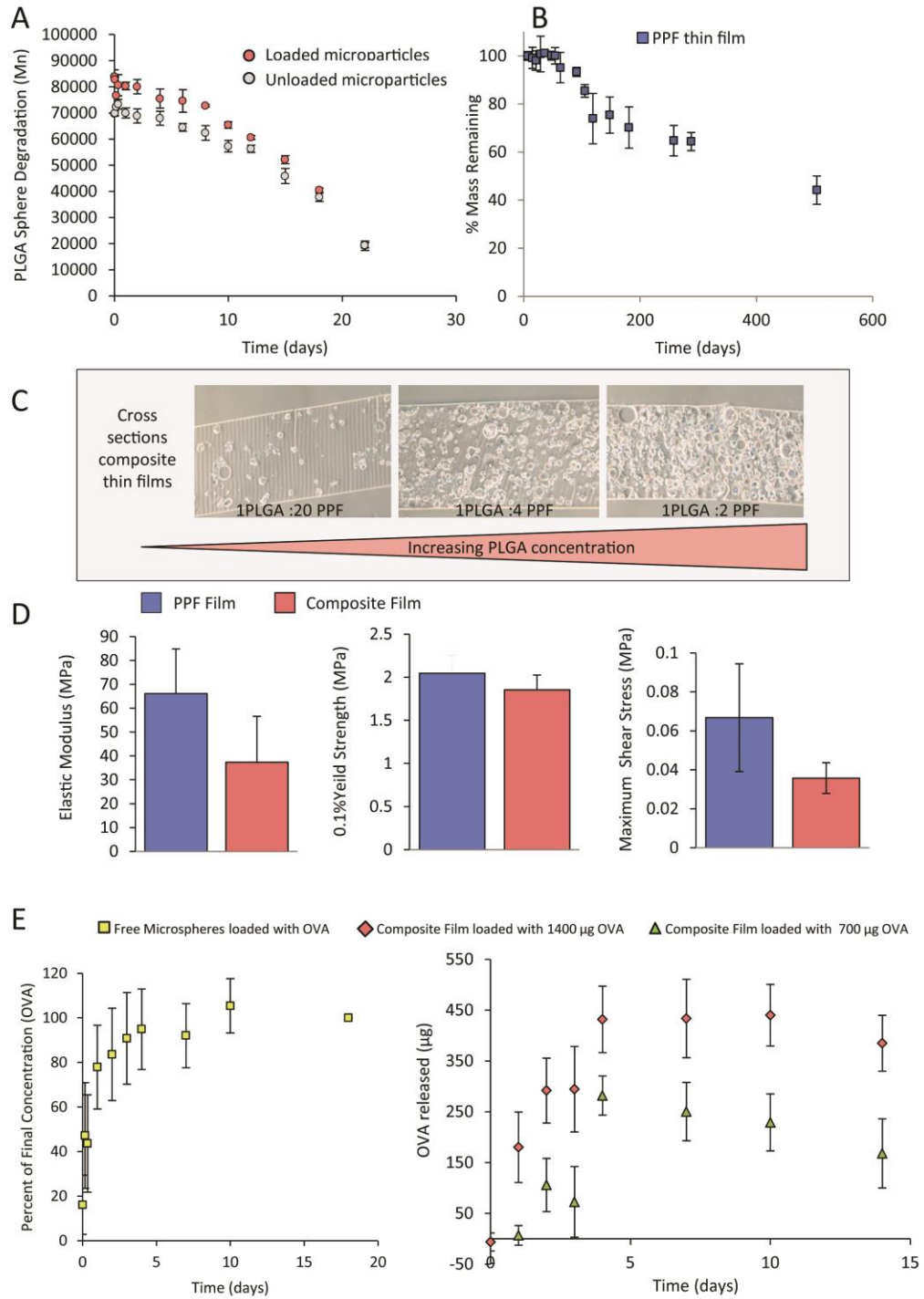


Figure 5. 4 Characterization of the Composite Polymer Layer. In A, degradation of PLGA microspheres with and without OVA encapsulated (loaded vs unloaded) as measured with GPC shows significant loss of molecular weight (Mn) over 20 days (n=3 per time point). This degradation is much faster than the degradation of PPF thin films (Figure 5.4 B), as measured by mass loss over 500 days

(n=6 per time point). C shows bright field images of composite thin films with mass concentrations of PLGA microparticles embedded within them. D shows mechanical analysis of the composite thin films, including elastic modulus, 0.1% yield strength, and the maximum shear stress that can be applied to the biohybrid material before the composite polymer layer separates (n=5 per group). A Student's t-test shows no significant difference between PPF with or without PLGA. Figure 5.4 E shows the release of OVA from PLGA microparticles contained within the PPF film (composite films) (n=6 per time point).

Within this first objective to characterize the composite material, the expected release of proteins as the polymer components degrade was also assessed. The microparticle fabrication resulted in spherical particles with a mean diameter of $25 \pm 11 \mu\text{m}$, which was measured using light microscopy. The degradation of the PLGA microparticles over 21 days is shown in Figure 5.4 A, as decreasing molecular weight from the starting number average molecular weight of 70,000 Da to an average of 20,000 Da by day 21. The average molecular weights between OVA loaded and blank microparticles do not differ statistically, as shown by a Student's t-test ($p > 0.05$) within each time point. The degradation of PPF thin films is also shown in Figure 5.4 B, represented by retained mass % over 500 days. The degradation of PLGA is much faster than PPF, which confirms that the PLGA microparticles will be able to degrade into solution and release bioactive molecules while the PPF remains. The lasting PPF construct retains strength and structure in order to hold PLGA microparticles in place while they completely degrade, as well as to maintain adherence to the pericardium substrate.

The release of OVA from microparticles both free in solution and from within thin films is shown in Figure 5.4 E. The amount of protein is normalized to the mass of PLGA microparticles tested in each experiment. The release of OVA from microparticles shows a constant initial release of protein until day three, at which point the rate of release slows and the concentration of protein in solution remains constant. This constant concentration is indicative of the maximal protein release from the microparticles. The release from composite thin films shows an initial

release during the first three days, and then the concentration in solution remains constant. The initial release from composite thin films was recorded at lower concentrations than that of microparticles alone. This difference is expected due to the reduced surface area of microparticles that are exposed to the solution. The timeline of release observed is in line with other studies that suggest a quick influence of growth factors like VEGF (on the order of days) can affect vascular remodeling and influence the early formation of an endothelial layer, contributing to success of the graft (146-148).

In objective two, the bioactivity of encapsulated cargo was confirmed, to ensure that molecules are not altered in the encapsulation or release process. From the composite thin film, we confirmed that three possible bioactive factors retained functionality through the embedding and release process. First, TGF β 3 concentration was measured in cell cultures with the composite thin films loaded with TGF β 3. This was compared to cultures supplemented with TGF β 3 and from cultures containing blank polymer microspheres and films. Results first show a matching concentration between what was measured with the ELISA to the amount added into culture media (until the media change after day two) (Figure 5.5 B).

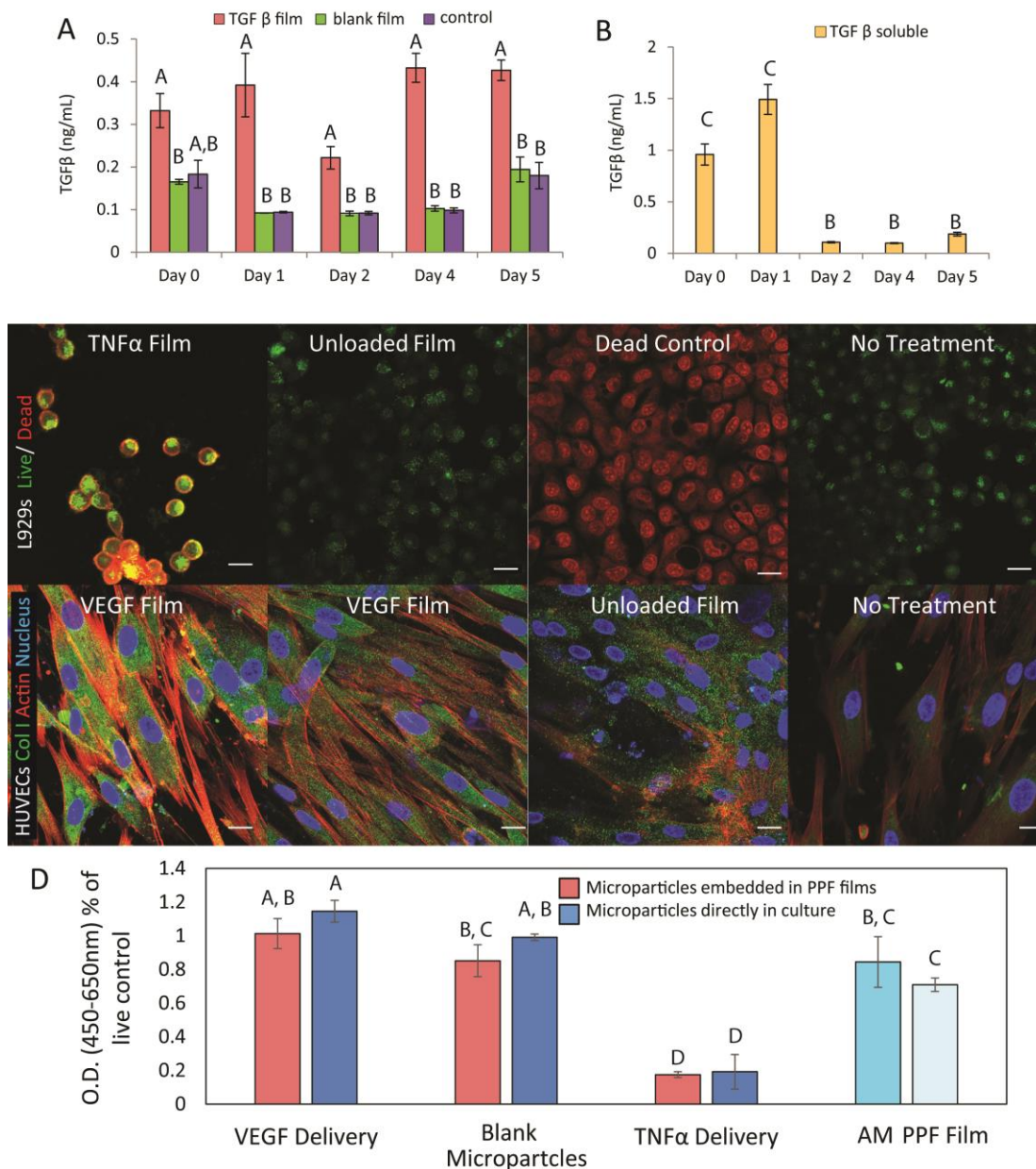


Figure 5.5 Release of Active Growth Factors from Composite Films. TGFβ is released into cell culture from composite films (A) and supplemented into culture (B); the data are separated into panels (A) and (B) due to the significant differences in the ordinate's scale. TGFβ released from composite films shows sustained presence in cell culture over 5 days that is significantly higher than both blank films and control cell cultures (n=3), as well as significantly higher than the supplemented media

groups (B) after the media change between day 1 and day 2. This was confirmed using a one way ANOVA and post hoc Tukey's test to compare groups within the same time point from both panel (A) and panel (B). Groups that do not share a letter in this graph are significantly different ($p < 0.05$). Figure 5.5 C shows fluorescently stained cell cultures after delivery of either TNF α , which is seen to kill L929s, or VEGF, which increases collagen and actin staining in HUVECS. The scale bar represents 20 μm . Figure D corroborates this result with metabolic activity assay of the tested cell cultures ($n=3$). Groups that do not share a letter are significantly different ($p < 0.05$) as determined with a one way ANOVA and post hoc Tukey's test.

Concentration of TGF β 3 in cultures with the composite thin films maintained a moderate level throughout the study, even after the media change, indicating a constant release of the molecule from the composite thin films. The TGF β concentration dips slightly after the media change between day one and day two, but composite films continue to release and sustain the concentration, creating a significantly higher concentration than the supplemented media samples, as determined with a one-way ANOVA and post hoc Tukey's test ($p < 0.05$). The ability of the ELISA to accurately bind and measure concentration of the molecule suggests the molecule retains at least a portion of its original physical conformation, meaning it is unaltered by the encapsulation or release processes. Maintenance of the molecule's physical conformation suggests that the molecule may retain biological activity, although this result for TGF β 3 is untested.

We continued to investigate the retained activity of encapsulated bioactive factors by performing two established bioassays. To confirm that the released factor and not the polymer carriers is responsible for changes cellular behavior, both a proliferative (VEGF to HUVECs) and a cytotoxic molecule (TNF α to L929s) were selected for investigation. Delivering TNF α to L929 cells through a composite thin film resulted in significantly reduced metabolic activity of the cells when compared to cells in culture with blank microparticles, blank microparticles in films, and plain films (Figure 5.5 D), as determined with a one-way ANOVA and post hoc Tukey's test between all groups. This result indicates that TNF α is successfully released from the composite in an active form capable of inducing apoptosis in L929 cells. TNF α doses

were independently confirmed by directly adding TNF α to L929 culture, and assessing metabolic activity (Figure 5.3). The effect of the TNF α composite films on L929s is visually confirmed with the Live/Dead stain (Figure 5.5 C). In Figure 5.5 C, L929s with TNF α composite thin films have reduced population and viability, indicated by the presence of the red stain within the cell membrane. On the other hand, HUVECs in culture with composite films with VEGF show improved metabolic activity when compared to cells in culture with blank microparticles, blank microparticles in films, and plain films (Figure 5.5 C). This result supports VEGF is successfully released from the composite in an active form, capable of inducing proliferation or matrix production in HUVECs. The effect of the composite films on HUVECs can be seen in the immunofluorescent images in Figure 5.5 C, where HUVECs with the composite film appear to have increased density, as well as increased collagen and actin staining compared with the control groups of cells. Both sets of results are consistent with metabolic activity data assessing the effect of soluble factor delivery to cells, which are presented in Figure 5.3A and 5.3B. We have also confirmed the viability of L929 cells in culture with the materials for 2 points over 48 hours, and have presented that information in Figure 5.6.

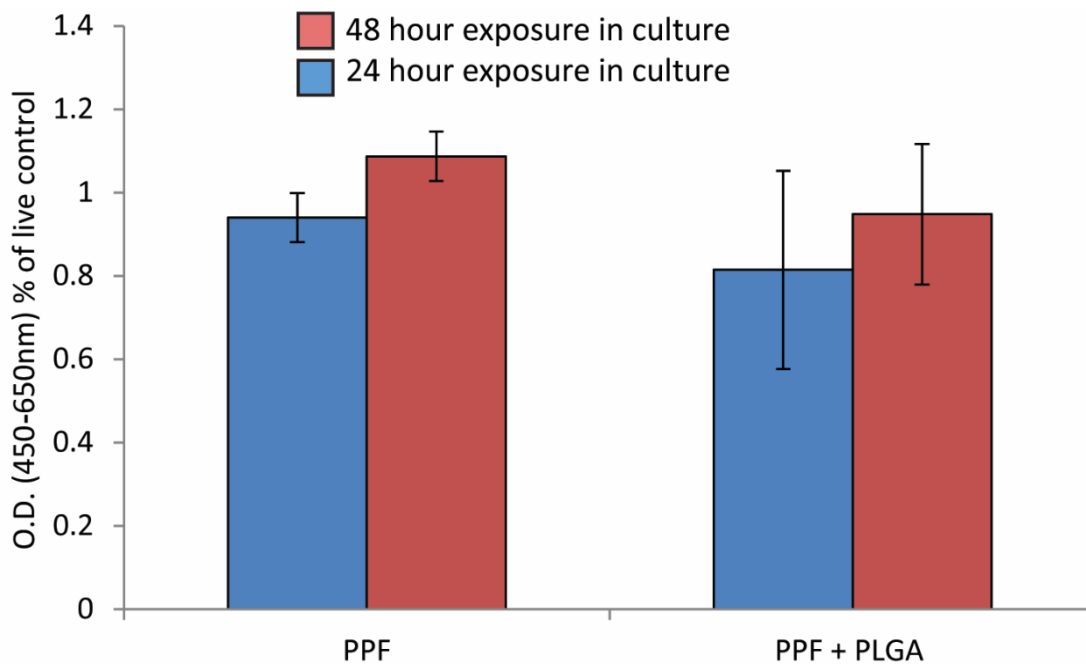


Figure 5. 6 Composite Polymers Effect on Viability. Confirmed viability of L929 cells in culture with the PPF/PLGA composite material for 2 points over 48 hours. Data is presented normalized to the positive, untreated control cells.

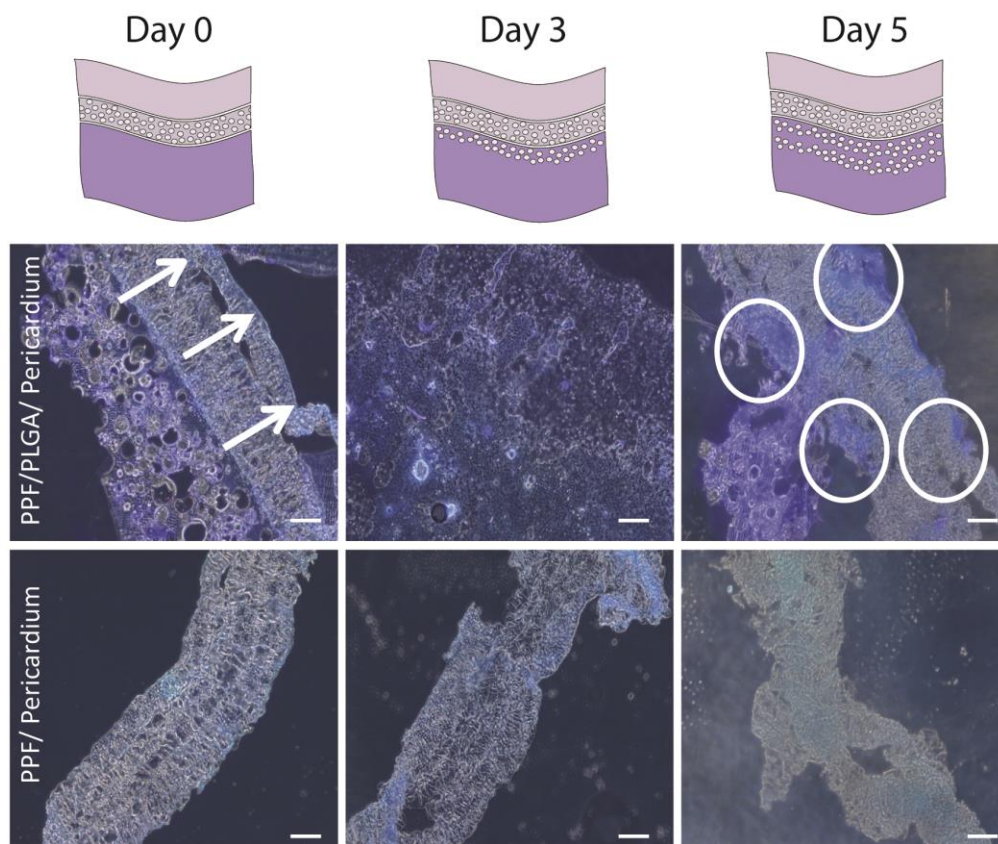


Figure 5. 7 Directional Delivery from Composite Layer into Pericardium Substrate. Pericardium tissue samples coupled with OVA-loaded composite films PLGA/PPF or with just PPF layers were immunostained using an antibody for OVA, indicated with a localized blue stain. Staining shows OVA contained primarily in the polymer layer on day 0, moving into the pericardium tissue by day 5. There is very low blue fluorescence observed in the PPF and pericardium samples, corresponding to the absence of OVA. The scale bar in these images is 50 μm .

In the third objective, the location of released proteins is confirmed in an *in vitro* analysis of the complete biohybrid material. Directional release of OVA into the pericardium substrate is demonstrated in Figure 5.7. A Bradford assay confirms no detectable free OVA in solution in either sample group. However, the histological stains confirm its presence in and around the pericardium layer when delivered with the PLGA/PPF layer of the hybrid. As shown in Figure 5.7, on day 0, before significant hydrolytic degradation has occurred, the OVA stain (blue) is primarily in the PLGA/PPF layer of the construct. By day three, some OVA staining is observed in the tissue, and increases by day five.

By using PPF as a scaffold to encapsulate PLGA microparticles, a tunable and directional release of bioactive molecules can be achieved. As PLGA microparticles degrade hydrolytically into biocompatible molecules, the encapsulated cargo is released and appears to move freely into the space created by degrading surrounding PLGA particles. In this design, that space preferentially sends the bioactive molecules into the pericardium or biomaterial substrate, and exposes the next plane of microspheres for hydrolytic degradation. In addition to the directional release, this design can also be used to achieve either a sequential or simultaneous delivery of multiple growth factors, by creating separate populations of microsphere carriers. Other studies have suggested that delivery of platelet-derived growth factor (149), hepatocyte growth factor (150), brain-derived neurotrophic factor (146) or stromal cell-derived factor-1(151) in addition to VEGF could be beneficial in vascular remodeling, each of which could be delivered using this mechanism.

The much slower degrading interconnected PPF network will initially remain intact as a strong and durable material, but eventually degrades into biocompatible molecules as well. During the remodeling process, the PPF support layer can provide critical mechanical support without causing detrimental side effects such as calcification and fibrosis formation, as demonstrated in previous *in vivo* studies in Chapter 2 and elsewhere (63, 142). In selecting spheres as the vehicle for delivery, we allow the PPF support layer to fill in the spaces between PLGA spheres, therefore ensuring the bulk polymer PPF is adhered to the pericardium substrate in this intermediate layer. This maintains the support relationship as the PLGA microspheres degrade.

Recent studies have reported on hybrid biomaterial systems that have been fabricated, by layering a polymer scaffold with a natural, decellularized matrix-type material for applications in skin (50), cardiac and vascular tissue (30, 53), and abdominal muscle injury(58). This paper serves to advance the technologies used in these systems as it describes a way to build ECM-based biohybrid material that promotes controlled regrowth of the injured site by not only the intrinsic material properties, but also by delivering growth factors and cytokines that can enhance the remodeling process.

5.4 Acknowledgements

Research reported in this publication was supported through a seed grant from Children's National Sheikh Zayed Institute for Pediatric Surgical Innovation and the A. James Clark School of Engineering at the University of Maryland, an American Heart Association Grant # 14PRE20380374 (Laura Bracaglia), as well as the National

Institutes of Health under the Award Number R01 AR061460. The content is solely the responsibility of the authors and does not necessarily represent the official views of the National Institutes of Health. This work was also supported with a Fulbright Fellowship.

Chapter 6: 3D Printed Pericardium Hydrogels Promote Wound Healing Response in Vascular Tissue Scaffolds

6.1 Introduction

Scaffolds that incorporate molecules from the extracellular matrix (ECM) of the target tissue create a bioactive platform upon implantation that can positively influence natural tissue regeneration. Incorporation of these molecules, such as proteins and growth factors, is aimed at mimicking one or more of the responsibilities of the ECM. Constituents of the ECM provide cues for diverse functions such as cell signaling pathways (152), shape and function (153), proliferation and migration (154-156), and cell differentiation (157, 158). Due to broad application, complexity, and tissue specificity of ECM, it is unlikely that a manmade or natural material can recapitulate all the features of the ECM. Evidence is emerging that simply incorporating predetermined building blocks into a tissue engineering scaffold may over simplify the environment, and ignore critical structures, binding sites, and signals critical to development at the implant site.

Scaffolds that instead use tissue derived and site specific ECM have been shown to significantly enhance cell recruitment, support remodeling of the scaffold, and modulate the immune response to enhance healing of the injured site over single or controlled component scaffolds (21, 114, 159). This mechanism is thought to be a result of tissue specific binding sites that promote stem cell differentiation on the

scaffold (160, 161), unique combinations of fibrous proteins like collagen, fibronectin and laminin that support host cell attachment (113), or peptides that modulate the phenotype of arriving macrophages (162).

Modulation of the immune response by these scaffolds is especially relevant in vascular tissue engineering. When scaffolds are implanted, macrophages are among the first responders (124, 125). Upon arrival and differentiation, macrophages can initiate and contribute to wound healing and/or inflammatory pathways that can support or exacerbate the healing process. Beginning with acute inflammatory response to injured endothelial and smooth muscle cells near the implant site, macrophages will phagocytose wound debris, secrete enzymes that work towards tissue reorganization, and produce cytokines and growth factors that cause migration and proliferation of fibroblasts (118) to initiate the reparative response. The dynamics of this process may be effected by the population of macrophages that develop and persist at the injured site (116, 163). If arriving macrophages adopt a healing phenotype, they will aid in the process of regeneration by secreting cytokines like vascular endothelial growth factor (VEGF), insulin-like growth factor 1 (IGF1), or transforming growth factor beta 1 (TGF- β 1) that signal for matrix reorganization and rebuilding, especially by stimulating vessel growth (VEGF) and stabilizing neovessels (platelet derived growth factor) (116). However, if a majority of arriving cells adopt and then sustain a classically activated (M1) phenotype, inflammatory chemoattractants (Interleukin (IL) 1, tumor necrosis factor α (TNF α), IL 12, C-C chemokine receptor type 7 (CCR7)) continue to be disseminated, which perpetuates

the inflammation. This can result in excessive proliferation and formation of a fibrotic capsule (118). In vascular tissue grafts, several studies have now linked an excessive and sustained inflammatory response marked with macrophages (164), natural killer (NK) cells and C-reactive protein (165) to stenosis in as fast as 2 weeks after implantation (166). It is suspected that a higher and sustained density of M1 macrophages impedes the initiation of the remodeling phase, where a more moderate ratio of M1:M2 phenotypes could initiate a healing response. Evidence of this process is observed in that the moderate infiltration of macrophages plays a role in regeneration and neovessel formation (166).

The presence of ECM has been shown to direct the healing response toward the scaffold in an anti-inflammatory way, by causing a macrophage to differentiate more towards the M2 phenotype and a TH2 favored cytokine profile (40, 118, 123, 167, 168). The mechanism, although not fully understood, likely involves cross talk between the arriving macrophages, endothelial cells, as well as other immune modulating cells in response to binding sites, cryptic peptides and adhered growth factors. The degradation of ECM scaffolding is mediated by enzymatic processes, which helps control the release of cryptic peptides from collagen, fibronectin and fibrinogen that can serve as chemoattractants for vascular specific cell types, initiate matrix rebuilding pathways, and modulate proliferation (115, 118, 169-171). In addition to, or perhaps as a result of decreased inflammatory response, ECM scaffolds encourage endogenous repair (113, 172) and promote cell differentiation and the production of new tissue specific markers (23). Most importantly, vascular site

specific ECM scaffolds have been developed by several groups. One such study demonstrates enhanced maturation of cardiomyocytes, cardiac progenitor cells on ECM scaffolds compared to collagen, gelatin, and nonspecific site ECM scaffolds (160, 173). Similarly, another group improved migration of rat endothelial cells, rat aortic smooth muscle cells, and human coronary artery cells compared to collagen scaffolds (172). A third report increased endothelial cell and smooth muscle cell infiltration and *in vivo* arteriole formation in myocardial matrix ECM compared to non-specific ECM (21).

Appropriate cell recruitment and modulation of the inflammatory response are clearly two important processes in vascular tissue engineering that can be achieved by using an ECM-based scaffold. In addition to the importance of chemical constituents, matrix stiffness controls numerous cell functions including durotaxis (174), focal adhesions, cell proliferation (175), and stem cell differentiation (176) of cells recruited to the injured site. Although some ECM components can re-assemble into robust 3D structures on their own, these hydrogels can be relatively weak compared to synthetic hydrogel components, and as such are not suitable as a compliant tissue replacement which is required in the vasculature. Several studies have indicated a change in endothelial cell proliferation and the formation of cell-cell networks depending on the modulus of the hydrogel scaffold (177, 178). Additionally, a compliance mismatch between the graft and the native vessel is linked to intimal hyperplasia of vascular grafts, indicating the importance of appropriate response to pressure of blood flow without permanent deformation (111). Therefore, we propose a

biohybrid material as an approach to combine the bioactivity of an ECM-based material with the strength and controlled degradation of a synthetic polymer.

To build a biohybrid material, we present research here combining decellularized and homogenized bovine pericardium with polyethylene glycol (PEG) diacrylate into a chemically crosslinked hydrogel. Pericardium is a matrix dense tissue, composed of many of the same proteins and glycans as vascular tissue, including the proteins collagen, elastin, fibrillin, and fibronectin (172). The fiber proteins provide tensile strength, while other components act as cell adhesion domains for cell-matrix interaction (118). In particular, glycosaminoglycans (GAGs) act as a reservoir for growth factors and preserve their activity by protecting against enzymatic degradation, while also holding them to a specific location (118). Additionally, pericardium is sparsely cellularized, and due to the easily removed, light DNA content, it is an ideal candidate to donate xenographic tissue (112, 179, 180). Pericardium has been used extensively in graft and scaffold material (113) although it is primarily used in cardiovascular applications (113) due to its high collagen content, which gives it superb mechanical strength.

PEG has been used extensively in biological scaffolds as well, and is often chosen to intentionally not react with the host due to the non-adhesive nature of PEG polymer chains (181). However, it can be modified to be included in scaffold that on the whole is both bioactive and biodegradable (78). In these applications, it is used primarily as an inert carrier to present proteins and other biomolecules to the host (60, 144), and in

this way does not interfere with the tissue specific composition of the ECM. PEG has been selected to enhance the mechanical properties of ECM hydrogels specifically in porcine cartilage and gelatin methacrylate (gelMA) (182), myocardial matrix (80) and collagen (183, 184).

To increase the elastic modulus of homogenized pericardium in a way that does not interfere with the biochemical content, we propose to chemically react PEG with the proteins in homogenized pericardium matrix (HPM). The objectives of this work are to first derive active matrix components from pericardium, and then form a controllable and structurally strong hydrogel scaffold. To achieve the utmost architectural control, we will develop this hydrogel for a cyto-compatible printing method using visible light photoinitiation and digital stereolithography. With this scaffold, we can then direct the signs of vascular regrowth and inflammatory response that are induced or supported by our scaffolds using various mechanical strengths to effect endothelial cell growth and concentrations of ECM to effect macrophage polarization. Understanding the interaction between arriving macrophages, endothelial cells, and the designed scaffold is essential in the regeneration process for vascular tissue. Looking at these two cell populations in co-culture can allow us to experimentally measure their interaction with each other and the material scaffold. We hypothesize that the addition of PEG to HPM will result in an increased elastic modulus, and will also slow the presentation of ECM, allowing for a moderate inflammatory response from co-cultured macrophages.

6.2 Methods

6.2.1 Tissue Homogenization

Whole bovine pericardium was obtained fresh from Innovative Research, Inc. Decellularization was conducted similarly to previously established methods (172, 185). To homogenize, the tissue was first rinsed to remove blood and excess fascia. Next, it was cut into 1 cm² squares which were flash frozen in liquid nitrogen. Frozen samples were then mechanically ground into a fine powder (Krupps, F203 Electric Grinder with Stainless Steel Blades). Pericardium powder was lyophilized to obtain total tissue mass. This powder was then digested at a concentration of 10 mg/mL with 1 mg/mL of the enzyme pepsin. For digestion, the pH of this solution was adjusted to 2 using 1M HCl. After 72 hours, the solution was neutralized to a pH of 7.4 using 1M NaOH, and the salt concentration adjusted by adding 10x phosphate buffered saline at 1/9th of the digest volume. The neutralized, homogenized pericardium matrix (HPM) was then frozen at -20 °C until time of use.

6.2.2 HPM Characterization

Concentrations of various protein components in the HPM were determined using the following assays: total protein was tested using the Bradford Assay (ThermoFisher), collagen concentration was determined using the hydroxyproline assay (Sigma Aldrich), and glycosaminoglycan (GAG) concentration was determined using the dimethyl-methylene blue (DMMB) assay. DNA content remaining in the HPM was quantified using a PicoGreen Assay. All concentrations determined were expressed as part of the mass of dry HPM.

Samples of HPM were diluted to 1 mg/mL total protein and prepared for sodium dodecyl sulfate-polyacrylamide gel electrophoresis (SDS-PAGE) following standard protocols (BioRad). Briefly, samples were mixed with 25% laemmli buffer containing 10% β -mercaptoethanol, heated at 95 °C for 5 min, and then loaded into a 4–15% Mini-PROTEAN® TGX Stain-Free™ Protein Gel (BioRad). Standard human collagen type I (Corning, Corning NY) was also run as a control. SDS-PAGE gels were stained with coomassie brilliant blue for total protein bands. Protein bands were also transferred to nitrocellulose membranes and stained using primary antibodies for collagen I (Rabbit Polyclonal Collagen I alpha 1 (1:5000 dilution), fibronectin (Rabbit Polyclonal Fibronectin/Anastellin 1:1000 dilution) and collagen IV (Rabbit Polyclonal Collagen IV alpha 1, 1:1000 dilution) (Novus Biologicals). Positive staining was detected using IRDye® 800CW Goat anti-Rabbit IgG fluorescent secondary antibodies (LI-COR) on an Odyssey CLx Platform (LI-COR).

For mass spectrometry and protein identification, SDS-PAGE gels were digested with sequencing grade Trypsin (Promega) and resulting peptides were extracted with Acetonitrile-Formic acid buffer. The peptide mixtures were sequentially analyzed by LC-MS/MS using nano-LC system (Easy nLC1000) connected to Q Exactive mass spectrometer (Thermo Scientific). The mass spectrometry data was collected in data-dependent manner switching between one full scan MS mode (m/z 380-1600, resolution 70,000, AGC 3×10^6) and 10 MS/MS mode (resolution 17,500); where

MS/MS analysis of the top 10 target ions were performed once and dynamically excluded from the list for 20 seconds.

6.2.3 PEG +HPM Hydrogel Formation

Two forms of modified PEG were investigated: 4arm PEG Acrylate (20,000 kDa, JenKem Technologies USA, Plano Texas) and PEG diacrylate (5,000 kDa, Laysan Biologics). PEG and HPM hydrogels were formed using the visible light photopolymerization method described by Bahney et al (186). In this reaction, eosin-Y acts as a photosensitizer, excited at a wavelength of 510 nm. Activated eosin-Y can then deprotonate triethanolamine (TEA), which in the presence of n-vinylpyrrolidone (NVP) can initiate crosslinking between the acrylates and the free amines in the ECM proteins. The following concentrations of initiators were investigated in this study:

Table 6.1 Photoinitiator Concentrations

<i>Reagent</i>	<i>Concentration</i>
<i>Eosin- Y</i>	<i>0.01- 0.1mM</i>
<i>TEA</i>	<i>0.05-0.75%</i>
<i>NVP</i>	<i>18-37nM</i>

To create 3 dimensional scaffolds, shapes were first designed using SolidWorks® (Waltham, MA). Scaffolds were then fabricated using an EnvisionTEC Perfactory® P4 (EnvisionTEC, Detroit, MI). Using digital stereolithography, the liquid resin (containing PEG, ±HPM, and photoinitiators) was crosslinked with an exposure of 800 mW/dm² for 240 seconds per 100 µm step size. Optimal combination of reagents were selected to minimize time to crosslink among samples that supported at least 70% cell viability.

6.2.4 Evaluation of PEG+HPM hydrogels

Hydrogels were formed as described above using 5% PEGda, 1% HPM, 0.5% TEA, 10 μ M EOSIN and 37 mM NVP. Concentration of free amines were quantified in pre and post-crosslinked materials and solutions using a TNBSA assay (Sigma) to confirm the reaction had taken place. In addition, pre and post crosslinked materials were examined using Fourier transform infrared spectroscopy (FTIR). FTIR measurements were acquired using a Smiths IlluminatIR II with samples mounted on MirrIR Low-e Microscope Slides (Kevley Technologies). 128 scans per sample were taken under ATR mode, imaging a 100 μ m² area, with background computed and removed for each measurement. Samples (n=6 per test set) were run per conditioned and the average absorbance vs. wavenumber (cm⁻¹) was computed.

Biodegradation was compared between PEG hydrogels without HPM (referred to as PEG (-)) and PEG hydrogels with 1% HPM (w/v) (referred to as PEG+HPM). For this test, 10 cylindrical scaffolds (diameter 7mm, height 5mm) were formed for each of the following compositions: 5% starPEG-acrylate + 1% HPM, 5% starPEG-acrylate without 1% HPM, 5% PEGDA + 1% HPM 5% PEGDA without 1% HPM. All scaffolds were crosslinked with 0.5% TEA, 10 μ M EOSIN and 37 mM NVP. Scaffolds were lyophilized to obtain starting mass. Five from each group were submerged in water, and the remaining 5 were submerged in 0.4 U/mL of collagenase. After 5 days, gels were rinsed with water and lyophilized again. Degradation is represented by percent mass loss using the following equation:

$$\% \text{ Mass Loss} = \left(1 - \frac{\text{Mass}_{\text{initial}} - \text{Mass}_{\text{final}}}{\text{Mass}_{\text{initial}}} \right) \times 100$$

Dynamic mechanical analysis (DMA) was conducted on a Q800 DMA (TA Instruments). Discs of hydrogel scaffolds were formed (diameter 7mm, height 5mm) using the formulations listed in Table 2. Scaffolds were first treated with a preload of 0.01 N, and then were tested using a strain sweep with a fixed frequency (1 Hz) to determine the stress-strain curve and the compressive modulus. From each formulation, 5 scaffolds were tested, and standard deviations are reported.

Table 6.2 Concentrations of Hybrid Hydrogels

PEGda	HPM
10%	0%
	0.5%
	1%
5%	0%
	0.5%
	0.2%
	1%
0%	10%

6.2.5 Cell Metabolic Activity Assay

The cell line L929 (ATCC) was cultured according to supplier instructions, and used for basic viability testing. Hydrogel scaffolds were formed using combinations of the reagents listed in Table 1, and crosslinked in 96 well plates to facilitate even and consistent surfaces for seeding. Cells were seeded onto scaffolds ($3.1 \times 10^4/\text{cm}^2$), and cultured at 37 °C for 3 days. Cell metabolic activity was quantitatively assessed using Cell Proliferation Kit II (Roche, Mainheim, Germany). XTT [2, 3-bis-(2-methoxy-4-nitro-5-sulfophenyl)-2H-tetrazolium-5-carboxanilide] was used in this assay following manufacturer’s instructions. The solution of XTT labeling and electron coupling reagents was added to cell culture wells and incubated at 37 °C for 4 hours.

Net absorbance was then measured (A450-A650) for each sample. Cells grown on tissue culture polystyrene were used to set 100% metabolic activity.

To assess the bioactivity of the incorporated HPM, PEG hydrogels were formed with and without HPM. Human umbilical vein endothelial cells (HUVECs) were seeded on top of hydrogel scaffolds, and cultured at 37 °C for 3 days. After 3 days, cells were lifted using trypsin, and the supernatant was collected and combined with an acetic acid rinse of the scaffold. Collagen was quantified using the hydroxyproline assay. Hydrogel scaffolds without HUVECs were included as a baseline for collagen content within the scaffold.

6.2.6 Isolation of Bone Marrow

Whole, unprocessed bone marrow was obtained from male adult Sprague Dawley rats and processed as described in published protocols (187, 188). Briefly, bone marrow is flushed from the femur and tibia to obtain bone marrow progenitor cells. Cells were plated onto non-treated petri dishes in macrophage complete media (DMEM/F12 supplemented with 10mM glutamine, 100 U/mL penicillin and 100ug/mL streptomycin and 10% (v/v) of fetal bovine serum plus 100 U/mL of recombinant granulocyte macrophage colony stimulating factor (Peprotech)). At day 4, media was supplemented with the same volume of fresh macrophage complete media. After 7 days of culture, non-adherent cells are eliminated. Adherent cells are harvested with light cell scraping, and plated at a density of 3.1×10^5 cells/cm².

6.2.7 Macrophage response to HPM components

Sterile filtered HPM was added to macrophage culture in the concentrations of 3 mg/mL, 1.5 mg/mL, and 0.3 mg/mL. As controls, separate macrophages were polarized using either 150 U/mL IFN γ or 120 ng/mL IL 4 and 40 ng/mL IL 13 (189). After 6 hours, 100 ng/mL lipopolysaccharide was added to control cultures to stimulate cells (190). After 6 hours of either HPM or LPS addition, cells were harvested using cell scraping to extract RNA. After 24 hours, other groups were fixed with 4% paraformaldehyde to stain for cell surface markers and media was collected for cytokine analysis.

6.2.8 Quantitative reverse transcriptase-polymerase chain reaction (QT-PCR)

RNA was isolated using an RNeasy Mini Plus Kit (Qiagen, Valencia, CA) following standard procedures. Isolated RNA was then reverse transcribed to cDNA using a High Capacity cDNA Reverse Transcription Kit (Applied Biosystems).

Glyceraldehyde-3-phosphatase dehydrogenase (GAPDH) was used as an endogenous control gene for all samples.

Gene expression assays were combined with the cDNA from each sample and TaqMan PCR Master Mix II (Applied Biosystems). The reaction was conducted on a 7900HT real-time PCR system (Applied Biosystems) using thermal conditions of 2 min at 50 °C, 10 min at 95, and 40 cycles of 15 seconds at 95 and 1 min at 60. The relative gene expression level of each target was normalized to the mean of the GAPDH level, and then fold change was calculated using the $\Delta\Delta$ CT method. Samples were completed in triplicate and the standard deviations are reported.

6.2.9 Co-culture experiment to evaluate response to ECM Hydrogel

Rat aortic endothelial cells (RAECs) were purchased from Cell Biologics, and cultured according to suppliers instructions. PEG + HPM scaffolds were prepared as previously described, following the concentrations in Table 2. To investigate the contribution from complete ECM, a PEG + Collagen scaffold was added. RAECs were seeded (1.3×10^5 cells/cm²) onto hydrogels and cultured at 37 °C for 3 days to allow them to come to confluency on the surface of the gel. Naïve monocytes were added to cell culture on Day 4 at a density of (3.1×10^5 cells/cm²). Media was replaced with a mixture of RAEC media and macrophage complete media in a 50:50 ratio for all samples. For QT-PCR analysis, cells were harvested (n=3 from each group) 6 hours after addition of monocytes. Media extracts from the remaining scaffolds (n=3 from each group) were taken at 24 hours for cytokine analysis, and the scaffolds were fixed using 4% paraformaldehyde 1% sucrose for immunostaining. Scaffolds were then rinsed with PBS, followed by a permeabilization buffer and background blocker for 15 min. Cells were stained using the following antibody set and stains: a mouse anti-CD68 antibody (Abcam, 1:100) and goat anti-mouse FITC conjugated secondary antibody (Abcam, 1:200), a rabbit anti-CD206 antibody (Abcam, 1:600) and a donkey anti-rabbit Alexa Fluor®647 secondary (Abcam, 1:200), a goat anti-CD86 antibody (Novus Biologics, 1:200) and donkey anti-goat Alexa Fluor®555 secondary (Abcam, 1:200), a rabbit anti-von Willebrand Factor antibody (Abcam, 1:100) and a donkey anti-rabbit Alexa Fluor®647 secondary (1:200), or finally, an actin stain Alexa Fluor® 594 Phalloidin (Invitrogen, 2.5%), and a cell nucleus stain DAPI (Vector Laboratories).

Table 6.3 Hydrogel Scaffolds for Co-Culture

	RBM	RAEC	RBM + RAEC
1%HPM	6	6	6
5% PEG	6	6	6
5%PEG + 0.5% HPM	6	6	6
5% PEG + 0.1% HPM	6	6	6
5% PEG + 0.1% Collagen	6	6	6

6.2.10 Statistical Analysis

Data was analyzed using a one way analysis of variance (ANOVA), followed by a post hoc Tukey's test using a 95% confidence interval. Data plotted represents the mean with standard deviation.

6.3 Results and Discussion

The first objective of this study was to extract active matrix components from pericardium that could be incorporated into a shape-controlled hydrogel scaffold. Bovine pericardium was successfully decellularized and homogenized, resulting in a water soluble, protein powder. If reconstituted at 10 mg/mL, the HPM assembles at 37 °C into a solid hydrogel (as compared to the same formulation at 4°C in Figure 6.1D, and in a cylindrical mold, Figure 6.1E). From 1 mg of tissue, the final components of homogenized pericardium matrix (HPM) were determined to be 0.8 mg of protein using a Bradford assay. Of that protein, at least 80% was determined to be collagen using a hydroxyproline quantification and compared to a collagen control. We additionally determined 7.8 µg GAG/mg HPM. Finally, in 10 mg of tissue, less than 50 ng of DNA content was detected. These results are detailed in Figure 6.1A. To more specifically identify the protein components, samples of HPM were analyzed using SDS-PAGE (Figure 6.1B). As shown, the total protein bands in HPM are in similar locations to the control rat tail collagen I, but are also present at several other distinct locations. Some of these bands were further assessed using antibody specific western blotting, and were identified as collagen I, collagen IV, and fibronectin.

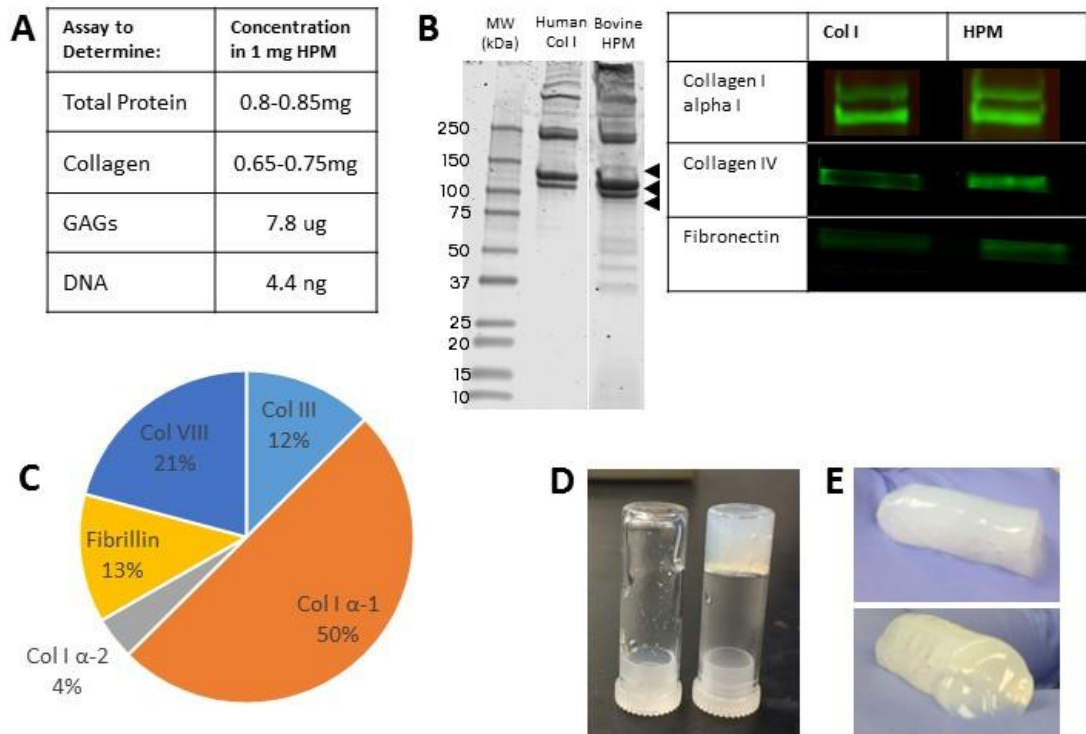


Figure 6. 1 HPM Characterization. Protein quantification and colorimetric assays were used to determine the molecular concentrations in the HPM, and displayed as concentrations per mg of dry HPM (n=15) (A). HPM was analyzed using SDS-PAGE (B) and stained for total protein. HPM is compared to a standard of rat tail collagen I, and arrows indicate bands appearing in HPM that were further characterized using antibody specific staining on the right. The final characterization was completed using mass spectrometry, and proteins existing in significant quantities are displayed by total percent (C). The final product HPM is capable of forming a thermally crosslinked hydrogel, as compared to the same material stored at 4C (D). The hydrogel can maintain shape integrity, as shown from a cylindrical mold (E).

As a control, a sample of gelatin was compared to the HPM electrophoresis (data not shown) to ensure the integrity of the protein molecules in HPM. The variety of structural proteins were confirmed using mass spectrometry (Figure 6.1C). We were able to confirm collagen I, III, VIII and fibrillin. These results support the design of using site specific ECM-based source for the bioactivity within a scaffold. Building a scaffold using a simple cocktail of collagen I and fibrillin for example, could oversimplify and eliminate some critical matrix components that HPM provides, such as fibronectin for cell adhesion points or GAGs for sequestering growth factors (118). The composition of the vascular environment is complex, and distinct from protein profiles identified in other tissues.

As described, although HPM is capable of forming a hydrogel on its own, the resulting hydrogel is weak and lacks spatial resolution that could be important in developing vascular scaffolds. To improve on the mechanical integrity and spatial control, we combine HPM with PEGacrylate using a photoinitiated crosslinking system. To confirm this reaction is taking place between the HPM and the PEGacrylate, we can compare the concentration of free amines before and after crosslinking. Crosslinking HPM with PEGacrylate reduced the primary amine concentration significantly when compared to the uncrosslinked materials, indicating that the free amines in HPM are now bound to acrylates in PEG (Figure 6.2A). Similarly, the FTIR spectra of the crosslinked sample displays a reduced peak around the 1600 wavenumber compared to the uncrosslinked HPM, demonstrating a change to the primary amine group (Figure 6.2B). Finally, in a degradation test, the PEG

HPM hydrogel is seen to lose significantly more mass in both water and with collagenase than PEG (-) gels in collagenase (Figure 6.2C). The average mass loss is greater than the 1% HPM incorporated into the gels, suggesting that this result is not simply the HPM content leaching out of a crosslinked PEG-PEG hydrogel. Taken together, these results indicate that a chemically crosslinked network is formed between the PEG molecules and the proteins in the HPM, creating a hybrid, biodegradable scaffold.

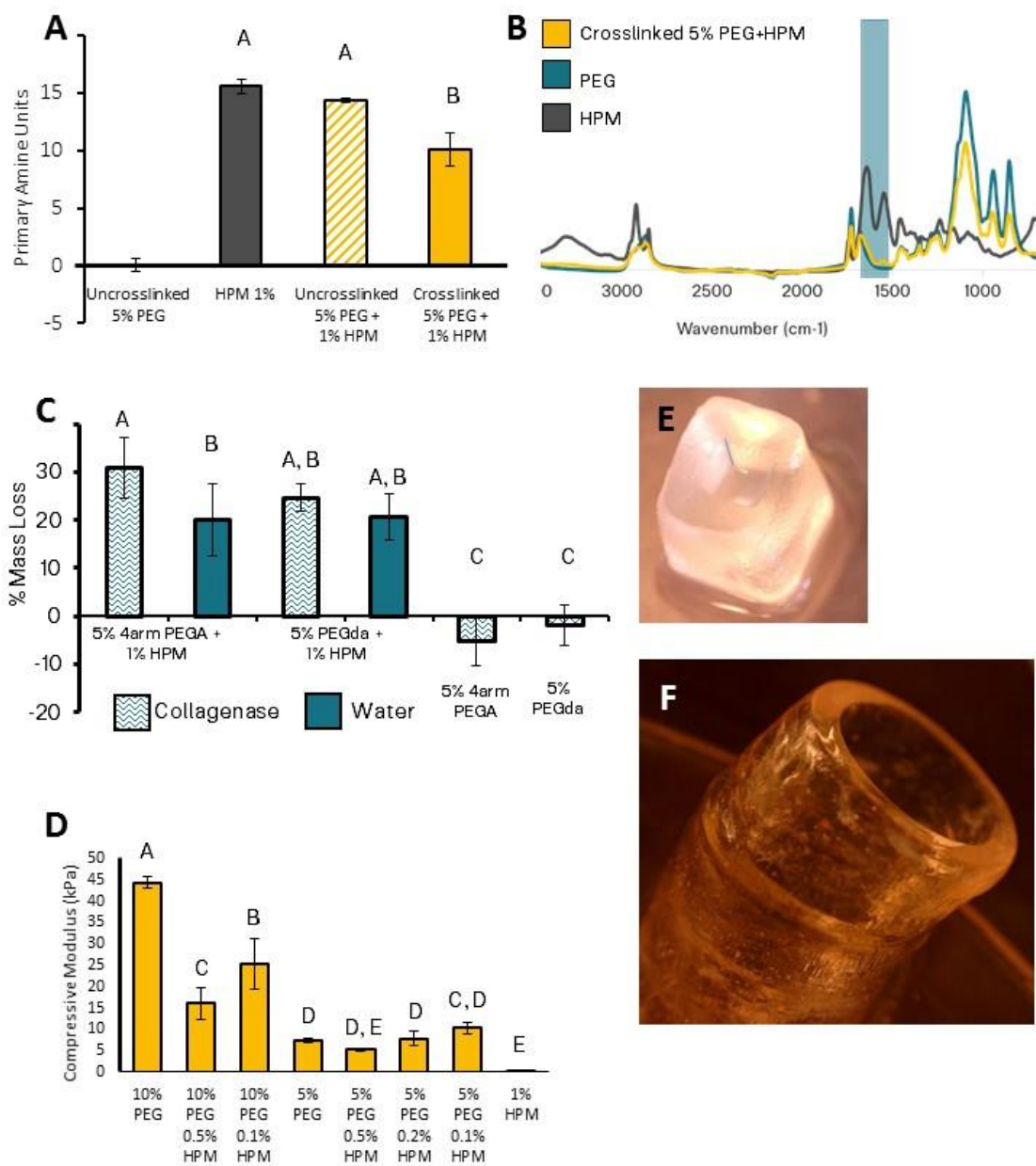


Figure 6. 2 HPM PEG Hydrogel Formation. A reduction in the total concentration of amines in the HPM PEG hydrogel compared to the uncrosslinked components demonstrates successful formation of the network (n=3) (A). In the FTIR spectra (B), a change near the 1600 wavenumber also indicates a change to the free amine group after crosslinking (n=6). Mass loss from hydrogels over 3 days with and without collagenase indicated the biodegradability of the hybrid hydrogels, as compared to PEG (-) hydrogels (n=5) (C). Compressive modulus was also evaluated in scaffolds formed with varying concentrations of HPM and PEG (n=5) (D). The greatest significance is seen as a result of PEG

content, however, changes to modulus are also seen as a result of HPM concentration. Images display the 3D printing capability of this hydrogel, showing a 5mm hollow prism with 1 mm wall thickness (E), and a curved vascular model, with an inner diameter of 6mm and a wall thickness of 1.5mm (F). Significance between groups was determined using an ANOVA, with a post hoc Tukey's test. Groups that do not share a letter are significantly different ($p < 0.05$).

Compressive modulus of hydrogels with degrees of HPM and PEG was determined to demonstrate that the strength of HPM can be supplemented by addition of PEG (shown in Figure 6.2D). The range of achievable modulus for the hybrid hydrogel is bound by the modulus of the two single component hydrogels: 10% PEGda (-) at 45 kPa and 1% HPM at 0.5 kPa. We observe that although the modulus of the hybrid hydrogels seems to be primarily controlled by the concentration of PEGda included, the amount of HPM can have a significant effect on the end result. As an example, the 10% PEG sample set is significantly stiffer than 10% PEG + 0.1% HPM, which is significantly stiffer than 10% PEG with 0.5% HPM. Gels with 5% PEG are all less stiff than any of the 10% PEG gels groups, but also have variations based on concentration of HPM incorporated. All of these groups (except 5% PEG + 0.5% HPM) are significantly distinct from 10% PEG or 1% HPM (the individual constituent hydrogels). Other groups have reported significant differences in parameters such as endothelial cell proliferation, ECM production, and cell-cell network formation on matrices spanning 0.05 to 10 kPa, with different stiffness promoting different behaviors (177, 191). In one study, endothelial cell proliferation was reported to increase on scaffolds of 20 kPa over scaffolds of 2 kPa (178). This indicates that the inclusion of PEG in the HPM scaffold could improve the formation of an endothelial layer by increasing the stiffness of the substrate. A well-formed endothelial layer could improve the long term success of a vascular graft, as well as contribute to a healing macrophage phenotype.

By successfully forming a photocrosslinked network of PEG and HPM, we can use 3D printing to achieve spatial control that unobtainable through casting methods. Figure 6.1E and Figure 6.1F demonstrate spatial resolution obtained using digital light projection (DLP) printing. Figure 6.1F shows a curved vascular graft with an inner diameter of 6mm, and a wall thickness of 1.5 mm, fitting approximately the size of an infant aortic arch.

After development of this hybrid hydrogel, the second objective of this work was to use the scaffold to show an environment that supports vascular regrowth and a moderate inflammatory response. We hypothesized that the addition of HPM would increase endothelial cell spreading matrix production, due to binding sites in the HPM. Furthermore, we hypothesized that the addition of PEG to HPM scaffolds would slow or dilute the presentation of ECM molecules, allowing for a decreased inflammatory response compared to HPM alone.

We first investigated cell viability in response to our hydrogels based on photoinitiator content, since PEG and HPM are established non cytotoxic materials. L929 cells seeded onto hydrogels with various initiator concentrations showed affected metabolic activities, compared to L929s on plastic (100% metabolic activity) and L929s on plastic fixed with methanol (0% metabolic activity). Results indicate that the initiator TEA appears to have the largest impact on cell metabolic activity, and was therefore kept at or below 0.5% for the remainder of the studies (Figure 6.3A). We suspect that the low cell metabolic activity from the highest initiator could

be in part attributed to ineffective crosslinking of the polymers at the highest concentrations of initiator.

We next investigated bioactivity of the incorporated HPM using HUVECs. A comparison of extracellular collagen production shows significantly higher concentrations after 3 days when HUVECs are seeded on PEG + HPM scaffolds compared to PEG (-) scaffolds (Figure 6.3B). This result suggests a favorable and familiar environment to vascular specific cells, indicated by the construction of tissue specific matrix. To confirm, HUVECs on HPM hydrogels and PEG hydrogels were stained for cytoskeletal actin to visualize morphology. HUVECs on HPM appear to have spread further, and formed more networks (Figure 6.3C). Additionally, RAECs seeded on the hydrogels were stained for von Willebrand factor, and show more cell-cell networks on the HPM hydrogel than the PEG hydrogel (Figure 6.3D).

Similarly, HPM added to macrophage culture directs different polarization depending on the concentration of HPM (Figure 6.3E). Looking at the expression of mRNA for 5 key cytokines, the control populations differ for several genes. In particular, the M2 control population has a more upregulated CD163 and IL 10 (M2 markers) and slightly less upregulated IL 1 β and TNF α than the M1 controls. Averaging the fold change for all the M1 markers and dividing by the average fold change for the M2 markers shows a ratio of either more than 1 in the M1 controls, indicating an M1 phenotype, and less than 1 in the M2 controls, indicating a M2 phenotype (Figure 6.3F). When low (0.03% w/v) HPM is added to the culture, macrophages behave in a

similar way to the M2 control, upregulating IL 10 more than the M1 controls. However, even though CD 163 is downregulated in this set, the ratio still favors an M2 response. As HPM concentration is increased, the IL10 and CD163 expression decreases, while IL1 β and TNF α slightly increase. These observations are noted in the ratio, showing a greater than 1 for both the medium and high concentrations of HPM.

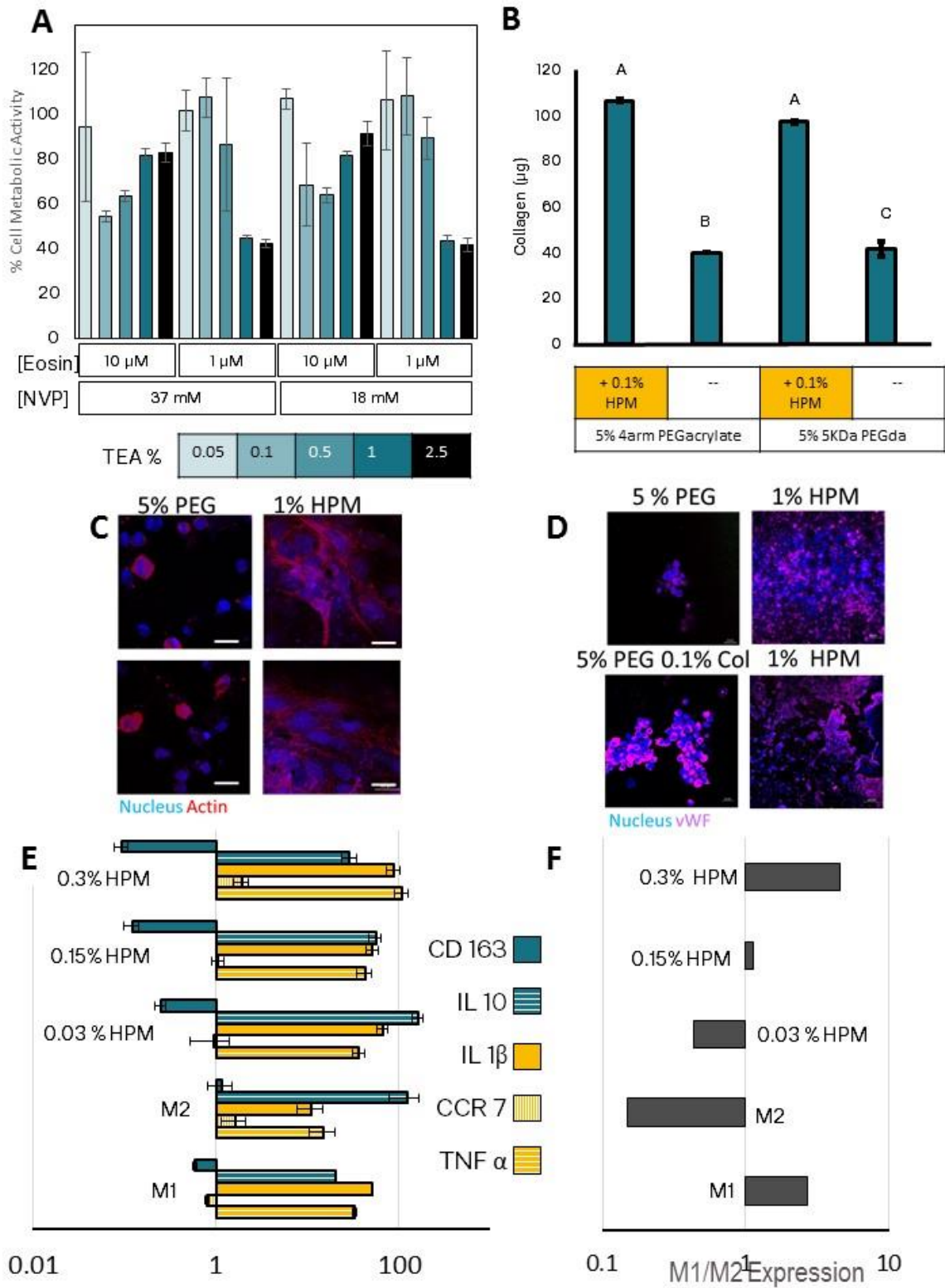


Figure 6. 3 Cell Response to Hybrid Hydrogel Components. L929 cells were found to maintain a metabolic activity of 70% or greater when TEA concentration was reduced to 0.5% or below (n=3 cell cultures) (A). When HUVECs were seeded on either hybrid hydrogels they lay more collagen matrix

than on PEG (-) hydrogels (n=3) (B). HUVECs on HPM hydrogels are stained for actin (red) in Figure 6.3C, and show morphology changes compared to HUVECs on PEG(-). Similarly, RAECs on HPM gels show more staining for von Willebrand factor (purple) than RAECs on PEG or PEG +Collagen scaffolds (D). RMCs expression of inflammatory or healing genes shows differences in response to HPM concentration (E). M1 and M2 control populations are shown after stimulation and polarization with soluble cytokines (represented as technical triplicates of RNA from 3 cell cultures). The gene profiles are summarized in Figure 6.3 F, showing a ratio of the expression of M1 genes over M2 genes for each group. Significance between groups was determined using an ANOVA, with a post hoc Tukey's test. Groups that do not share a letter are significantly different ($p < 0.05$).

Using this information, to develop the scaffolds for the co-culture, we combined a moderate (0.1%) and large (0.5%) amount of HPM with PEG. RAECs and RMCs were grown separately and together on hydrogels of PEG + HPM, PEG (-), HPM (-) and PEG + Collagen. PEG and HPM hybrid hydrogels all result in macrophage polarizations characterized by upregulated IL 4 and down regulated TNF α compared to macrophages on the single component and control scaffolds (Figure 6.4A). However, upregulated IL 1 β and downregulated CD163 in these same groups results in a phenotypic ratio near one (Figure 6.4B). The M1:M2 ratio flips however, when RMCs are cultured together with RAECs. This could be a result of matrix or other signals produced by the RAECs in response to the different hydrogel scaffolds.

Interestingly, IL10 upregulation increases as more HPM is added to the scaffold. The highest expression of this cytokine is observed on 1% HPM scaffolds. IL10 is anti-inflammatory cytokine, and a known activator and product of the regulatory macrophage. These macrophages act to limit tissue damage by reducing the activation of M1 macrophages, although they do not appear to participate actively in wound healing (192).

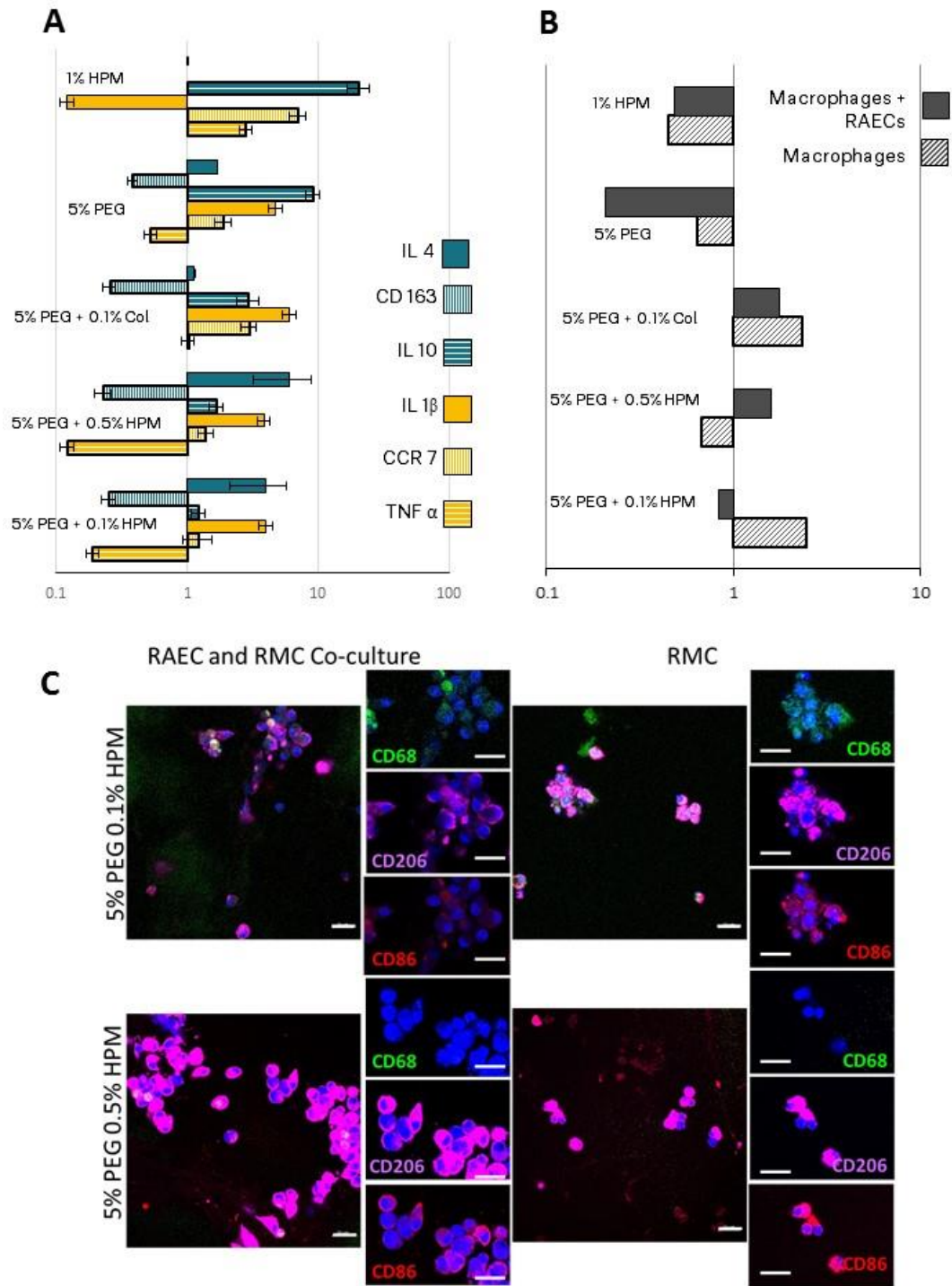


Figure 6.4 Co-Culture of RAECs and RMCs on Hybrid Hydrogels. RMCs expression of inflammatory or healing genes shows differences in response to HPM concentration including in the hybrid hydrogel (A). The gene profiles are summarized in Figure 6.4B, showing a ratio of the expression of M1 genes over M2 genes for each group. In this figure, we also show the change in gene

expression as a result of the presence of RAECs. Cells in the co-culture on hybrid hydrogels were stained for macrophage phenotypic markers CD68 (green, all), CD86 (red, M1), and CD206 (purple, M2) (C).

The M1:M2 ratio (Figure 6.4B) shows a mixed population of macrophages, with most ratios resulting near one. This result is confirmed using immunostaining (Figure 6.4C) to determine macrophage phenotype through surface markers. Cells positive for both markers appear on HPM + PEG scaffolds, regardless of HPM % added. It is important to note here that the presence of M1 macrophages, indicating an inflammatory response, is not purely pathogenic in vascular tissue regeneration (193). In fact, M1 macrophages have been reported to secrete VEGF (117), making them relevant in angiogenesis, and M2 macrophages more important for vessel maturation (116). In this way, macrophages along a spectrum of phenotypes participate in important ways at different times of wound healing. Therefore, the inclusion of HPM in the PEG hydrogels could support a moderate response from M1 macrophages, and allow for an easy re-polarization to M2 macrophages as healing progresses and more HPM is exposed.

We describe here a hydrogel scaffold with bioactivity to support a moderate inflammatory response and support endothelial cell growth. Incorporating this bioactivity into a gel with spatial and mechanical tenability is especially key parameters in vascular tissue. By using a visible light crosslinking system and a DLP printer, we have developed a cyto-compatible printing method with excellent resolution as an alternative to other extrusion based approaches with the restraint of fiber resolution. Additionally the use of visible light and elimination of harmful shear stress allow for the encapsulation of cells into the hydrogel during the printing process in a way that UV cured PEG gels would not.

Chapter 7: Summary and Future Directions

7.1 Summary

In this dissertation, we demonstrate the potential of a biohybrid material for cardiovascular tissue engineering, combining synthetic polymers with pericardium tissue. This work details the development of two distinct materials that can both contribute to endothelial cell growth as well modulate the inflammatory action from macrophages by controlled presentation of extracellular matrix (ECM) molecules. These two parameters are key indicators of successful tissue development in vascular grafts, and suggest strong potential for a permanent living tissue replacement of implanted material. A grafting solution that supports functional vessel development in the injured site has immense impacts for cardiovascular surgery, especially in young patients with congenital cardiovascular disease. Grafting material that supports the re-growth of a pediatric patient's own tissue can eliminate multiple operations and morbidities associated with congenital heart defects (CHD) and other vascular diseases.

The first objective of this work was to develop an ECM-based material for vascular wall repair that retains strength during remodeling and promotes functional tissue regrowth. Chapter 2 details the development of a novel hybrid material consisting of a layer of pericardium tissue and a layer of the biodegradable polymer, poly(propylene fumarate) (PPF). This technique was hypothesized to slow the enzymatic degradation of the tissue, but avoid chemical crosslinking and masking of molecules beneficial to remodeling. As such, the PPF reinforced pericardium was evaluated against untreated

pericardium, which is subject to easy and rapid enzymatic degradation, and GA crosslinked pericardium, the chemically crosslinked surgical standard material. A 12-day *in vitro* degradation challenge resulted in no significant difference between the elastic modulus or 1% yield strength of PPF reinforced pericardium compared to the glutaraldehyde (GA) treated pericardium ($p < 0.05$). However, PPF reinforced pericardium accumulated significantly less calcification than GA treated pericardium in an *in vivo* subdermal implant. Furthermore, the overall percentage of macrophages in responding cells at 6 weeks *in vivo* is significantly less in PPF reinforced pericardium than in GA crosslinked or untreated pericardium. Less overall macrophages may explain the observed differences in pericardium degradation and remodeling between the PPF reinforced tissue and untreated tissue. These outcomes together indicate that PPF reinforcement directs a response that is closer to functional healing than the chronic inflammation or foreign body response that could result from GA crosslinked or untreated tissue.

The difference in inflammation around the PPF reinforced pericardium compared to the untreated pericardium could have impactful outcomes for the use of xenographic ECM-based scaffolds in tissue engineering. In chapter 3, we look further into the phenotype of macrophages responding to the implants to characterize the relationship between inflammation and amount of ECM exposed. After 6 weeks *in vivo*, the untreated pericardium (100% exposed) has more overall staining of macrophages of both phenotypes. The GA treated pericardium (0% exposed) has notably more M1 macrophages in the dense band surrounding the implant than the other samples. These

noted differences in inflammation at the scaffolds motivated the evaluation of PPF in isolated cell culture. To determine what contribution, if any, PPF makes to the inflammation, it was cultured together with splenocytes and endothelial cells. Splenocytes became activated in the presence of PPF films, but not more so than the inflammatory control lipopolysaccharide (LPS), and without any strong presence from one phenotype over the other. Additionally, PPF was found to induce moderate upregulation of tumor necrosis factor α (TNF α) in human endothelial cells (HUVECs), but the effect could fade after initial degradation of the PPF within 5 days. The investigation culminated with a final subdermal implant study in athymic rats, to isolate the role of macrophages alone from other immune cells in response to 3 degrees of pericardium presentation. Fewer overall cells were observed near the implants in athymic rats compared to Sprague Dawley (SD) samples, indicating the response is markedly different without a full cast of immune system cells. Nevertheless, some differences in macrophage phenotypes were observed. The cells present in the high PPF coverage sample had the least intensity of the CD68 general macrophage stain. There also appeared to be distinct CD206 stain in both of the PPF reinforced samples. This observation after 6 weeks, together with the reduced TNF α compared to untreated samples, could indicate a shift in macrophage action towards healing and away from inflammation propagation.

Based on results presented in these two chapters, we believe that PPF reinforcement is a valuable tool to control the presentation of ECM molecules and could reduce the propagation of inflammatory pathways brought on by highly concentrated

accumulation of matrix breakdown products, cryptic peptides, and M1 macrophages. In chapter 4, we describe an approach to utilize this tool as a platform to directionally release pro-angiogenic factors to the tissue substrate. This directional and time controlled delivery could be used to direct or further promote vascular regrowth and reduced inflammation. Specifically, we hypothesized that by using PPF as a scaffold to encapsulate poly (lactic-co-glycolic) acid (PLGA) microparticles, a tunable and directional release would be achieved from the intact scaffold into the bioactive substrate, pericardium. Release of bioactive molecules occurs as PLGA microparticles degrade hydrolytically into biocompatible molecules, leaving the PPF scaffold unchanged within the release time frame and able to mechanically support the pericardium substrate through remodeling. In this proof-of-concept study, we first evaluated the degradation time frame and strength of the composite polymer layer. We determined the release of encapsulated factors to occur over eight days, while the bulk polymer remained intact with near 100% of its original mass. Next, this study demonstrated sustained bioactive molecule release from the composite into cell culture, causing significant changes to cellular metabolic activity. In particular, delivering vascular endothelial growth factor (VEGF) from the composite material to endothelial cells increased metabolic activity over the same cells with unloaded composite material. Additionally, delivering TNF α from the composite material to L929 cells significantly reduced metabolic activity compared to the same cells with unloaded composite material ($p < 0.05$). Finally, directional release into a bioactive substrate was confirmed with localized immunostaining of encapsulated ovalbumin as a model. It follows that this design could then successfully include time and location

controlled cytokines and growth factors in the pericardium substrate during remodeling as a tool to further promote endothelialization and reduce inflammation.

The material developed as part of this first objective fills the need for a compliant and versatile material for use in vascular patches, with demonstrated ability to encourage and support functional tissue remodeling. Based on the success of pericardium, the second of objective of this work seeks to expand on the potential uses for this platform. In chapter 5, we establish through 3D printing a shape and modulus controlled hydrogel combining homogenized pericardium and polyethylene glycol (PEG). The hybrid hydrogel can retain the benefits discovered in objective one in promoting wound healing response and endothelial cell growth in vascular tissue. Homogenization of the pericardium tissue resulted in a water soluble powder containing a unique profile of collagen, fibrillin, fibronectin, and glycosaminoglycans. Through a visible light photoinitiated reaction, the homogenized pericardium (HPM) was combined with PEGacrylate, and formed a hydrogel with varying modulus depending on concentration of each component between 0.5 and 20 kPa. Cell viability and preferential growth when compared to PEGacrylate hydrogels was evaluated using L929 cells, HUVECs, and ultimately a co-culture of rat aortic endothelial cells (RAECs) and rat macrophages (RMCs). HUVECs cultured on HPM hydrogels laid more matrix, and maintained a more natural morphology with positive von Willebrand factor staining. Macrophages developed an M2 phenotype in response to low amounts (0.03%, w/v) of HPM in culture, but responded with inflammatory phenotypes to high concentrations (0.3%, w/v). In the co-culture

analysis, both M1 and M2 macrophages were detected, along with a combination of both inflammatory and healing cytokines. This result, as discussed in Chapter 5, may not be pathogenic, as some inflammation is important to early wound repair. Based on results of pericardium *in vivo* in chapters 2 and 3, as well as pericardium in isolated macrophage culture, we suspect this material will support a dynamic shift in macrophage population to an M2 dominated environment at later time points. Finally, specific shape formation of the biohybrid hydrogel using DLP 3D printing demonstrates the utility of this approach to building specific structures for use in pediatric congenital heart defect reconstruction.

In conclusion, through this work we have demonstrated the use of an ECM-based hybrid material to positively influence cells to respond with healing and repair to a vascular graft. A successful tissue engineered vascular graft embodies potential for growth, long term incorporation and maintenance in the body. These characteristics are essential in the pediatric population, as well as for general cardiovascular disease patients. As such, tissue engineered vascular grafts, since they can meet these criteria, are a popular area of research. There are several promising approaches currently under investigation in animal and even clinical trials. In one such study, a completely synthetic but biodegradable polymer scaffold was implanted in sheep. Researchers found that the polymer graft was slowly replaced with native cells, which laid new collagen and elastic matrix over the graft as it degraded (194). The benefits of this purely synthetic approach include a simplified manufacturing method, since a more repeatable and controllable material can be formed using only synthetic materials.

However, it is possible that without control over the cellular infiltration, either through biological signals or pre-seeding of cells, over stimulation of the inappropriate type of cells could be propagated to quickly lay matrix, ultimately leading to inappropriate tissue formation. This possibility is supported by the success seen in two different but impactful clinical trials, implementing a blend of polymer and cell populations. In one approach, biomimetic in vitro mechanical stimulation is used to develop a mechanically functioning graft tissue in vitro. These grafts can be developed with non-species specific cells, decellularized, and the reseeded with autologous cells (195). It is more than possible that the long term success and functional tissue development of these grafts could be related to the biological activity of the substrate. In another approach currently in clinical trials, a synthetic backbone of degradable polymers is pre-seeded mononuclear cells. The presence of these cells is suspected to influence the healing response, and encourage the formation of neotissue (193). However, it is interesting to note that the seeded cells may not be incorporated into the newly formed tissue, but rather recruit and signal for healing and infiltration of nearby cells (196). These graphs demonstrate growth and show appropriate vessel tissue formation, although thickening at anastomosis sites, stenosis and thrombosis are still notable concerns for failure at 5.6 years (197). Upon further investigation into this mechanism, the stenosis could be macrophage derived (193). Control over macrophage infiltration is therefore critical for neovessel formation and the inhibition of stenosis. ECM has been described here and in other research as a potent controller of macrophage activation.

Based on these current investigations, it is clear that a biologically relevant surface and scaffold are essential to re-building native tissue around an implant site. The material described here builds on the success seen in other grafts with biologically relevant surfaces, but incorporates this surface with minimal in vitro cell development or without the need for autologous cells. Furthermore, the combination of materials in the ratios described here could influence infiltration and matrix breakdown rates, which can positively modulate the immune response, and possibly reduce macrophage directed stenosis. Controlled macrophage population and infiltration, appropriate tissue formation, and patency beyond 5 years would be important benchmarks to evaluate in the continued development of the hybrid materials developed in this thesis.

The ECM-based hybrid material can be enhanced through variations to the concentration of polymer, or more overtly by adding bioactive factor reservoirs to the polymer layer that can further promote and signal for reconstruction and regrowth. Based on these accomplishments, we believe pericardium based biohybrid materials are extremely well suited for a tissue engineering strategy for vascular repair. Complex pediatric and general cardiac surgeries demand the use of tissue or synthetic patch material in reconstruction and repair. As described, outcomes of these surgeries would be significantly improved and frequency of subsequent surgeries would be decreased with innovative design of material that can create a lasting solution through the eventual formation of native site appropriate tissue.

7.2 Contributions

The work presented in this dissertation has resulted in three first author publications, along with two manuscripts in the preparation and submission process. My research related to this work is included in 3 additional publications. Over the course of my research, I was in part supported by the American Heart Association Predoctoral Fellowship (# 14PRE20380374) and the National Institute of Health Ruth L. Kirschstein National Research Service Award F31 Predoctoral Fellowship (Award Number F31HL132541). The novel combination of PPF and pericardium is also contained in a full patent application. The work to develop ECM-based biomaterials with polymer reinforcement a significant step in tissue to provide a mechanically suitable and biologically preferable substrate, with the possibility for long term incorporation and remodeling.

7.3 Future Directions

The work focused on material development for surgical applications, and provides compelling evidence that indicates success as a vascular graft. Future developments could begin to prepare this material for interaction with blood in circulation. This work could begin with more isolated studies to investigate parameters such as compliance and burst pressure in closed system, suture retention or hemocompatibility with platelets and coagulation factors. Eventually, studies could progress to investigate tissue development in a site specific study in the vascular wall. Based on the work presented here, a pro-healing immune and rebuilding response would be observed at later time points. Scaffolds would show evidence of new collagen and elastin strand formation, endothelial cell presence, and with minimal

fibroblasts, M1 macrophages, and concentrations of inflammatory cytokines. To correlate results directly with previous studies, this study could be conducted in SD rats in order to observe the healing response to a significant vessel injury with the multiple systems at play *in vivo*. Blood sampled at early time points would help detail immune system activated cells. The implanted and surrounding tissue could be excised to determine local immune activity and remodeling of the injured site at later time points, providing a broad view of the response.

ECM-based implants are currently a field with great attention in tissue engineering. The involvement of these molecules in the immune system as whole is a complex study, and one that is just beginning to be understood. The results presented in this work suggest that pericardium based scaffolds may recruit M1 and initiate other inflammatory pathways initially or if exposed in high concentration, but overtime this response could shift towards a healing, M2 dominated outcome. An in depth investigation into this mechanism could first break down the pericardium into categories, including but not limited to: intact proteins, peptide fragments, peptides chemically bound to a PEG molecule, etc., and investigate the role that these molecules have in overall inflammation. Each of these molecules listed could have separate roles, and all may be present at one time or another in the degradation of the scaffold (115). A second investigation could test specific components of the pericardium compared to other tissue ECMs. Comparisons between other tissues have shown different immune activation profiles in recently published work (159, 162). Understanding the temporal and component dynamics of ECM interaction with the

immune system would allow the engineer to make more informed and directed design changes, specifically regarding synthetic polymer concentration and delivery of angiogenic or anti-inflammatory signals.

Finally, the work presented here is aimed at repair for existing and functional vasculature. However, many of the same cells and pathways are involved in the development of microvasculature into tissue engineered organs or into ischemic zones affected by peripheral artery disease. Many of the concepts developed in the hybrid hydrogel study could be translatable to promote new vessel development and stabilization. To apply this concept, mechanical properties, degradation rates, and possible cell encapsulation would be appropriate to areas of optimization for this new system. The incorporation of vascular-specific ECM could cause more endothelial cells to participate in vascular structure formation by providing signals for chemotaxis, proliferation and vascular sprouting. This could be measured by the upregulation of angiogenic genes including: VEGF, brain-derived neurotrophic factor, platelet derived growth factor, and epidermal growth factor in an *in vitro* study.

The research presented in this thesis, along with future investigations, describes an approach to hybrid scaffold development that has potential to dramatically improve results for tissue engineered vascular scaffolds. Through the combined incorporation of bioactive molecules from tissue-specific ECM and the control of a synthetic

polymer, a scaffold can be built that supports ordered remodeling and functional development of new tissue.

Chapter 8: References

1. Benjamin EJ, Blaha MJ, Chiuve SE, Cushman M, Das SR, Deo R, de Ferranti SD, Floyd J, Fornage M, Gillespie C, Isasi CR, Jiménez MC, Jordan LC, Judd SE, Lackland D, Lichtman JH, Lisabeth L, Liu S, Longenecker CT, Mackey RH, Matsushita K, Mozaffarian D, Mussolino ME, Nasir K, Neumar RW, Palaniappan L, Pandey DK, Thiagarajan RR, Reeves MJ, Ritchey M, Rodriguez CJ, Roth GA, Rosamond WD, Sasson C, Towfighi A, Tsao CW, Turner MB, Virani SS, Voeks JH, Willey JZ, Wilkins JT, Wu JH, Alger HM, Wong SS, Muntner P, Subcommittee AHASCaSS. Heart Disease and Stroke Statistics-2017 Update: A Report From the American Heart Association. *Circulation*. 2017. Epub 2017/01/25. doi: 10.1161/CIR.0000000000000485. PubMed PMID: 28122885.
2. Ozaki S, Kawase I, Yamashita H, Nozawa Y, Takatoh M, Hagiwara S, Kiyohara N. Aortic valve reconstruction using autologous pericardium for patients aged less than 60 years. *J Thorac Cardiovasc Surg*. 2014;148(3):934-8. Epub 2014/06/24. doi: 10.1016/j.jtcvs.2014.05.041. PubMed PMID: 24954174.
3. Ong CS, Kasai Y, Fukushima S, Hibino N, Magruder T, Suarez-Pierre A, Cameron D, Vricella L. Single-Stage Total Arch Replacement Including Resection of Kommerell Diverticulum in a Patient With Loeys-Dietz Syndrome. *World J Pediatr Congenit Heart Surg*. 2016;7(5):651-4. Epub 2016/08/12. doi: 10.1177/2150135116656979. PubMed PMID: 27521346.
4. Loeys BL, Schwarze U, Holm T, Callewaert BL, Thomas GH, Pannu H, De Backer JF, Oswald GL, Symoens S, Manouvrier S, Roberts AE, Faravelli F, Greco MA, Pyeritz RE, Milewicz DM, Coucke PJ, Cameron DE, Braverman AC, Byers PH, De Paepe AM, Dietz HC. Aneurysm syndromes caused by mutations in the TGF-beta receptor. *N Engl J Med*. 2006;355(8):788-98. doi: 10.1056/NEJMoa055695. PubMed PMID: 16928994.
5. Hughes GC. Aggressive aortic replacement for Loeys-Dietz syndrome. *Tex Heart Inst J*. 2011;38(6):663-6. PubMed PMID: 22199429; PMCID: PMC3233316.
6. DiBardino DJ, Jacobs JP. Current readings: long-term management of patients undergoing successful pediatric cardiac surgery. *Semin Thorac Cardiovasc Surg*. 2014;26(2):132-44. Epub 2014/08/07. doi: 10.1053/j.semtcvs.2014.08.002. PubMed PMID: 25441004.
7. Downing TE, Kim YY. Tetralogy of Fallot: General Principles of Management. *Cardiol Clin*. 2015;33(4):531-41, vii-viii. Epub 2015/08/29. doi: 10.1016/j.ccl.2015.07.002. PubMed PMID: 26471818.
8. Carpentier A, Lemaigre G, Robert L, Carpentier S, Dubost C. Biological factors affecting long-term results of valvular heterografts. *J Thorac Cardiovasc Surg*. 1969;58(4):467-83. PubMed PMID: 5344189.
9. Escande Rémi NK, Isabelle Di Centa, Caroline Roques, Maguette Ba, Fatima Medjahed-Hamidi, Frederic Chaubet, Didier Letourneur, Emmanuel Lansac and Anne Meddahi-Pelle. Pericardial Processing: Challenges, Outcomes and Future Prospects. 2011. In: *Biomaterials Science and Engineering* [Internet]: InTech; [437-57]. Available from: <http://www.intechopen.com/books/biomaterials-science-and-engineering/pericardial-processing-challenges-outcomes-and-future-prospects>.

10. Guldner NW, Jasmund I, Zimmermann H, Heinlein M, Girndt B, Meier V, Fluss F, Rohde D, Gebert A, Sievers HH. Detoxification and endothelialization of glutaraldehyde-fixed bovine pericardium with titanium coating: a new technology for cardiovascular tissue engineering. *Circulation*. 2009;119(12):1653-60. Epub 2009/03/18. doi: 10.1161/CIRCULATIONAHA.108.823948. PubMed PMID: 19289635.
11. Li X, Guo Y, Ziegler KR, Model LS, Eghbalieh SD, Brenes RA, Kim ST, Shu C, Dardik A. Current usage and future directions for the bovine pericardial patch. *Annals of vascular surgery*. 2011;25(4):561-8. Epub 2011/02/01. doi: 10.1016/j.avsg.2010.11.007. PubMed PMID: 21276709; PMCID: 3085588.
12. Kumar SP, Prabhakar G, Kumar M, Kumar N, Shahid M, Ali ML, Becker A, Duran CM. Comparison of fresh and glutaraldehyde-treated autologous stented pericardium as pulmonary valve replacement. *Journal of cardiac surgery*. 1995;10(5):545-51. Epub 1995/09/01. PubMed PMID: 7488776.
13. Schoen FJ. Future directions in tissue heart valves: impact of recent insights from biology and pathology. *J Heart Valve Dis*. 1999;8(4):350-8. Epub 1999/08/26. PubMed PMID: 10461233.
14. Sung HW, Chang Y, Chiu CT, Chen CN, Liang HC. Crosslinking characteristics and mechanical properties of a bovine pericardium fixed with a naturally occurring crosslinking agent. *J Biomed Mater Res*. 1999;47(2):116-26. Epub 1999/08/17. PubMed PMID: 10449623.
15. Leong J, Munnely A, Liberio B, Cochrane L, Vyavahare N. Neomycin and carbodiimide crosslinking as an alternative to glutaraldehyde for enhanced durability of bioprosthetic heart valves. *J Biomater Appl*. 2013;27(8):948-60. Epub 2011/12/31. doi: 10.1177/0885328211430542. PubMed PMID: 22207605.
16. Mohler ER, 3rd, Gannon F, Reynolds C, Zimmerman R, Keane MG, Kaplan FS. Bone formation and inflammation in cardiac valves. *Circulation*. 2001;103(11):1522-8. Epub 2001/03/21. PubMed PMID: 11257079.
17. Schoen FJ, Levy RJ. Calcification of tissue heart valve substitutes: progress toward understanding and prevention. *Ann Thorac Surg*. 2005;79(3):1072-80. Epub 2005/03/01. doi: 10.1016/j.athoracsur.2004.06.033. PubMed PMID: 15734452.
18. Sugiura T, Hibino N, Breuer CK, Shinoka T. Tissue-engineered cardiac patch seeded with human induced pluripotent stem cell derived cardiomyocytes promoted the regeneration of host cardiomyocytes in a rat model. *J Cardiothorac Surg*. 2016;11(1):163. Epub 2016/12/01. doi: 10.1186/s13019-016-0559-z. PubMed PMID: 27906085; PMCID: PMC5131419.
19. Hoerstrup SP, Cummings Mrcs I, Lachat M, Schoen FJ, Jenni R, Leschka S, Neuschwander S, Schmidt D, Mol A, Günter C, Gössi M, Genoni M, Zund G. Functional growth in tissue-engineered living, vascular grafts: follow-up at 100 weeks in a large animal model. *Circulation*. 2006;114(1 Suppl):I159-66. doi: 10.1161/CIRCULATIONAHA.105.001172. PubMed PMID: 16820566.
20. Shin'oka T, Matsumura G, Hibino N, Naito Y, Watanabe M, Konuma T, Sakamoto T, Nagatsu M, Kurosawa H. Midterm clinical result of tissue-engineered vascular autografts seeded with autologous bone marrow cells. *J Thorac Cardiovasc Surg*. 2005;129(6):1330-8. doi: 10.1016/j.jtcvs.2004.12.047. PubMed PMID: 15942574.

21. Singelyn JM, DeQuach JA, Seif-Naraghi SB, Littlefield RB, Schup-Magoffin PJ, Christman KL. Naturally derived myocardial matrix as an injectable scaffold for cardiac tissue engineering. *Biomaterials*. 2009;30(29):5409-16. Epub 2009/07/15. doi: 10.1016/j.biomaterials.2009.06.045. PubMed PMID: 19608268; PMCID: PMC2728782.
22. Brown BN, Badylak SF. Extracellular matrix as an inductive scaffold for functional tissue reconstruction. *Translational research : the journal of laboratory and clinical medicine*. 2014;163(4):268-85. Epub 2013/12/03. doi: 10.1016/j.trsl.2013.11.003. PubMed PMID: 24291155; PMCID: 4203714.
23. Pati F, Jang J, Ha DH, Won Kim S, Rhie JW, Shim JH, Kim DH, Cho DW. Printing three-dimensional tissue analogues with decellularized extracellular matrix bioink. *Nat Commun*. 2014;5:3935. Epub 2014/06/02. doi: 10.1038/ncomms4935. PubMed PMID: 24887553; PMCID: PMC4059935.
24. Nelson CM, Bissell MJ. Of extracellular matrix, scaffolds, and signaling: tissue architecture regulates development, homeostasis, and cancer. *Annual review of cell and developmental biology*. 2006;22:287-309. Epub 2006/07/11. doi: 10.1146/annurev.cellbio.22.010305.104315. PubMed PMID: 16824016; PMCID: 2933192.
25. Sicari BM, Rubin JP, Dearth CL, Wolf MT, Ambrosio F, Boninger M, Turner NJ, Weber DJ, Simpson TW, Wyse A, Brown EH, Dziki JL, Fisher LE, Brown S, Badylak SF. An acellular biologic scaffold promotes skeletal muscle formation in mice and humans with volumetric muscle loss. *Science translational medicine*. 2014;6(234):234ra58. Epub 2014/05/03. doi: 10.1126/scitranslmed.3008085. PubMed PMID: 24786326.
26. Jacobs JP, Mavroudis C, Quintessenza JA, Chai PJ, Pasquali SK, Hill KD, Vricella LA, Jacobs ML, Dearani JA, Cameron D. Reoperations for pediatric and congenital heart disease: an analysis of the Society of Thoracic Surgeons (STS) congenital heart surgery database. *Semin Thorac Cardiovasc Surg Pediatr Card Surg Annu*. 2014;17(1):2-8. doi: 10.1053/j.pcsu.2014.01.006. PubMed PMID: 24725711; PMCID: PMC4276147.
27. Hynes RO. The extracellular matrix: not just pretty fibrils. *Science*. 2009;326(5957):1216-9. Epub 2009/12/08. doi: 10.1126/science.1176009. PubMed PMID: 19965464; PMCID: 3536535.
28. Lu H, Oh HH, Kawazoe N, Yamagishi K, Chen G. PLLA–collagen and PLLA–gelatin hybrid scaffolds with funnel-like porous structure for skin tissue engineering. *Sci Technol Adv Mater*. 2012;13(6).
29. Brown BN, Badylak SF. Expanded applications, shifting paradigms and an improved understanding of host-biomaterial interactions. *Acta biomaterialia*. 2013;9(2):4948-55. Epub 2012/10/27. doi: 10.1016/j.actbio.2012.10.025. PubMed PMID: 23099303.
30. Nimni ME, Cheung D, Strates B, Kodama M, Sheikh K. Chemically modified collagen: a natural biomaterial for tissue replacement. *J Biomed Mater Res*. 1987;21(6):741-71. Epub 1987/06/01. doi: 10.1002/jbm.820210606. PubMed PMID: 3036880.
31. Hansen KC, Kiemele L, Maller O, O'Brien J, Shankar A, Fornetti J, Schedin P. An in-solution ultrasonication-assisted digestion method for improved extracellular

- matrix proteome coverage. *Molecular & cellular proteomics : MCP*. 2009;8(7):1648-57. Epub 2009/04/09. doi: 10.1074/mcp.M900039-MCP200. PubMed PMID: 19351662; PMCID: 2709248.
32. Xu Y, Patnaik S, Guo X, Li Z, Lo W, Butler R, Claude A, Liu Z, Zhang G, Liao J, Anderson PM, Guan J. Cardiac differentiation of cardiosphere-derived cells in scaffolds mimicking morphology of the cardiac extracellular matrix. *Acta biomaterialia*. 2014;10(8):3449-62. Epub 2014/04/29. doi: 10.1016/j.actbio.2014.04.018. PubMed PMID: 24769114.
33. Guaccio A, Guarino V, Perez MA, Cirillo V, Netti PA, Ambrosio L. Influence of electrospun fiber mesh size on hMSC oxygen metabolism in 3D collagen matrices: experimental and theoretical evidences. *Biotechnology and bioengineering*. 2011;108(8):1965-76. Epub 2011/02/26. doi: 10.1002/bit.23113. PubMed PMID: 21351071.
34. Seif-Naraghi SB, Singelyn JM, Salvatore MA, Osborn KG, Wang JJ, Sampat U, Kwan OL, Strachan GM, Wong J, Schup-Magoffin PJ, Braden RL, Bartels K, DeQuach JA, Preul M, Kinsey AM, DeMaria AN, Dib N, Christman KL. Safety and efficacy of an injectable extracellular matrix hydrogel for treating myocardial infarction. *Science translational medicine*. 2013;5(173):173ra25. Epub 2013/02/22. doi: 10.1126/scitranslmed.3005503. PubMed PMID: 23427245; PMCID: 3848875.
35. Gilbert TW, Stewart-Akers AM, Simmons-Byrd A, Badylak SF. Degradation and remodeling of small intestinal submucosa in canine Achilles tendon repair. *The Journal of bone and joint surgery American volume*. 2007;89(3):621-30. Epub 2007/03/03. doi: 10.2106/JBJS.E.00742. PubMed PMID: 17332112.
36. Zhu C, Ma X, Xian L, Zhou Y, Fan D. Characterization of a co-electrospun scaffold of HLC/CS/PLA for vascular tissue engineering. *Bio-medical materials and engineering*. 2014;24(6):1999-2005. Epub 2014/09/18. doi: 10.3233/BME-141009. PubMed PMID: 25226896.
37. Kumbar SG, James R, Nukavarapu SP, Laurencin CT. Electrospun nanofiber scaffolds: engineering soft tissues. *Biomedical materials*. 2008;3(3):034002. Epub 2008/08/12. doi: 10.1088/1748-6041/3/3/034002. PubMed PMID: 18689924.
38. Barnes CP, Sell SA, Boland ED, Simpson DG, Bowlin GL. Nanofiber technology: designing the next generation of tissue engineering scaffolds. *Advanced drug delivery reviews*. 2007;59(14):1413-33. Epub 2007/10/06. doi: 10.1016/j.addr.2007.04.022. PubMed PMID: 17916396.
39. Tatekawa Y, Kawazoe N, Chen G, Shirasaki Y, Komuro H, Kaneko M. Tracheal defect repair using a PLGA-collagen hybrid scaffold reinforced by a copolymer stent with bFGF-impregnated gelatin hydrogel. *Pediatr Surg Int*. 2010;26(6):575-80. Epub 2010/04/29. doi: 10.1007/s00383-010-2609-2. PubMed PMID: 20425118.
40. Wolf MT, Carruthers CA, Dearth CL, Crapo PM, Huber A, Burnsed OA, Londono R, Johnson SA, Daly KA, Stahl EC, Freund JM, Medberry CJ, Carey LE, Nieponice A, Amoroso NJ, Badylak SF. Polypropylene surgical mesh coated with extracellular matrix mitigates the host foreign body response. *J Biomed Mater Res A*. 2014;102(1):234-46. Epub 2013/07/23. doi: 10.1002/jbm.a.34671. PubMed PMID: 23873846; PMCID: 3808505.

41. Zhang J-G, Mo X-M. Current research on electrospinning of silk fibroin and its blends with natural and synthetic biodegradable polymers. *Front Mater Sci.* 2013;7(2):129-42. doi: 10.1007/s11706-013-0206-8.
42. Jung S-M, Kim DS, Ju JH, Shin HS. Evaluation of EPS-PCL Nanofibers as a Nanobiocomposite for Artificial Skin Based on Dermal Fibroblast Culture. *Journal of Nanomaterials.* 2013;2013(2013):1-6.
43. Koch S, Flanagan TC, Sachweh JS, Tanios F, Schnoering H, Deichmann T, Ella V, Kellomaki M, Gronloh N, Gries T, Tolba R, Schmitz-Rode T, Jockenhoevel S. Fibrin-poly lactide-based tissue-engineered vascular graft in the arterial circulation. *Biomaterials.* 2010;31(17):4731-9. Epub 2010/03/23. doi: 10.1016/j.biomaterials.2010.02.051. PubMed PMID: 20304484.
44. Jang YS, Jang CH, Cho YB, Kim M, Kim GH. Tracheal regeneration using polycaprolactone/collagen-nanofiber coated with umbilical cord serum after partial resection. *International journal of pediatric otorhinolaryngology.* 2014;78(12):2237-43. Epub 2014/12/04. doi: 10.1016/j.ijporl.2014.10.022. PubMed PMID: 25465447.
45. Song JEL, Yujung ; Lee, Yun Me ; Cho, Sun Ah ; Jang, Ji Eun ; Lee, Dongwon ; Khang, Gilson ;. Effects of PLGA/Fibrin Scaffolds on Attachment and Proliferation of Costal Cartilage Cells. *Polymer-Korea.* 2013;37(2):141-7.
46. Hong S, Kim GH. Electrospun Polycaprolactone/Silk Fibroin/Small Intestine Submucosa Composites for Biomedical Applications. *Macromolecular Materials and Engineering.* 2010;295(6):529-34. doi: 10.1002/mame.201000051.
47. Cai C, Chen C, Chen G, Wang F, Guo L, Yin L, Feng D, Yang L. Type I collagen and polyvinyl alcohol blend fiber scaffold for anterior cruciate ligament reconstruction. *Biomedical materials.* 2013;8(3):035001. Epub 2013/03/28. doi: 10.1088/1748-6041/8/3/035001. PubMed PMID: 23531980.
48. Han J, Gerstenhaber JA, Lazarovici P, Lelkes PI. Tissue factor activity and ECM-related gene expression in human aortic endothelial cells grown on electrospun biohybrid scaffolds. *Biomacromolecules.* 2013;14(5):1338-48. Epub 2013/04/09. doi: 10.1021/bm400450m. PubMed PMID: 23560456.
49. Hong Y, Huber A, Takanari K, Amoroso NJ, Hashizume R, Badylak SF, Wagner WR. Mechanical properties and in vivo behavior of a biodegradable synthetic polymer microfiber-extracellular matrix hydrogel biohybrid scaffold. *Biomaterials.* 2011;32(13):3387-94. Epub 2011/02/10. doi: 10.1016/j.biomaterials.2011.01.025. PubMed PMID: 21303718; PMCID: 3184831.
50. Ekaputra AK, Prestwich GD, Cool SM, Hutmacher DW. The three-dimensional vascularization of growth factor-releasing hybrid scaffold of poly (epsilon-caprolactone)/collagen fibers and hyaluronic acid hydrogel. *Biomaterials.* 2011;32(32):8108-17. Epub 2011/08/03. doi: 10.1016/j.biomaterials.2011.07.022. PubMed PMID: 21807407.
51. Song JE, Lee Y, Lee YM, Cho SA, Jang JE, Lee D, Khang G. Effects of PLGA/Fibrin Scaffolds on Attachment and Proliferation of Costal Cartilage Cells. *Polymer-Korea.* 2013;37(2):141-7.
52. Han J, Lazarovici P, Pomerantz C, Chen X, Wei Y, Lelkes PI. Co-electrospun blends of PLGA, gelatin, and elastin as potential nonthrombogenic scaffolds for vascular tissue engineering. *Biomacromolecules.* 2011;12(2):399-408. Epub 2010/12/25. doi: 10.1021/bm101149r. PubMed PMID: 21182235.

53. Choi JS, Lee SJ, Christ GJ, Atala A, Yoo JJ. The influence of electrospun aligned poly(ϵ -caprolactone)/collagen nanofiber meshes on the formation of self-aligned skeletal muscle myotubes. *Biomaterials*. 2008;29(19):2899-906. doi: <http://dx.doi.org/10.1016/j.biomaterials.2008.03.031>.
54. Liang D, Hsiao BS, Chu B. Functional electrospun nanofibrous scaffolds for biomedical applications. *Adv Drug Deliv Rev*. 2007;59(14):1392-412. Epub 2007/09/22. doi: S0169-409X(07)00185-8 [pii] 10.1016/j.addr.2007.04.021. PubMed PMID: 17884240; PMCID: 2693708.
55. Mendoza-Novelo B, Alvarado-Castro DI, Mata-Mata JL, Cauich-Rodriguez JV, Vega-Gonzalez A, Jorge-Herrero E, Rojo FJ, Guinea GV. Stability and mechanical evaluation of bovine pericardium cross-linked with polyurethane prepolymer in aqueous medium. *Mater Sci Eng C Mater Biol Appl*. 2013;33(4):2392-8. Epub 2013/03/19. doi: 10.1016/j.msec.2013.02.001. PubMed PMID: 23498274.
56. Samal SK, Dash M, Chiellini F, Wang X, Chiellini E, Declercq HA, Kaplan DL. Silk/chitosan biohybrid hydrogels and scaffolds via green technology. *RSC Advances*. 2014;4(96):53547-56. doi: 10.1039/c4ra10070k.
57. Daniele MA, Adams AA, Naciri J, North SH, Ligler FS. Interpenetrating networks based on gelatin methacrylamide and PEG formed using concurrent thiol click chemistries for hydrogel tissue engineering scaffolds. *Biomaterials*. 2014;35(6):1845-56. Epub 2013/12/10. doi: 10.1016/j.biomaterials.2013.11.009. PubMed PMID: 24314597.
58. Chong EJ, Phan TT, Lim IJ, Zhang YZ, Bay BH, Ramakrishna S, Lim CT. Evaluation of electrospun PCL/gelatin nanofibrous scaffold for wound healing and layered dermal reconstitution. *Acta biomaterialia*. 2007;3(3):321-30. doi: <http://dx.doi.org/10.1016/j.actbio.2007.01.002>.
59. Ghasemi-Mobarakeh L, Prabhakaran MP, Morshed M, Nasr-Esfahani M-H, Ramakrishna S. Electrospun poly(ϵ -caprolactone)/gelatin nanofibrous scaffolds for nerve tissue engineering. *Biomaterials*. 2008;29(34):4532-9. doi: <http://dx.doi.org/10.1016/j.biomaterials.2008.08.007>.
60. Jung JP, Sprangers AJ, Byce JR, Su J, Squirrel JM, Messersmith PB, Eliceiri KW, Ogle BM. ECM-incorporated hydrogels cross-linked via native chemical ligation to engineer stem cell microenvironments. *Biomacromolecules*. 2013;14(9):3102-11. Epub 2013/07/24. doi: 10.1021/bm400728e. PubMed PMID: 23875943; PMCID: 3880157.
61. Liang D, Hsiao BS, Chu B. Functional electrospun nanofibrous scaffolds for biomedical applications. *Advanced drug delivery reviews*. 2007;59(14):1392-412. doi: <http://dx.doi.org/10.1016/j.addr.2007.04.021>.
62. Pan JF, Liu NH, Sun H, Xu F. Preparation and characterization of electrospun PLCL/Pluronic nanofibers and dextran/gelatin hydrogels for skin tissue engineering. *PloS one*. 2014;9(11):e112885. Epub 2014/11/19. doi: 10.1371/journal.pone.0112885. PubMed PMID: 25405611; PMCID: 4236104.
63. Bracaglia LG, Yu L, Hibino N, Fisher JP. Reinforced pericardium as a hybrid material for cardiovascular applications. *Tissue Eng Part A*. 2014;20(21-22):2807-16. Epub 2014/09/23. doi: 10.1089/ten.TEA.2014.0516. PubMed PMID: 25236439; PMCID: 4229701.

64. Loke WK, Khor E, Wee A, Teoh SH, Chian KS. Hybrid biomaterials based on the interaction of polyurethane oligomers with porcine pericardium. *Biomaterials*. 1996;17(22):2163-72. Epub 1996/11/01. PubMed PMID: 8922602.
65. Nogueira GM, Rodas ACD, Weska RF, Aimoli CG, Higa OZ, Maizato M, Leiner AA, Pitombo RNM, Polakiewicz B, Beppu MM. Bovine pericardium coated with biopolymeric films as an alternative to prevent calcification: In vitro calcification and cytotoxicity results. *Materials Science and Engineering: C*. 2010;30(4):575-82. doi: <http://dx.doi.org/10.1016/j.msec.2010.02.011>.
66. Mathapati S, Bishi DK, Venugopal JR, Cherian KM, Guhathakurta S, Ramakrishna S, Verma RS. Nanofibers coated on acellular tissue-engineered bovine pericardium supports differentiation of mesenchymal stem cells into endothelial cells for tissue engineering. *Nanomedicine*. 2014;9(5):623-34. Epub 2014/05/16. doi: 10.2217/nnm.13.76. PubMed PMID: 24827842.
67. Ricchetti ET, Aurora A, Iannotti JP, Derwin KA. Scaffold devices for rotator cuff repair. *Journal of shoulder and elbow surgery / American Shoulder and Elbow Surgeons [et al]*. 2012;21(2):251-65. Epub 2012/01/17. doi: 10.1016/j.jse.2011.10.003. PubMed PMID: 22244069.
68. Wojak-Cwik IM, Hintze V, Schnabelrauch M, Moeller S, Dobrzynski P, Pamula E, Scharnweber D. Poly(L-lactide-co-glycolide) scaffolds coated with collagen and glycosaminoglycans: impact on proliferation and osteogenic differentiation of human mesenchymal stem cells. *Journal of biomedical materials research Part A*. 2013;101(11):3109-22. Epub 2013/03/26. doi: 10.1002/jbm.a.34620. PubMed PMID: 23526792.
69. Kawazoe N, Xiaoting Lin, Tateishi T, Guoping Chen. Three-dimensional Cultures of Rat Pancreatic RIN-5F Cells in Porous PLGA-collagen Hybrid Scaffolds. *Journal of Bioactive and Compatible Polymers*. 2009;24(1):25-42. doi: 10.1177/0883911508099439.
70. Martinez-Ramos C, Rodriguez-Perez E, Garnes MP, Chachques JC, Moratal D, Valles-Lluch A, Monleon Pradas M. Design and assembly procedures for large-sized biohybrid scaffolds as patches for myocardial infarct. *Tissue engineering Part C, Methods*. 2014;20(10):817-27. Epub 2014/03/19. doi: 10.1089/ten.tec.2013.0489. PubMed PMID: 24628399.
71. Chachques JC, Pradas MM, Bayes-Genis A, Semino C. Creating the bioartificial myocardium for cardiac repair: challenges and clinical targets. *Expert review of cardiovascular therapy*. 2013;11(12):1701-11. Epub 2013/11/13. doi: 10.1586/14779072.2013.854165. PubMed PMID: 24215199.
72. Faulk DM, Londono R, Wolf MT, Ranallo CA, Carruthers CA, Wildemann JD, Dearth CL, Badylak SF. ECM hydrogel coating mitigates the chronic inflammatory response to polypropylene mesh. *Biomaterials*. 2014;35(30):8585-95. Epub 2014/07/22. doi: 10.1016/j.biomaterials.2014.06.057. PubMed PMID: 25043571.
73. Chang CC, Boland ED, Williams SK, Hoying JB. Direct-write bioprinting three-dimensional biohybrid systems for future regenerative therapies. *Journal of biomedical materials research Part B, Applied biomaterials*. 2011;98(1):160-70. Epub 2011/04/20. doi: 10.1002/jbm.b.31831. PubMed PMID: 21504055; PMCID: 3772543.

74. Mintz BR, Cooper JA, Jr. Hybrid hyaluronic acid hydrogel/poly(varepsilon-caprolactone) scaffold provides mechanically favorable platform for cartilage tissue engineering studies. *Journal of biomedical materials research Part A*. 2014;102(9):2918-26. Epub 2013/10/12. doi: 10.1002/jbm.a.34957. PubMed PMID: 24115629.
75. Danti S, Stefanini C, D'Alessandro D, Moscato S, Pietrabissa A, Petrini M, Berrettini S. Novel biological/biohybrid prostheses for the ossicular chain: fabrication feasibility and preliminary functional characterization. *Biomedical microdevices*. 2009;11(4):783-93. Epub 2009/03/19. doi: 10.1007/s10544-009-9293-9. PubMed PMID: 19294514.
76. Shtrichman R, Zeevi-Levin N, Zaid R, Barak E, Fishman B, Ziskind A, Shulman R, Novak A, Avrahami R, Livne E, Lowenstein L, Zussman E, Itskovitz-Eldor J. The generation of hybrid electrospun nanofiber layer with extracellular matrix derived from human pluripotent stem cells, for regenerative medicine applications. *Tissue engineering Part A*. 2014;20(19-20):2756-67. Epub 2014/09/04. doi: 10.1089/ten.TEA.2013.0705. PubMed PMID: 25185111.
77. Antebi B, Zhang Z, Wang Y, Lu Z, Chen XD, Ling J. Stromal-cell-derived extracellular matrix promotes the proliferation and retains the osteogenic differentiation capacity of mesenchymal stem cells on three-dimensional scaffolds. *Tissue engineering Part C, Methods*. 2015;21(2):171-81. Epub 2014/06/27. doi: 10.1089/ten.TEC.2014.0092. PubMed PMID: 24965227; PMCID: 4313424.
78. Zhu J. Bioactive modification of poly(ethylene glycol) hydrogels for tissue engineering. *Biomaterials*. 2010;31(17):4639-56. doi: <http://dx.doi.org/10.1016/j.biomaterials.2010.02.044>.
79. Stocco E, Barbon S, Dalzoppo D, Lora S, Sartore L, Folin M, Parnigotto PP, Grandi C. Tailored PVA/ECM scaffolds for cartilage regeneration. *BioMed research international*. 2014;2014:762189. Epub 2014/08/26. doi: 10.1155/2014/762189. PubMed PMID: 25147814; PMCID: 4131468.
80. Grover GN, Rao N, Christman KL. Myocardial matrix-polyethylene glycol hybrid hydrogels for tissue engineering. *Nanotechnology*. 2014;25(1):014011. Epub 2013/12/18. doi: 10.1088/0957-4484/25/1/014011. PubMed PMID: 24334615; PMCID: 3914302.
81. Xiao W, He J, Nichol JW, Wang L, Hutson CB, Wang B, Du Y, Fan H, Khademhosseini A. Synthesis and characterization of photocrosslinkable gelatin and silk fibroin interpenetrating polymer network hydrogels. *Acta biomaterialia*. 2011;7(6):2384-93. Epub 2011/02/08. doi: 10.1016/j.actbio.2011.01.016. PubMed PMID: 21295165; PMCID: 3085717.
82. Hutson CB, Nichol JW, Aubin H, Bae H, Yamanlar S, Al-Haque S, Koshy ST, Khademhosseini A. Synthesis and characterization of tunable poly(ethylene glycol): gelatin methacrylate composite hydrogels. *Tissue engineering Part A*. 2011;17(13-14):1713-23. Epub 2011/02/11. doi: 10.1089/ten.TEA.2010.0666. PubMed PMID: 21306293; PMCID: 3118706.
83. Van Vlierberghe S, Samal SK, Dubruel P. Development of Mechanically Tailored Gelatin-Chondroitin Sulphate Hydrogel Films. *Macromolecular Symposia*. 2011;309-310(1):173-81. doi: 10.1002/masy.201100030.

84. Haroun AA, Gamal-Eldeen A, Harding DR. Preparation, characterization and in vitro biological study of biomimetic three-dimensional gelatin-montmorillonite/cellulose scaffold for tissue engineering. *Journal of materials science Materials in medicine*. 2009;20(12):2527-40. Epub 2009/07/25. doi: 10.1007/s10856-009-3818-x. PubMed PMID: 19629650.
85. Welzel PB, Friedrichs J, Grimmer M, Vogler S, Freudenberg U, Werner C. Cryogel micromechanics unraveled by atomic force microscopy-based nanoindentation. *Advanced healthcare materials*. 2014;3(11):1849-53. Epub 2014/04/15. doi: 10.1002/adhm.201400102. PubMed PMID: 24729299.
86. Shin SR, Jung SM, Zalabany M, Kim K, Zorlutuna P, Kim SB, Nikkhah M, Khabiry M, Azize M, Kong J, Wan KT, Palacios T, Dokmeci MR, Bae H, Tang XS, Khademhosseini A. Carbon-nanotube-embedded hydrogel sheets for engineering cardiac constructs and bioactuators. *ACS nano*. 2013;7(3):2369-80. Epub 2013/02/01. doi: 10.1021/nn305559j. PubMed PMID: 23363247; PMCID: 3609875.
87. Malik AF, Hoque R, Ouyang X, Ghani A, Hong E, Khan K, Moore LB, Ng G, Munro F, Flavell RA, Shi Y, Kyriakides TR, Mehal WZ. Inflammasome components Asc and caspase-1 mediate biomaterial-induced inflammation and foreign body response. *Proceedings of the National Academy of Sciences of the United States of America*. 2011;108(50):20095-100. Epub 2011/11/24. doi: 10.1073/pnas.1105152108. PubMed PMID: 22109549; PMCID: 3250158.
88. Avula MN, Rao AN, McGill LD, Grainger DW, Solzbacher F. Foreign body response to subcutaneous biomaterial implants in a mast cell-deficient Kit(w-Sh) murine model. *Acta biomaterialia*. 2014;10(5):1856-63. Epub 2014/01/11. doi: 10.1016/j.actbio.2013.12.056. PubMed PMID: 24406200.
89. Wolf MT, Vodovotz Y, Tottey S, Brown BN, Badylak SF. Predicting in vivo responses to biomaterials via combined in vitro and in silico analysis. *Tissue engineering Part C, Methods*. 2015;21(2):148-59. Epub 2014/07/02. doi: 10.1089/ten.TEC.2014.0167. PubMed PMID: 24980950; PMCID: 4313398.
90. Lu HK, Ko MT, Wu MF. Comparison of Th1/Th2 cytokine profiles of initial wound healing of rats induced by PDCM and e-PTFE. *Journal of biomedical materials research Part B, Applied biomaterials*. 2004;68(1):75-80. Epub 2003/12/23. doi: 10.1002/jbm.b.10081. PubMed PMID: 14689499.
91. Brown BN, Valentin JE, Stewart-Akers AM, McCabe GP, Badylak SF. Macrophage phenotype and remodeling outcomes in response to biologic scaffolds with and without a cellular component. *Biomaterials*. 2009;30(8):1482-91. Epub 2009/01/06. doi: 10.1016/j.biomaterials.2008.11.040 S0142-9612(08)00927-7 [pii]. PubMed PMID: 19121538; PMCID: 2805023.
92. Sahoo S, Toh SL, Goh JC. A bFGF-releasing silk/PLGA-based biohybrid scaffold for ligament/tendon tissue engineering using mesenchymal progenitor cells. *Biomaterials*. 2010;31(11):2990-8. Epub 2010/01/22. doi: 10.1016/j.biomaterials.2010.01.004. PubMed PMID: 20089300.
93. Daley WP, Peters SB, Larsen M. Extracellular matrix dynamics in development and regenerative medicine. *Journal of cell science*. 2008;121(Pt 3):255-64. Epub 2008/01/25. doi: 10.1242/jcs.006064. PubMed PMID: 18216330.
94. Lu P, Takai K, Weaver VM, Werb Z. Extracellular matrix degradation and remodeling in development and disease. *Cold Spring Harbor perspectives in biology*.

- 2011;3(12). Epub 2011/09/16. doi: 10.1101/cshperspect.a005058. PubMed PMID: 21917992; PMCID: 3225943.
95. Schmidt CE, Baier JM. Acellular vascular tissues: natural biomaterials for tissue repair and tissue engineering. *Biomaterials*. 2000;21(22):2215-31. Epub 2000/10/12. PubMed PMID: 11026628.
96. Vande Geest JP, Sacks MS, Vorp DA. The effects of aneurysm on the biaxial mechanical behavior of human abdominal aorta. *J Biomech*. 2006;39(7):1324-34. Epub 2005/05/12. doi: S0021-9290(05)00132-6 [pii] 10.1016/j.jbiomech.2005.03.003. PubMed PMID: 15885699.
97. Sacks MS, Chuong CJ. Orthotropic mechanical properties of chemically treated bovine pericardium. *Ann Biomed Eng*. 1998;26(5):892-902. Epub 1998/10/21. PubMed PMID: 9779962.
98. Cohn D, Younes H, Milgarter E, Uretzky G. Mechanical behaviour of isolated pericardium: species, isotropy, strain rate and collagenase effect on pericardial tissue. *Clinical Materials*. 1987;2(2):115-24. doi: [http://dx.doi.org/10.1016/0267-6605\(87\)90030-8](http://dx.doi.org/10.1016/0267-6605(87)90030-8).
99. Sung HW, Hsu CS, Wang SP, Hsu HL. Degradation potential of biological tissues fixed with various fixatives: an in vitro study. *Journal of biomedical materials research*. 1997;35(2):147-55. Epub 1997/05/01. PubMed PMID: 9135163.
100. Tamura K, Jones M, Yamada I, Ferrans VJ. A comparison of failure modes of glutaraldehyde-treated versus antibiotic-preserved mitral valve allografts implanted in sheep. *The Journal of thoracic and cardiovascular surgery*. 1995;110(1):224-38. Epub 1995/07/01. PubMed PMID: 7609546.
101. Go AS, Mozaffarian D, Roger VL, Benjamin EJ, Berry JD, Blaha MJ, Dai S, Ford ES, Fox CS, Franco S, Fullerton HJ, Gillespie C, Hailpern SM, Heit JA, Howard VJ, Huffman MD, Judd SE, Kissela BM, Kittner SJ, Lackland DT, Lichtman JH, Lisabeth LD, Mackey RH, Magid DJ, Marcus GM, Marelli A, Matchar DB, McGuire DK, Mohler ER, 3rd, Moy CS, Mussolino ME, Neumar RW, Nichol G, Pandey DK, Paynter NP, Reeves MJ, Sorlie PD, Stein J, Towfighi A, Turan TN, Virani SS, Wong ND, Woo D, Turner MB. Heart disease and stroke statistics--2014 update: a report from the American Heart Association. *Circulation*. 2014;129(3):e28-e292. Epub 2013/12/20. doi: 10.1161/01.cir.0000441139.02102.80 01.cir.0000441139.02102.80 [pii]. PubMed PMID: 24352519.
102. Schoen FJ, Levy RJ. Founder's Award, 25th Annual Meeting of the Society for Biomaterials, perspectives. Providence, RI, April 28-May 2, 1999. Tissue heart valves: current challenges and future research perspectives. *Journal of biomedical materials research*. 1999;47(4):439-65. Epub 1999/09/25. doi: 10.1002/(SICI)1097-4636(19991215)47:4<439::AID-JBM1>3.0.CO;2-O [pii]. PubMed PMID: 10497280.
103. Eckert CE, Fan R, Mikulis B, Barron M, Carruthers CA, Friebe VM, Vyavahare NR, Sacks MS. On the biomechanical role of glycosaminoglycans in the aortic heart valve leaflet. *Acta Biomater*. 2013;9(1):4653-60. Epub 2012/10/06. doi: 10.1016/j.actbio.2012.09.031 S1742-7061(12)00468-0 [pii]. PubMed PMID: 23036945; PMCID: 3508081.
104. Dweck MR, Jones C, Joshi NV, Fletcher AM, Richardson H, White A, Marsden M, Pessotto R, Clark JC, Wallace WA, Salter DM, McKillop G, van Beek EJ, Boon NA, Rudd JH, Newby DE. Assessment of valvular calcification and

- inflammation by positron emission tomography in patients with aortic stenosis. *Circulation*. 2012;125(1):76-86. Epub 2011/11/18. doi: 10.1161/CIRCULATIONAHA.111.051052
CIRCULATIONAHA.111.051052 [pii]. PubMed PMID: 22090163.
105. Fisher JP, Vehof JW, Dean D, van der Waerden JP, Holland TA, Mikos AG, Jansen JA. Soft and hard tissue response to photocrosslinked poly(propylene fumarate) scaffolds in a rabbit model. *Journal of biomedical materials research*. 2002;59(3):547-56. Epub 2002/01/05. PubMed PMID: 11774313.
106. Wang MO, Etheridge JM, Thompson JA, Vorwald CE, Dean D, Fisher JP. Evaluation of the in vitro cytotoxicity of cross-linked biomaterials. *Biomacromolecules*. 2013;14(5):1321-9. Epub 2013/05/01. doi: 10.1021/bm301962f. PubMed PMID: 23627804; PMCID: 3670822.
107. Fisher JP, Lalani Z, Bossano CM, Brey EM, Demian N, Johnston CM, Dean D, Jansen JA, Wong ME, Mikos AG. Effect of biomaterial properties on bone healing in a rabbit tooth extraction socket model. *J Biomed Mater Res A*. 2004;68(3):428-38.
108. Fisher JP, Dean D, Mikos AG. Photocrosslinking characteristics and mechanical properties of diethyl fumarate/poly(propylene fumarate) biomaterials. *Biomaterials*. 2002;23(22):4333-43. Epub 2002/09/11. PubMed PMID: 12219823.
109. Kasper FK, Tanahashi K, Fisher JP, Mikos AG. Synthesis of poly(propylene fumarate). *Nat Protoc*. 2009;4(4):518-25. Epub 2009/03/28. doi: 10.1038/nprot.2009.24
nprot.2009.24 [pii]. PubMed PMID: 19325548; PMCID: 3076598.
110. Sinha P, Zurakowski D, Kumar TK, He D, Rossi C, Jonas RA. Effects of glutaraldehyde concentration, pretreatment time, and type of tissue (porcine versus bovine) on postimplantation calcification. *The Journal of thoracic and cardiovascular surgery*. 2012;143(1):224-7. Epub 2011/11/04. doi: 10.1016/j.jtcvs.2011.09.043. PubMed PMID: 22047684.
111. Pashneh-Tala S, MacNeil S, Claeysens F. The Tissue-Engineered Vascular Graft-Past, Present, and Future. *Tissue Eng Part B Rev*. 2015. Epub 2015/10/08. doi: 10.1089/ten.teb.2015.0100. PubMed PMID: 26447530; PMCID: PMC4753638.
112. Badylak SF, Gilbert TW. Immune response to biologic scaffold materials. *Semin Immunol*. 2008;20(2):109-16. Epub 2008/02/20. doi: 10.1016/j.smim.2007.11.003. PubMed PMID: 18083531; PMCID: PMC2605275.
113. Badylak SF. The extracellular matrix as a biologic scaffold material. *Biomaterials*. 2007;28(25):3587-93. Epub 2007/05/08. doi: 10.1016/j.biomaterials.2007.04.043. PubMed PMID: 17524477.
114. Balestrini JL, Niklason LE. Extracellular matrix as a driver for lung regeneration. *Ann Biomed Eng*. 2015;43(3):568-76. Epub 2014/10/25. doi: 10.1007/s10439-014-1167-5. PubMed PMID: 25344351; PMCID: PMC4380778.
115. Li F, Li W, Johnson S, Ingram D, Yoder M, Badylak S. Low-molecular-weight peptides derived from extracellular matrix as chemoattractants for primary endothelial cells. *Endothelium*. 2004;11(3-4):199-206. doi: 10.1080/10623320490512390. PubMed PMID: 15370297.
116. Spiller KL, Nassiri S, Witherel CE, Anfang RR, Ng J, Nakazawa KR, Yu T, Vunjak-Novakovic G. Sequential delivery of immunomodulatory cytokines to facilitate the M1-to-M2 transition of macrophages and enhance vascularization of

- bone scaffolds. *Biomaterials*. 2015;37:194-207. Epub 2014/10/23. doi: 10.1016/j.biomaterials.2014.10.017. PubMed PMID: 25453950; PMCID: PMC4312192.
117. Spiller KL, Anfang RR, Spiller KJ, Ng J, Nakazawa KR, Daulton JW, Vunjak-Novakovic G. The role of macrophage phenotype in vascularization of tissue engineering scaffolds. *Biomaterials*. 2014;35(15):4477-88. Epub 2014/02/28. doi: 10.1016/j.biomaterials.2014.02.012. PubMed PMID: 24589361; PMCID: PMC4000280.
118. Franz S, Rammelt S, Scharnweber D, Simon JC. Immune responses to implants - a review of the implications for the design of immunomodulatory biomaterials. *Biomaterials*. 2011;32(28):6692-709. Epub 2011/06/28. doi: 10.1016/j.biomaterials.2011.05.078. PubMed PMID: 21715002.
119. Gordon S. Alternative activation of macrophages. *Nat Rev Immunol*. 2003;3(1):23-35. doi: 10.1038/nri978. PubMed PMID: 12511873.
120. Wynn TA, Vannella KM. Macrophages in Tissue Repair, Regeneration, and Fibrosis. *Immunity*. 2016;44(3):450-62. doi: 10.1016/j.immuni.2016.02.015. PubMed PMID: 26982353; PMCID: PMC4794754.
121. McDonald SM, Matheson LA, McBane JE, Kuraitis D, Suuronen E, Santerre JP, Labow RS. Use of monocyte/endothelial cell co-cultures (in vitro) and a subcutaneous implant mouse model (in vivo) to evaluate a degradable polar hydrophobic ionic polyurethane. *J Cell Biochem*. 2011;112(12):3762-72. doi: 10.1002/jcb.23307. PubMed PMID: 21826703.
122. Higgins DM, Basaraba RJ, Hohnbaum AC, Lee EJ, Grainger DW, Gonzalez-Juarrero M. Localized immunosuppressive environment in the foreign body response to implanted biomaterials. *Am J Pathol*. 2009;175(1):161-70. Epub 2009/06/15. doi: 10.2353/ajpath.2009.080962. PubMed PMID: 19528351; PMCID: PMC2708803.
123. Badylak SF, Valentin JE, Ravindra AK, McCabe GP, Stewart-Akers AM. Macrophage phenotype as a determinant of biologic scaffold remodeling. *Tissue Eng Part A*. 2008;14(11):1835-42. doi: 10.1089/ten.tea.2007.0264. PubMed PMID: 18950271.
124. Anderson JM, Rodriguez A, Chang DT. Foreign body reaction to biomaterials. *Semin Immunol*. 2008;20(2):86-100. Epub 2007/12/26. doi: 10.1016/j.smim.2007.11.004. PubMed PMID: 18162407; PMCID: PMC2327202.
125. Barnett-Vanes A, Sharrock A, Birrell MA, Rankin S. A Single 9-Colour Flow Cytometric Method to Characterise Major Leukocyte Populations in the Rat: Validation in a Model of LPS-Induced Pulmonary Inflammation. *PLoS One*. 2016;11(1):e0142520. Epub 2016/01/14. doi: 10.1371/journal.pone.0142520. PubMed PMID: 26764486; PMCID: PMC4713146.
126. Wolf MT, Dearth CL, Ranallo CA, LoPresti ST, Carey LE, Daly KA, Brown BN, Badylak SF. Macrophage polarization in response to ECM coated polypropylene mesh. *Biomaterials*. 2014;35(25):6838-49. Epub 2014/05/27. doi: 10.1016/j.biomaterials.2014.04.115
S0142-9612(14)00528-6 [pii]. PubMed PMID: 24856104; PMCID: 4347831.
127. Wei Y, Ji Y, Xiao LL, Lin QK, Xu JP, Ren KF, Ji J. Surface engineering of cardiovascular stent with endothelial cell selectivity for in vivo re-endothelialisation.

Biomaterials. 2013;34(11):2588-99. Epub 2013/01/29. doi: 10.1016/j.biomaterials.2012.12.036 S0142-9612(12)01416-0 [pii]. PubMed PMID: 23352039.

128. Rocha FG, Sundback CA, Krebs NJ, Leach JK, Mooney DJ, Ashley SW, Vacanti JP, Whang EE. The effect of sustained delivery of vascular endothelial growth factor on angiogenesis in tissue-engineered intestine. *Biomaterials*. 2008;29(19):2884-90. Epub 2008/04/09. doi: 10.1016/j.biomaterials.2008.03.026 S0142-9612(08)00197-X [pii]. PubMed PMID: 18396329; PMCID: 2685178.

129. Lee K, Silva EA, Mooney DJ. Growth factor delivery-based tissue engineering: general approaches and a review of recent developments. *J R Soc Interface*. 2011;8(55):153-70. Epub 2010/08/20. doi: 10.1098/rsif.2010.0223 rsif.2010.0223 [pii]. PubMed PMID: 20719768; PMCID: 3033020.

130. Vehof JW, Fisher JP, Dean D, van der Waerden JP, Spauwen PH, Mikos AG, Jansen JA. Bone formation in transforming growth factor beta-1-coated porous poly(propylene fumarate) scaffolds. *J Biomed Mater Res*. 2002;60(2):241-51. Epub 2002/02/22. doi: 10.1002/jbm.10073 [pii]. PubMed PMID: 11857430.

131. Fisher JP, Holland TA, Dean D, Mikos AG. Photoinitiated cross-linking of the biodegradable polyester poly(propylene fumarate). Part II. In vitro degradation. *Biomacromolecules*. 2003;4(5):1335-42. Epub 2003/09/10. doi: 10.1021/bm0300296. PubMed PMID: 12959603.

132. Fisher JP, Timmer MD, Holland TA, Dean D, Engel PS, Mikos AG. Photoinitiated cross-linking of the biodegradable polyester poly(propylene fumarate). Part I. Determination of network structure. *Biomacromolecules*. 2003;4(5):1327-34. Epub 2003/09/10. doi: 10.1021/bm030028d. PubMed PMID: 12959602.

133. Fisher JP, Holland TA, Dean D, Engel PS, Mikos AG. Synthesis and properties of photocross-linked poly(propylene fumarate) scaffolds. *J Biomater Sci Polym Ed*. 2001;12(6):673-87. Epub 2001/09/15. PubMed PMID: 11556743.

134. Hedberg EL, Kroese-Deutman HC, Shih CK, Crowther RS, Carney DH, Mikos AG, Jansen JA. Effect of varied release kinetics of the osteogenic thrombin peptide TP508 from biodegradable, polymeric scaffolds on bone formation in vivo. *J Biomed Mater Res A*. 2005;72(4):343-53. Epub 2005/01/25. doi: 10.1002/jbm.a.30265. PubMed PMID: 15666357.

135. Ruhe PQ, Hedberg EL, Padron NT, Spauwen PH, Jansen JA, Mikos AG. Biocompatibility and degradation of poly(DL-lactic-co-glycolic acid)/calcium phosphate cement composites. *J Biomed Mater Res A*. 2005;74(4):533-44. Epub 2005/07/26. doi: 10.1002/jbm.a.30341. PubMed PMID: 16041795.

136. Hedberg EL, Shih CK, Solchaga LA, Caplan AI, Mikos AG. Controlled release of hyaluronan oligomers from biodegradable polymeric microparticle carriers. *J Control Release*. 2004;100(2):257-66. Epub 2004/11/17. doi: S0168-3659(04)00401-8 [pii] 10.1016/j.jconrel.2004.08.020. PubMed PMID: 15544873.

137. Humphreys DT, Wilson MR. Modes of L929 cell death induced by TNF-alpha and other cytotoxic agents. *Cytokine*. 1999;11(10):773-82. Epub 1999/10/20. doi: 10.1006/cyto.1998.0492 S1043-4666(98)90492-6 [pii]. PubMed PMID: 10525316.

138. Aggarwal BB, Eessalu TE, Hass PE. Characterization of receptors for human tumour necrosis factor and their regulation by gamma-interferon. *Nature*. 1985;318(6047):665-7. Epub 1985/12/19. PubMed PMID: 3001529.
139. Han DW, Park YH, Kim JK, Jung TG, Lee KY, Hyon SH, Park JC. Long-term preservation of human saphenous vein by green tea polyphenol under physiological conditions. *Tissue Eng*. 2005;11(7-8):1054-64. Epub 2005/09/08. doi: 10.1089/ten.2005.11.1054. PubMed PMID: 16144441.
140. Fung YC. Blood Flow in Arteries. *Biomechanics: Circulation*. New York, NY: Springer New York; 1997. p. 108-205.
141. Yamada H, Evans FG. Strength of biological materials. Huntington, N.Y.: Robert E. Krieger Pub. Co.; 1973.
142. Melchiorri AJ, Hibino N, Best CA, Yi T, Lee YU, Kraynak CA, Kimerer LK, Krieger A, Kim P, Breuer CK, Fisher JP. 3D-Printed Biodegradable Polymeric Vascular Grafts. *Adv Healthc Mater*. 2016;5(3):319-25. Epub 2015/12/03. doi: 10.1002/adhm.201500725. PubMed PMID: 26627057; PMCID: 4749136.
143. Sell SA, McClure MJ, Barnes CP, Knapp DC, Walpoth BH, Simpson DG, Bowlin GL. Electrospun polydioxanone-elastin blends: potential for bioresorbable vascular grafts. *Biomed Mater*. 2006;1(2):72-80. Epub 2008/05/08. doi: 10.1088/1748-6041/1/2/004S1748-6041(06)22179-X [pii]. PubMed PMID: 18460759.
144. Bracaglia LG, Fisher JP. Extracellular Matrix-Based Biohybrid Materials for Engineering Compliant, Matrix-Dense Tissues. *Adv Healthc Mater*. 2015;4(16):2475-87. Epub 2015/08/01. doi: 10.1002/adhm.201500236. PubMed PMID: 26227679; PMCID: 4715589.
145. Heydrick S, Roberts E, Kim J, Emani S, Wong JY. Pediatric cardiovascular grafts: historical perspective and future directions. *Curr Opin Biotechnol*. 2016;40:119-24. Epub 2016/04/06. doi: 10.1016/j.copbio.2016.03.013S0958-1669(16)30069-6 [pii]. PubMed PMID: 27046072.
146. Melchiorri AJ, Hibino N, Fisher JP. Strategies and techniques to enhance the in situ endothelialization of small-diameter biodegradable polymeric vascular grafts. *Tissue Eng Part B Rev*. 2013;19(4):292-307. Epub 2012/12/21. doi: 10.1089/ten.TEB.2012.0577. PubMed PMID: 23252992; PMCID: 3690089.
147. Yang S, Xin X, Zlot C, Ingle G, Fuh G, Li B, Moffat B, de Vos AM, Gerritsen ME. Vascular endothelial cell growth factor-driven endothelial tube formation is mediated by vascular endothelial cell growth factor receptor-2, a kinase insert domain-containing receptor. *Arterioscler Thromb Vasc Biol*. 2001;21(12):1934-40. Epub 2001/12/18. PubMed PMID: 11742867.
148. Hao X, Silva EA, Mansson-Broberg A, Grinnemo KH, Siddiqui AJ, Dellgren G, Wardell E, Brodin LA, Mooney DJ, Sylven C. Angiogenic effects of sequential release of VEGF-A165 and PDGF-BB with alginate hydrogels after myocardial infarction. *Cardiovasc Res*. 2007;75(1):178-85. Epub 2007/05/08. doi: S0008-6363(07)00159-9 [pii] 10.1016/j.cardiores.2007.03.028. PubMed PMID: 17481597.
149. Richardson TP, Peters MC, Ennett AB, Mooney DJ. Polymeric system for dual growth factor delivery. *Nat Biotechnol*. 2001;19(11):1029-34. Epub 2001/11/02. doi: 10.1038/nbt1101-1029

- nbt1101-1029 [pii]. PubMed PMID: 11689847.
150. Chapanian R, Amsden BG. Combined and sequential delivery of bioactive VEGF165 and HGF from poly(trimethylene carbonate) based photo-cross-linked elastomers. *J Control Release*. 2010;143(1):53-63. Epub 2009/12/08. doi: 10.1016/j.jconrel.2009.11.025
S0168-3659(09)00822-0 [pii]. PubMed PMID: 19961885.
151. De Visscher G, Mesure L, Meuris B, Ivanova A, Flameng W. Improved endothelialization and reduced thrombosis by coating a synthetic vascular graft with fibronectin and stem cell homing factor SDF-1alpha. *Acta Biomater*. 2012;8(3):1330-8. Epub 2011/10/04. doi: 10.1016/j.actbio.2011.09.016
S1742-7061(11)00400-4 [pii]. PubMed PMID: 21964214.
152. Ducey P. Molecular signaling. *Ann N Y Acad Sci*. 2002;961:161. PubMed PMID: 12081889.
153. Alford AI, Rannels DE. Extracellular matrix fibronectin alters connexin43 expression by alveolar epithelial cells. *Am J Physiol Lung Cell Mol Physiol*. 2001;280(4):L680-8. PubMed PMID: 11238008.
154. Vorotnikova E, McIntosh D, Dewilde A, Zhang J, Reing JE, Zhang L, Cordero K, Bedelbaeva K, Gourevitch D, Heber-Katz E, Badylak SF, Braunhut SJ. Extracellular matrix-derived products modulate endothelial and progenitor cell migration and proliferation in vitro and stimulate regenerative healing in vivo. *Matrix Biol*. 2010;29(8):690-700. Epub 2010/08/24. doi: 10.1016/j.matbio.2010.08.007. PubMed PMID: 20797438.
155. Plotnikov SV, Pasapera AM, Sabass B, Waterman CM. Force fluctuations within focal adhesions mediate ECM-rigidity sensing to guide directed cell migration. *Cell*. 2012;151(7):1513-27. doi: 10.1016/j.cell.2012.11.034. PubMed PMID: 23260139; PMCID: PMC3821979.
156. Daub JT, Merks RM. A cell-based model of extracellular-matrix-guided endothelial cell migration during angiogenesis. *Bull Math Biol*. 2013;75(8):1377-99. Epub 2013/03/15. doi: 10.1007/s11538-013-9826-5. PubMed PMID: 23494144; PMCID: PMC3738846.
157. Flaim CJ, Chien S, Bhatia SN. An extracellular matrix microarray for probing cellular differentiation. *Nat Methods*. 2005;2(2):119-25. Epub 2005/01/21. doi: 10.1038/nmeth736. PubMed PMID: 15782209.
158. Bonnans C, Chou J, Werb Z. Remodelling the extracellular matrix in development and disease. *Nat Rev Mol Cell Biol*. 2014;15(12):786-801. doi: 10.1038/nrm3904. PubMed PMID: 25415508; PMCID: PMC4316204.
159. Wang RM, Christman KL. Decellularized myocardial matrix hydrogels: In basic research and preclinical studies. *Adv Drug Deliv Rev*. 2016;96:77-82. Epub 2015/06/06. doi: 10.1016/j.addr.2015.06.002. PubMed PMID: 26056717; PMCID: PMC4670814.
160. French KM, Boopathy AV, DeQuach JA, Chingozha L, Lu H, Christman KL, Davis ME. A naturally derived cardiac extracellular matrix enhances cardiac progenitor cell behavior in vitro. *Acta Biomater*. 2012;8(12):4357-64. Epub 2012/07/27. doi: 10.1016/j.actbio.2012.07.033. PubMed PMID: 22842035; PMCID: PMC3488121.

161. Duan Y, Liu Z, O'Neill J, Wan LQ, Freytes DO, Vunjak-Novakovic G. Hybrid gel composed of native heart matrix and collagen induces cardiac differentiation of human embryonic stem cells without supplemental growth factors. *J Cardiovasc Transl Res.* 2011;4(5):605-15. Epub 2011/07/09. doi: 10.1007/s12265-011-9304-0. PubMed PMID: 21744185; PMCID: PMC3196310.
162. Meng FW, Slivka PF, Dearth CL, Badylak SF. Solubilized extracellular matrix from brain and urinary bladder elicits distinct functional and phenotypic responses in macrophages. *Biomaterials.* 2015;46:131-40. Epub 2015/01/24. doi: 10.1016/j.biomaterials.2014.12.044. PubMed PMID: 25678122.
163. Mosser DM. The many faces of macrophage activation. *J Leukoc Biol.* 2003;73(2):209-12. PubMed PMID: 12554797.
164. Welt FG, Rogers C. Inflammation and restenosis in the stent era. *Arterioscler Thromb Vasc Biol.* 2002;22(11):1769-76. PubMed PMID: 12426203.
165. Gaspardone A, Crea F, Versaci F, Tomai F, Pellegrino A, Chiariello L, Giofrè PA. Predictive value of C-reactive protein after successful coronary-artery stenting in patients with stable angina. *Am J Cardiol.* 1998;82(4):515-8. PubMed PMID: 9723643.
166. Hibino N, Mejias D, Pietris N, Dean E, Yi T, Best C, Shinoka T, Breuer C. The innate immune system contributes to tissue-engineered vascular graft performance. *FASEB J.* 2015;29(6):2431-8. Epub 2015/02/20. doi: 10.1096/fj.14-268334. PubMed PMID: 25713026; PMCID: PMC4447224.
167. Allman AJ, McPherson TB, Badylak SF, Merrill LC, Kallakury B, Sheehan C, Raeder RH, Metzger DW. Xenogeneic extracellular matrix grafts elicit a TH2-restricted immune response. *Transplantation.* 2001;71(11):1631-40. PubMed PMID: 11435976.
168. Valentin JE, Stewart-Akers AM, Gilbert TW, Badylak SF. Macrophage participation in the degradation and remodeling of extracellular matrix scaffolds. *Tissue Eng Part A.* 2009;15(7):1687-94. doi: 10.1089/ten.tea.2008.0419. PubMed PMID: 19125644; PMCID: PMC2792102.
169. Zantop T, Gilbert TW, Yoder MC, Badylak SF. Extracellular matrix scaffolds are repopulated by bone marrow-derived cells in a mouse model of achilles tendon reconstruction. *J Orthop Res.* 2006;24(6):1299-309. doi: 10.1002/jor.20071. PubMed PMID: 16649228.
170. Badylak SF, Park K, Peppas N, McCabe G, Yoder M. Marrow-derived cells populate scaffolds composed of xenogeneic extracellular matrix. *Exp Hematol.* 2001;29(11):1310-8. PubMed PMID: 11698127.
171. Mott JD, Werb Z. Regulation of matrix biology by matrix metalloproteinases. *Curr Opin Cell Biol.* 2004;16(5):558-64. doi: 10.1016/j.ceb.2004.07.010. PubMed PMID: 15363807; PMCID: PMC2775446.
172. Seif-Naraghi SB, Salvatore MA, Schup-Magoffin PJ, Hu DP, Christman KL. Design and characterization of an injectable pericardial matrix gel: a potentially autologous scaffold for cardiac tissue engineering. *Tissue Eng Part A.* 2010;16(6):2017-27. doi: 10.1089/ten.TEA.2009.0768. PubMed PMID: 20100033; PMCID: PMC2949214.
173. DeQuach JA, Mezzano V, Miglani A, Lange S, Keller GM, Sheikh F, Christman KL. Simple and high yielding method for preparing tissue specific

extracellular matrix coatings for cell culture. *PLoS One*. 2010;5(9):e13039. Epub 2010/09/27. doi: 10.1371/journal.pone.0013039. PubMed PMID: 20885963; PMCID: PMC2946408.

174. Lo CM, Wang HB, Dembo M, Wang YL. Cell movement is guided by the rigidity of the substrate. *Biophys J*. 2000;79(1):144-52. doi: 10.1016/S0006-3495(00)76279-5. PubMed PMID: 10866943; PMCID: PMC1300921.

175. Balestrini JL, Chaudhry S, Sarrazy V, Koehler A, Hinz B. The mechanical memory of lung myofibroblasts. *Integr Biol (Camb)*. 2012;4(4):410-21. Epub 2012/03/13. doi: 10.1039/c2ib00149g. PubMed PMID: 22410748.

176. Engler AJ, Sen S, Sweeney HL, Discher DE. Matrix elasticity directs stem cell lineage specification. *Cell*. 2006;126(4):677-89. doi: 10.1016/j.cell.2006.06.044. PubMed PMID: 16923388.

177. Murikipudi S, Methe H, Edelman ER. The effect of substrate modulus on the growth and function of matrix-embedded endothelial cells. *Biomaterials*. 2013;34(3):677-84. Epub 2012/10/24. doi: 10.1016/j.biomaterials.2012.09.079. PubMed PMID: 23102623; PMCID: PMC3505450.

178. Yeh YT, Hur SS, Chang J, Wang KC, Chiu JJ, Li YS, Chien S. Matrix stiffness regulates endothelial cell proliferation through septin 9. *PLoS One*. 2012;7(10):e46889. Epub 2012/10/31. doi: 10.1371/journal.pone.0046889. PubMed PMID: 23118862; PMCID: PMC3485289.

179. Lotze MT, Deisseroth A, Rubartelli A. Damage associated molecular pattern molecules. *Clin Immunol*. 2007;124(1):1-4. Epub 2007/04/30. doi: 10.1016/j.clim.2007.02.006. PubMed PMID: 17468050; PMCID: PMC2000827.

180. Zheng MH, Chen J, Kirilak Y, Willers C, Xu J, Wood D. Porcine small intestine submucosa (SIS) is not an acellular collagenous matrix and contains porcine DNA: possible implications in human implantation. *J Biomed Mater Res B Appl Biomater*. 2005;73(1):61-7. doi: 10.1002/jbm.b.30170. PubMed PMID: 15736287.

181. Lee JH, Lee HB, Andrade JD. Blood compatibility of polyethylene oxide surfaces. *Progress in Polymer Science*. 1995;20(6):1043-79. Epub 2000. doi: 10.1016/0079-6700(95)00011-4.

182. Beck EC, Barragan M, Tadros MH, Gehrke SH, Detamore MS. Approaching the compressive modulus of articular cartilage with a decellularized cartilage-based hydrogel. *Acta Biomater*. 2016;38:94-105. Epub 2016/04/22. doi: 10.1016/j.actbio.2016.04.019. PubMed PMID: 27090590; PMCID: PMC4903909.

183. Sargeant TD, Desai AP, Banerjee S, Agawu A, Stopek JB. An in situ forming collagen-PEG hydrogel for tissue regeneration. *Acta Biomater*. 2012;8(1):124-32. Epub 2011/08/26. doi: 10.1016/j.actbio.2011.07.028. PubMed PMID: 21911086.

184. Stahl PJ, Romano NH, Wirtz D, Yu SM. PEG-based hydrogels with collagen mimetic peptide-mediated and tunable physical cross-links. *Biomacromolecules*. 2010;11(9):2336-44. doi: 10.1021/bm100465q. PubMed PMID: 20715762; PMCID: PMC3006224.

185. Freytes DO, Martin J, Velankar SS, Lee AS, Badylak SF. Preparation and rheological characterization of a gel form of the porcine urinary bladder matrix. *Biomaterials*. 2008;29(11):1630-7. Epub 2008/01/16. doi: 10.1016/j.biomaterials.2007.12.014. PubMed PMID: 18201760.

186. Bahney CS, Lujan TJ, Hsu CW, Bottlang M, West JL, Johnstone B. Visible light photoinitiation of mesenchymal stem cell-laden bioresponsive hydrogels. *Eur Cell Mater.* 2011;22:43-55; discussion Epub 2011/07/15. PubMed PMID: 21761391; PMCID: PMC5050040.
187. Zhang X, Goncalves R, Mosser DM. The isolation and characterization of murine macrophages. *Curr Protoc Immunol.* 2008;Chapter 14:Unit 14.1. doi: 10.1002/0471142735.im1401s83. PubMed PMID: 19016445; PMCID: PMC2834554.
188. Boltz-Nitulescu G, Wiltschke C, Holzinger C, Fellingner A, Scheiner O, Gessl A, Förster O. Differentiation of rat bone marrow cells into macrophages under the influence of mouse L929 cell supernatant. *J Leukoc Biol.* 1987;41(1):83-91. PubMed PMID: 3543182.
189. Mosser DM, Zhang X. Activation of murine macrophages. *Curr Protoc Immunol.* 2008;Chapter 14:Unit 14.2. doi: 10.1002/0471142735.im1402s83. PubMed PMID: 19016446; PMCID: PMC2822273.
190. Barrett JP, Costello DA, O'Sullivan J, Cowley TR, Lynch MA. Bone marrow-derived macrophages from aged rats are more responsive to inflammatory stimuli. *J Neuroinflammation.* 2015;12:67. Epub 2015/04/09. doi: 10.1186/s12974-015-0287-7. PubMed PMID: 25890218; PMCID: PMC4397943.
191. Mason BN, Reinhart-King CA. Controlling the mechanical properties of three-dimensional matrices via non-enzymatic collagen glycation. *Organogenesis.* 2013;9(2):70-5. Epub 2013/04/01. doi: 10.4161/org.24942. PubMed PMID: 23811696; PMCID: PMC3812287.
192. Fleming BD, Mosser DM. Regulatory macrophages: setting the threshold for therapy. *Eur J Immunol.* 2011;41(9):2498-502. doi: 10.1002/eji.201141717. PubMed PMID: 21952805; PMCID: PMC4299459.
193. Hibino N, Yi T, Duncan DR, Rathore A, Dean E, Naito Y, Dardik A, Kyriakides T, Madri J, Pober JS, Shinoka T, Breuer CK. A critical role for macrophages in neovessel formation and the development of stenosis in tissue-engineered vascular grafts. *FASEB J.* 2011;25(12):4253-63. Epub 2011/08/24. doi: 10.1096/fj.11-186585. PubMed PMID: 21865316; PMCID: PMC3236622.
194. Kluin J, Talacua H, Smits AI, Emmert MY, Brugmans MC, Fioretta ES, Dijkman PE, Söntjens SH, Duijvelshoff R, Dekker S, Janssen-van den Broek MW, Lintas V, Vink A, Hoerstrup SP, Janssen HM, Dankers PY, Baaijens FP, Bouten CV. In situ heart valve tissue engineering using a bioresorbable elastomeric implant - From material design to 12 months follow-up in sheep. *Biomaterials.* 2017;125:101-17. Epub 2017/02/08. doi: 10.1016/j.biomaterials.2017.02.007. PubMed PMID: 28253994.
195. Gui L, Boyle MJ, Kamin YM, Huang AH, Starcher BC, Miller CA, Vishnevetsky MJ, Niklason LE. Construction of tissue-engineered small-diameter vascular grafts in fibrin scaffolds in 30 days. *Tissue Eng Part A.* 2014;20(9-10):1499-507. Epub 2014/02/06. doi: 10.1089/ten.TEA.2013.0263. PubMed PMID: 24320793; PMCID: PMC4011429.
196. Pepper VK, Clark ES, Best CA, Onwuka EA, Sugiura T, Heuer ED, Moko LE, Miyamoto S, Miyachi H, Berman DP, Cheatham SL, Chisolm JL, Shinoka T, Breuer CK, Cheatham JP. Intravascular Ultrasound Characterization of a Tissue-

Engineered Vascular Graft in an Ovine Model. *J Cardiovasc Transl Res.* 2017. Epub 2017/01/17. doi: 10.1007/s12265-016-9725-x. PubMed PMID: 28097523.

197. Hibino N, McGillicuddy E, Matsumura G, Ichihara Y, Naito Y, Breuer C, Shinoka T. Late-term results of tissue-engineered vascular grafts in humans. *J Thorac Cardiovasc Surg.* 2010;139(2):431-6, 6.e1-2. doi: 10.1016/j.jtcvs.2009.09.057. PubMed PMID: 20106404.